IntechOpen

Effects of Sediment Transport on Hydraulic Structures

Edited by Vlassios Hrissanthou

EFFECTS OF SEDIMENT TRANSPORT ON HYDRAULIC STRUCTURES

Edited by **Vlassios Hrissanthou**

Effects of Sediment Transport on Hydraulic Structures
http://dx.doi.org/10.5772/59636
Edited by Vlassios Hrissanthou

Contributors

Jose Ramon Barros Cantalice, Wagner Luis Sousa, Yuri Silva, Alex Araujo, Douglas Cavalcante, Sergio Monthezuma Guerra, Levent Yilmaz, Jueyi Sui, Peng Wu, Ram Balachandar, Anastasios Georgoulas, Manolia Andredaki, Vlassios Hrissanthou, Nikolaos Kotsovinos, Marcus Schindewolf, Constance Bornkampf, Michael Von Werner, Jürgen Schmidt

Notice

First published in Croatia, 2015 by INTECH d.o.o.
eBook (PDF) Published by IN TECH d.o.o.
Place and year of publication of eBook (PDF): Rijeka, 2019.
IntechOpen is the global imprint of IN TECH d.o.o.
Printed in Croatia

Legal deposit, Croatia: National and University Library in Zagreb

Additional hard and PDF copies can be obtained from orders@intechopen.com

Effects of Sediment Transport on Hydraulic Structures
Edited by Vlassios Hrissanthou

p. cm.

ISBN 978-953-51-2231-9

eBook (PDF) ISBN 978-953-51-5060-2

Meet the editor

Prof. Vlassios Hrissanthou has studied Civil Engineering at the Aristotle University of Thessaloniki, Greece and Hydraulic Engineering at the University of Karlsruhe, Germany. His doctorate was elaborated at the University of Karlsruhe, Institute of Hydrology and Water Resources Management. The theme of his doctoral dissertation concerns the mathematical simulation of soil erosion and sediment transport in large basins. Prof. Hrissanthou has continued the research activities experimentally at the University of the Armed Forces Munich, Germany. The subject of his postdoctoral research concerns sediment transport in sewers. In the last 23 years, he had successively hold the positions of Assistant, Associate and Full Professor at the Democritus University of Thrace, Greece. Prof. Hrissanthou has taught 11 different graduate courses and 6 different postgraduate courses, and supervised a great number of diploma, postgraduate and doctoral dissertations. He was principal investigator or leader in many national and international projects regarding computation of rainfall-runoff, soil erosion and sediment transport in small and large basins, as well as reservoir sedimentation. Prof. Hrissanthou's research work is imprinted in over 115 peer reviewed articles in scientific journals, books and conference proceedings, in English, German and Greek. He is a reviewer in over 25 international scientific journals.

Contents

Preface XI

Section 1 Alluvial Channel Hydraulics 1

Chapter 1 **General Hydraulic Geometry 3**
Levent Yilmaz

Section 2 Reservoir Sedimentation and its Effects 17

Chapter 2 **Bedload and Suspended Sediment of a Watershed Impacted by Dams 19**
Jose Ramon B. Cantalice, Wagner Luis da Silva Souza, Yuri Jacques Agra Bezerra Silva, Sergio M.S. Guerra, Alex Mauricio Araújo, Douglas Monteiro Cavalcante and Cinthia Maria Cordeiro Atanazio Cruz Silva

Chapter 3 **Simulation of Reservoir Siltation with a Process-based Soil Loss and Deposition Model 41**
Marcus Schindewolf, Constanze Bornkampf, Michael von Werner and Jürgen Schmidt

Chapter 4 **Assessment of Reservoir Sedimentation Effect on Coastal Erosion and Evaluation of Sediment Removal Techniques for Its Reduction — The Case of Nestos River, Greece 59**
Manolia Andredaki, Anastasios Georgoulas, Vlassios Hrissanthou and Nikolaos Kotsovinos

Section 3 Local Scour 89

Chapter 5 **The Impact of Ice Cover and Sediment Nonuniformity on Erosion Around Hydraulic Structures 91**
Peng Wu, Jueyi Sui and Ram Balachandar

Preface

Sediment transport in rivers is a complicated phenomenon, the quantification of which could not be implemented satisfactorily up to now. Hydraulic engineers mainly, but also geomorphologists, have attempted to quantify sediment transport in rivers because of the unfavorable consequences of it in hydraulic structures, in example: dams, reservoirs, bridge piers, harbors, etc. Especially during floods, rivers transport large quantities of sediments, which in combination with river flow endanger landscapes and settlements.

Sediment transport is a significant part of the scientific area of river hydraulics. Therefore, the first section of the present book concerns alluvial channel hydraulics. The second section refers to a serious consequence of river sediment transport, namely reservoir sedimentation. Sediment transported in a river originates from the corresponding basin, that is eroded by rainfall water. Hence, the quantification of soil erosion is also addressed in the second section. While soil erosion is the original physical process that causes reservoir sedimentation, the latter process may increase coastal erosion in case that the river feeding the reservoir, discharges its water into the sea. So, the effect of reservoir sedimentation on coastal erosion is further treated in the second section. Finally, the third section of the book is dedicated to the phenomenon of local scour around bridge piers, in particular the conditions of ice cover.

Prof. Dr.-Ing. Vlassios Hrissanthou
Department of Civil Engineering,
Section of Hydraulic Engineering,
Democritus University of Thrace,
Greece

Section 1

Alluvial Channel Hydraulics

Chapter 1

General Hydraulic Geometry

Levent Yilmaz

Additional information is available at the end of the chapter

http://dx.doi.org/10.5772/61643

Abstract

Employing bed load formulae hydraulic geometry relations were derived for stream width, meander wave length, and bed slope. The relations are in terms of friction factor, bed load discharge, bed load diameter, and water discharge. The bed load formulae are those of Engelund and Hansen (1966) [1], Einstein (1950) [2], Shields (1936) [3], and Meyer-Peter and Muller (1948) [4].

Keywords: Hydraulic Geometry, sediment transport, bed load, alluvium

1. Introduction

The water and sediment discharge of a river are primarily determined by the hydrology, geology, and topography of the drainage area. According to the influx water and sediment, the river creates its own geometry, i.e., slope, depth, width, and meandering pattern. Since the slope and meander pattern do not respond quickly enough to follow seasonal variations of discharge, it is natural to invoke some measure of dominant discharge values for these variables (Engelund and Hansen, 1966 [1] ; Hansen, 1967 [5]; Kennedy and Alam, 1967 [6]).

In a given river, the water and sediment discharges normally increase in the downstream direction, and so do the depth and the width of the stream. The slope and the grain size usually decrease gradually from the source to estuary. According to Leviavsky (1955) [7], the grain size decreases approximately exponentially in the downstream direction. These observations point towards the existence of relations for the depth, width, and slope as functions of the water and sediment discharge. To that end, a number of "regime" relations have been suggested using it. An account of such relations has been given by Blench (1957[8], 1966[9]). Accordingly,

$$B \sim Q^{1/2} \tag{1}$$

$$D \sim Q^{1/3} \tag{2}$$

$$S \sim Q^{-1/6} \tag{3}$$

where B = the width, D = the depth, S = the slope, and Q = the water discharge. An empirical relation expressing the meander " wave-length" has been suggested by Inglis (1947) [10] as:

$$L \sim Q^{1/2} \tag{4}$$

Equations (1) and (4) describe a direct proportionality between the width of the stream and the meander length. Using the data from a large number of rivers in U.S.A and Indian as well as from several small scale model tests, Leopold and Wolman (1957) [11]derived the following popular relation:

$$L=10B \tag{5}$$

Engelund and Hansen (1967)[12] derived equation (5) using the similarity principle. Due to the complex mechanics of the bed load and water transport, a number of variations of the above formulae have been proposed in the literature.

The objective of this paper is to derive hydraulic geometry relations using bed load formulae and compare them.

2. Derivation of hydraulic geometry relations

2.1. Engelund and Hansen (1966) [1] Bed Load Formula

The Darcy-Weisbach relation for the energy slope can be expressed as:

$$S = f\frac{V^2}{2g}\frac{1}{D} \tag{6}$$

where S = energy gradient (slope), f = friction factor, V= mean velocity, g = acceleration due to gravity, D = mean flow depth. Engelund and Hansen (1967) [12] expressed f as

http://dx.doi.org/10.5772/61643

$$f = 0.1\theta^{5/2}/\Phi \tag{7}$$

where θ = the dimensionless form of the bed shear stress τ_0, and Φ= non-dimensional sediment transport rate, and d = mean fall diameter.

The non-dimensional transport rate is expressed as

$$\Phi = \frac{q_T}{\sqrt{(s-1)gd^3}} \tag{8}$$

where $q_T = Q_T/B$= sediment discharge per unit width, Q_T = total sediment discharge ($=Q_B + Q_S$), Q_B=bed load discharge, Q_s= suspended load discharge, $s = \gamma_s / \gamma$ = relative density of sediment grains,γ=specific gravity of water, γ_s= specific gravity of sediment grains, B = flow width,. Substitution for $q_T = Q_T/B$ in equation (8) yields

$$\Phi = \frac{Q_T}{B\sqrt{(s-1)gd^3}} \tag{9}$$

The bed shear shear stress $\tau_{0,}$ can be expressed in dimensionless form, θ, as (Shields, 1936)[3]:

$$\theta = \frac{DS}{(s-1)d} \tag{10}$$

Substituting equations (7) – (10) into the Darcy-Weisbach equation (6) one gets

$$S = 0.1\left[\frac{DS}{(s-1)d}\right]^{5/2} \frac{1}{\Phi}(V)^2 \frac{1}{2g}\frac{1}{D} \tag{11}$$

Substitution of equation (10) for Φ, the non-dimensional transport rate and the continuity equation V=Q/BD in equation (11) yields

$$S = 0.1\left[\frac{DS}{(s-1)d}\right]^{5/2} \frac{B\sqrt{(s-1)gd^3}}{Q_T}(Q/BD)^2 \frac{1}{2g}\frac{1}{D} \tag{12}$$

Recalling the definition of s and putting the values of s = 2.65 and g = 9.81 in equation (12), one obtains:

$$S = 0.1\left[\frac{DS}{(1.65)d}\right]^{5/2}\frac{B\sqrt{(1.65)gd^3}}{Q_T}\left(\frac{Q}{BD}\right)^2\frac{1}{19.62}\frac{1}{D} \tag{13}$$

A little rearrangement of equation (13) yields

$$\frac{S}{S^{5/2}} = \frac{0.005}{(1.65)^{5/2}}d^{-5/2}D^{5/2}Q^2 / Q_T[(1.65)(9.81)]^{1/2}d^{3/2}BD^{-3} \tag{14}$$

Equation (14) can be simplified as

$$S = \left[0.20\ d^{-1}BD^{1/2}\left(Q^2/Q_T\right)\right]^{-2/3} \tag{15}$$

The mean depth can be expressed from equation (15) as

$$D = \left[5S^{-3/2}\ Bd\left(Q_T/Q^2\right)\right]^2 \tag{16}$$

The water surface width B can be expressed from equation (16) as

$$B = 0.20\ D^{1/2}S^{3/2}d\ \left(Q^2/Q_T\right) \tag{17}$$

or using L = 10B,one obtains from equation (17):

$$L = 2.0\ D^{1/2}S^{3/2}d\ \left(Q^2/Q_T\right) \tag{18}$$

Shields' (1936) [3] Bed Load Formula:

On the basis of his experimental results, Shields (1936) [3] proposed a dimensionally homogeneous transport function:

$$Q_B\gamma_s / Q\gamma S = 10(\tau_0 - \tau_c) / (\gamma_s - \gamma)d_m \tag{19}$$

where Q_B = bed load transport rate (tons/hour), d_m = the effective diameter of sediment (mm), γ_s = the specific weight of sediment (T/m^3), γ = the specific weight of water (T/m^3), τ_o = the shear stress (T/m^2); τ_c = critical shear stress (T/m^2), and S = the energy slope.

http://dx.doi.org/10.5772/61643

Shields (1936) [3] hypothesized that the rate of transport was a function of the dimensionless resistance coefficient:

$$\tau_o\left[(\gamma_S-\gamma)d_m\right]^{-1} \tag{20}$$

the critical value controlling the incipient motion of the bed load. The computation of the shear stress uses the hydraulic radius R and the bed slope S:

$$\tau_o=\gamma RS \tag{21}$$

whereas the critical shear stress is obtained from Straub's graph (1935) [3] for various sediment sizes. The bed load transport rate obtained from the Shields formula is the mass

of the solid particles. This rate value should be multiplied by a factor 1.60, in accordance with the density of sand, to obtain the volumetric value.

Recalling that

$$\tau_o-\tau_c=\tau=\gamma DS \tag{22}$$

Substituting of equation (22) in equation (19) gives

$$\frac{\gamma_s Q_B}{\gamma QS}=\frac{10\gamma DS}{(\gamma_s-\gamma)d_m}=\frac{10DS}{\left(\frac{\gamma_s}{\gamma}-1\right)d_m} \tag{23}$$

where $s=\frac{\gamma_s}{\gamma}$. This can be simplified as

$$\frac{\gamma_s Q_B}{\gamma QS^2}=\frac{10D}{\left(\frac{\gamma_s}{\gamma}-1\right)d_m} \tag{24}$$

Substituting $Q_B=q_BB$ and equation (6) into equation (24), one obtains

$$\frac{q_B BD4g^2B^4D^4}{Qf^2Q^4}=\frac{10D}{\frac{\gamma_s}{\gamma}\left(\frac{\gamma_s}{\gamma}-1\right)d_m} \tag{25}$$

Using the continuity equation V=Q/A, one gets from equation (25)

$$Q_B = \frac{10Q^5 f^2}{\frac{\gamma_s}{\gamma}\left(\frac{\gamma_s}{\gamma}-1\right)d_m B^4 D^5 4g^2} \tag{26}$$

D is expressed from equation (26) as

$$D = 0.3587 \frac{Q}{Q_B^{0.20}} f^{0.4} d_m^{-0.2} B^{-0.8} \tag{27}$$

Using L=10B, one obtains from equation (27)

$$L = 2.776 \frac{Q^{1.25}}{Q_B^{0.25}} f^{0.5} d_m^{-0.25} D^{-1.25} \tag{28}$$

From equation (28) the width B is computed as

$$B = (0.2776) \frac{Q^{1.25}}{Q_B^{0.25}} f^{0.5} d_m^{-0.25} D^{-1.25} \tag{29}$$

S is derived from equation (23)

$$S = 0.6612 \left(\frac{Q_B}{Q}\right)^{0.5} d^{0.5} D^{-0.5} \tag{30}$$

2.2. Einstein's (1950) [2] bed load formula

The bedload formula due to Einstein (1950) [2] can be expressed as

$$q_{sbi} = P_i \Phi_* \gamma_s \Big/ \left\{\left[\gamma/\gamma_s - \gamma\right]/g d_{si}^{\,3}\right\}^{1/2} \tag{31}$$

where d_{si} = the grain diameter for which si per cent is finer, q_{sbi} = the intensity of bed load movement of size class i, Φ_* = the bed load intensity, γ = the unit weight of water; γ_s = the unit weight of sediment particles, g = the gravitational acceleration, P_i = the particle availability parameter~ G_{di}/G_d (bed surface gradation),G_d = the total weight of sediment in the bed surface layer, and G_{di} = the weight of the i th size class in the bed surface layer.

http://dx.doi.org/10.5772/61643

The bed surface layer in this equation is a zone near the bed surface called the "active layer". The surface elevation is changed as sediment is deposited into or scoured out of this layer.

Setting the particle availability parameter, P_1, equal to 1. One obtains from equation (31)

$$\frac{Q_B}{B} = \frac{\Phi_* \gamma_s}{\left[\left(\gamma / \gamma_s - \gamma\right) / g d_{si}^3\right]^{1/2}} \qquad q_s = \frac{Q_B}{B} \qquad \text{B = water surface width} \tag{32}$$

where $q_s = P_i \Sigma q_{sbi'}$ and q_{sbi} = the intensity of bed load movement of size class i.

The water surface width can finally be expressed from the equation (32) as

$$B = Q_B \Phi_*^{-1} \gamma_s^{-1} \left[\left(\gamma^2 / \left(s-1\right)\gamma_s\right) / g d_{si}^3\right]^{1/2} \tag{33}$$

Using L=10B, one obtains from the equation (36) as

$$L = 10 Q_B \Phi_*^{-1} \gamma_s^{-1} [\left(\gamma^2 / \left(s-1\right)\gamma_s\right) / g d_{si}^3]^{1/2} \tag{34}$$

The Darcy-Weisbach relation, equation (6) can be written as

$$S == f \frac{Q^2}{B^2 D^3} \frac{1}{2g} \tag{35}$$

Substituting the water surface width B from the equation (32) into the equation (35) and using the continuity equation Q=V BD,

D is expressed from Equation (35) as

$$D = 0.2529 f^{0.571} Q^{0.571} B^{-0.571} V^{0.28571} \tag{36}$$

The mean velocity is derived from equation (36) as

$$V = 122.93 f^{-1.998} Q^{-1.998} B^{1.998} D^{3.5} \tag{37}$$

and the slope S is derived from the equation (38) as

$$S = fQ^2B^2 0.0509D^{-3} \tag{38}$$

2.3. Bed load formula of Meyer-Peter and Muller (MPM) model (1948) [4]

This formula was derived from experiments using a laboratory flume with a maximum width of 2 m, very different from the conditions encountered in large channels. The formula depends primarily on the grain diameter and water discharge. They derived a formula for bed load discharge with the aim to develop a more practical formula. Bogardi (1978) indicated several difficulties that are encountered in application of this formula.

According to the Meyer-Peter and Muller(1948) [4] (MPM) Model:

$$\gamma DS = 0.047(\gamma_s - \gamma)d_s + 0.25\rho^{1/3}q_b^{1/3} \tag{39}$$

where γ = specific gravity of water, γ_s = specific gravity of sediment grains,

D= mean depth, S= energy gradient (slope), d_s= mean sediment diameter,

ϱ = density of water, q_b= sediment discharge per unit width.

From equation (39) the slope S is computed as

$$S = \left(\gamma D\right)^{-1}\left[0.047(\gamma_s - \gamma)d_s + 0.25\rho^{1/3}q_b^{1/3}\right] \tag{40}$$

Putting equation (6) into the equation (40)

$$\gamma f\frac{Q^2}{B^2D^2}\frac{1}{2g} = 0.047(\gamma_s - \gamma)d_s + 0.25\rho^{1/3}q_b^{1/3} \tag{41}$$

Equation (41) is rearranged for computing the width B as

$$B^{-2} = 19.62D^2\left[0.047(\gamma_s - \gamma)d_s + 0.25\rho^{1/3}q_b^{1/3}\right]f^{-1}\gamma^{-1}Q^{-2} \tag{42}$$

From the equation (42), is computed the width B is computed

$$B = 0.226D^{-1}\left[0.047(\gamma_s - \gamma)d_s + 0.25\rho^{1/3}q_b^{1/3}\right]^{1/2} f^{1/2}\gamma^{1/2}Q^{-1} \tag{43}$$

http://dx.doi.org/10.5772/61643

Using L=10B, one obtains the wave length L as

$$L = 2.26D^{-1}\left[0.047(\gamma_s - \gamma)d_s + 0.25\rho^{1/3}q_b^{1/3}\right]^{1/2} f^{1/2}\gamma^{1/2}Q^{-1} \tag{44}$$

The water depth D is derived from equation (42) as

$$D = 0.226B^{-1}\left[0.047(\gamma_s - \gamma)d_s + 0.25\rho^{1/3}q_b^{1/3}\right]^{1/2} f^{1/2}\gamma^{1/2}Q^{-1} \tag{45}$$

3. Discussion

The hydraulic geometry relationships, B, D, S, L computed with DuBoys (1879) [13] sediment transport formula (Huang and Nanson, 2000) [14] were similar, those computed with Einstein's (1950) [2] model and Shields' (1936) [3] model, but MPM (1948) [4] model have differences by using the specific gravity of water and sediment grains, and density of water. Although there are four dependent variables (width, depth, velocity and slope) with only three basic flow relations of continuity, resistance and sediment transport. This study finds that the long-recognized problem of no closure can be solved directly in terms of the analytical approach advocated here for understanding the self-adjusting mechanism of alluvial channels.

With stable canal flow relations (Lacey's flow resistance relation and DuBoys' (1879) [13] sediment transport formula) and rectangular sections, introducing a channel form factor (width/depth ratio) as a dependent variable identifies an optimum condition for sediment transport by adjusting width/depth ratio for a given flow discharge, channel slope and sediment size (Huang and Nanson, 2000) [14].

Theoretically derived channel geometry relations are highly consistent with their counterparts obtained from " Darcy-Weisbach relation", except that ' threshold theory' provides a larger value of friction factor coefficient. This may be due to the use of rectangular cross-sections in our analytical study. Furthermore, the maximum friction value is greater in natural rivers using relationships not so dependent on canal data.

A comparison of the averaged channel geometry relations with downstream hydraulic geometry relations developed by Huang and co-workers (Huang and Warner, 1995 [15]; Huang and Nanson, 1995 [16], 1998 [17]) and by Julien and Wargadalam (1995) [18] based on numerous sets of field observations, reveals high level of consistency. When sediment concentration varies in a limited range, the averaged relationships are very similar to empirical regime formulations ('regime theory') (Huang and Nanson, 2000) [4].

Table I presents a comparison of equations with downstream hydraulic geometry relations obtained by Huang and co-workers (2000) and by Julien and Wargadalam (1995) [18], based on numerous sets of field observations.

Huang and co-workers' model (1995)[16]	Julien and Wargadalam's model(1995)[18]
$B \alpha Q^{0.501}S\text{-}0.156$	$B\alpha Q^{0.4\text{-}0.5} S^{-(0.2\text{-}0.25)}$
$D\alpha$ Q0.299 S-0.206	$D\alpha Q^{0.4\text{-}0.25}S^{-(0..2\text{-}0.125)}$
$V\alpha$ Q0.200 S0.362	$V\alpha Q^{0.2\text{-}0.25} S^{0.4\text{-}0.375}$
Huang and Nanson (2000) [14]	**Engelund and Hansen (1967) model [12]**
$B\alpha Q^{0.478}S0.076$	$B\alpha Q^2 (Q^{-4} S^{-3})^{0.5}S1.5$
$D\alpha$ Q0.289 S-0.350	$D\alpha$ Q-4 S-3
$V\alpha$ Q0.233 S0.274	
Shields (1936) model [3]	
$B\alpha Q^{1.25} f^{0.5} D^{-1.25} d_m^{-0.25}$	
$D\alpha (Q/Q_B^{0.20}) f^{0.4} d_m^{-0.2} B^{-0.8}$	
Einstein's (1950) model [2]	
$B\alpha \Phi_*^{-1} d_{si}^{1.5}$	
$D\alpha S^{-0.33} f^{0.33} Q^{0.66} (\Phi_*^{-1} d_{si}^{1.5})^{0.66}$	
MPM (1948) model [4]	
$B\alpha Q^{-1} f^{0.5} D^{-1}$	
$D\alpha Q^{-1} f^{0.5} B^{-1}$	

Table 1. Downstream hydraulic geometry relations defined as the functions of flow discharge and channel slope

To reflect how channel geometry adjusts within the range, this study is only able to present acceptably averaged relationships for channel geometry by assigning the four variables depth, width, slope and wave length.

Although as stated earlier τ_c and the other coefficients are determined only by sediment size d, their combined effects on natural channel geometry are much more complicated with both bank strength and channel roughness (or sediment size) being often particularly examined (Millar and Quick, 1993 [19]; Huang and Nanson, 1998 [17]). When the constant terms and the terms related to sediment size d are ignored, the equations of Einstein's (1950) [2] and Shields' (1936) [3] agree very closely with the widely observed empirical regime channel relationships, when sediment concentration (Q_s/Q) remains unchanged or varies within a limited range. This is consistent with the study by Simons and Albertson (1960) [20]. In an analysis of numerous observations that were collected from stable canals in different parts of the world, Simons and Albertson (1960) [20] identified that the relations closest to this equations occur only when sediment concentration varies in a limited range (less than 500 ppm).

In many circumstances, sediment discharge Q_s is unknown and consequently channel slope S is used as an alternative. The consistency of the theoretical results of equations (Engelund and Hansen, 1967 [12]; Shields [3], 1936; Einstein, 1950 [2]; MPM model, 1948 [4]) with the studies

based on direct observations suggests strongly that most natural alluvial channels are able to adjust their channel form, so as to reach an optimum state. This must be a general principle for flow in rivers and canals that causes channels in very different environments to exhibit remarkably similar hydraulic geometry relations.

The physical relationships of flow continuity, flow resistance and sediment transport determine the degree of channel adjustment and consequently illustrate a condition of maximum sediment transporting capacity, subject to the conditions of flow discharge, channel slope and sediment size.

Mathematically, it can be defined a minimum slope subject to the conditions of flow discharge, sediment discharge and sediment size; or a minimum flow discharge subject to the conditions of sediment discharge, channel slope and sediment size; or an optimum sediment size subject to the conditions of flow and sediment discharges, and channel slope. This formulation provides the maximum sediment transporting capacity per unit of approximate total stream power (actual total stream power is γQS where γ is the specific weight of water). This concept includes the following specific optimum conditions that have long been hypothesized and applied for practical problem solving:

1. for fixed S and Q, Q_s= a maximum as proposed by Pickup (1976) [21], Kirkby (1977) [22] and White et al. (1982) [23];
2. for fixed Q_S and Q, S= a minimum as proposed by Chang (1979 a [24], b [25], 1988 [26]);
3. for fixed Q_S, $S^{7/11}Q^{8/11}$= a minimum or $SQ^{1.142}$= a minimum, close to γQS= a minimum as proposed by Chang (1980 a [27], b [28], 1986 [29], 1988 [26]).

Hence, the use of the analytical approaches proposed by Pickup (1976) [21], Kirkby (1977) [22] and White et al. (1982) [23] with the maksimum sediment transport capacity, and by Chang (1979 a [24], b [25], 1980 a [27], b [28], 1988 [26]) based on the minimum stream power hypothesis should produce consistent stable channel geometry relations with the theoretical approach advocated in this study.

This study shows that the optimum condition for sediment transport with regard to downstream hydraulic geometry relations for a given flow discharge, channel slope and sediment size results from the general condition of maksimum flow efficiency according to Huang and Nanson, 2000 [14], defined as the maximum sediment transporting capacity per unit available stream power. Maksimum flow efficiency is an internal optimum condition and includes the conditions of maximum sediment transporting capacity and minimum stream power as proposed by Pickup (1976) [21], Kirkby (1977) [22] and White et al. (1982) [23], and by Chang (1979 a [24], b [25], 1980 a [27], b [28], 1986 [29], 1988 [26]) respectively.

Despite criticism of the use of extremal hypotheses (Griffiths, 1984)[30], this study offers strong support for the use of bed-load concepts of different authors for hydraulic-geometry relation derivations and for understanding natural channel-form adjustment.

Finally, this study indicates that the general principle of sediment transport approaches in the variational theory of mechanics is able to provide a physical explanation for the existence of

the optimum conditions of natural channel-form adjustment. However, these findings are of a preliminary nature and further detailed research is ongoing.

4. Conclusion

Strictly speaking, Engelund and Hansen's equation should be applied to flows with dune beds in accordance with the similarity principle. According to Yang(1987) [31], a river can adjust its roughness, geometry, profile and pattern through the processes of sediment transport. Qualitative descriptions of these dynamic adjustments of natural streams have been made mainly by geologists and geomorphologists. Empirical regime types of equation have been developed by engineers to solve design problems. Attempts have been made in recent years to explain these adjustments based on different extremal theories and hypotheses.

Author details

Levent Yilmaz*

Address all correspondence to: lyilmaz@itu.edu.tr

Technical University of Istanbul, Civil Engineering Department, Hydraulics Division, Maslak, Istanbul, Turkey

References

[1] Engelund, F. and E. Hansen, 1966: Investigations of Flow in Alluvial Streams. Acta Polytechnical Scandinavica. Civil Engineering and Building Construction Series No. 35, Copenhagen.

[2] Einstein, H. A., 1950: The Bed-Load Function for Sediment Transportation in Open Channel Flows. Technical Bulletin No. 1026. U. S. Dept. of Agriculture.

[3] Shields, I. A., 1936: Anwendung der Ahnlichkeitmechanik und der Turbulenzforschung auf die Geschiebebewegung. Mitt. Preuss. Ver. –Anst., Berlin, No. 26.

[4] Meyer-Peter, E.,and R. Muller, 1948: Formulas for Bed-Load Transport. Proc. 3rd Meet. Int. Ass. Hydr. Res., Stockholm.

[5] Hansen, E., 1967 : On the formation of Meanders as a Stability problem. Basic Research-Progress Report No. 13, Jan., Hydraulic Laboratory, Tech. Uni. of Denmark.

[6] Kennedy, J. F., and A. M. Z. Alam, 1967: Discussion of "Hydraulic Resistance of Alluvial Streams" in Journ. Hydr. Div. Vol. 93, HY 1, January.

[7] Leviavsky, S., 1955: An Introduction to Fluvial Hydraulics. Constable and Company Ltd., London.

[8] Blench, T., 1957: Regime Behavious of Canals and Rivers. Butterworths Scientific Publications, London.

[9] Blench, T., 1966 : Mobile-Bed Fluviology. Dept. Tech. Serv., Tech III. Div., Univ. of Alberta, Edmonto, Alberta, Canada.

[10] Inglis, C. C., 1947: Meanders and their Bearing on River Training. Proc. Instn. Civ. Engrs., Maritime and Waterways Pap. No.7, January.

[11] Leopold, L. B., and Wolman, M.G., 1957: River channel patterns: braided, meandering and straight. U.S. Geological Survey Profl. Paper, 282-B, pp. 39-85.

[12] Engelund, F., and E. Hansen, 1967: Comparison Between Similarity Theory and Regime Formulae. Basic Research-Progress Report No. 13, January, Hydraulic Laboratory, Techn. Un. of Denmark.

[13] Du Boys, P. 1879 : " Etudes du regime du Rhone et de I'action execee par les eaux sur un lit a fond de gravirs indefiniment affouillable", Annales des Ponts et Chausees, Series 5, 18(49), part 2, pp. 141- 195

[14] Huang, H. Q. and G.C.,Nanson, 2000 : Hydraulic Geometry and maximum flow efficiency as products of the principle of least action. Earth Surface Processes and Landforms, 25, pp. 1-16

[15] Huang, H. Q. and R.F, Warner, 1995 : The multivariate controls of hydraulic geometry; a causal investigation in terms of boundary shear distribution. Earth Surfaces Processes and Landforms 20, pp. 115-130

[16] Huang, H. Q. and G.C.,Nanson, 1995 : On a multivariate model of channel geometry. Proceedings of the XXVIth Congress of the International Association of Hydraulic Research, Vol. 1. Thomas Telford: London; pp. 510-515

[17] Huang, H. Q. and G.C.,Nanson, 1998 : The influence of bank strength on channel geometry. Earth Surface Processes and Landforms, 23, pp. 865-876

[18] Julien, P. Y. and J., Wargadalam, 1995 : Alluvial channel geometry : theory and applications. Journal of Hydraulic Engineering, ASCE, 121, pp. 312-325

[19] Millar, R.G. and M.C. Quick, 1993 : Effect of bank stability on geometry of gravel rivers. Journal of Hydraulic Engineering, ASCE, 119, pp. 1343-1363.

[20] Simons, D.B. and M.L. Albertson, 1960 : Uniform water conveyance channels in alluvial materials. Journal of the Hydraulics Division, ASCE, 86, pp. 33-71

[21] Pickup, G., 1976 : Adjustment of stream channel shape to hydrologic regime. Journal of Hydrology, 30, pp. 365-373

[22] Kirkby, M. J. 1977 : Maximum sediment efficiency as a criterion for alluvial channels. In River Channel Changes, Gregory, K. J. (ed.). Wiley : Chichester; pp. 429-442

[23] White, W. R., Bettess, R. and Paris, E., 1982 : Analytical approach to river regime. Journal of the Hydraulics Division, ASCE, 108, pp. 1179- 1193

[24] Chang, H.H., 1979a: Geometry of rivers in regime, Journal of the Hydraulics Division, ASCE 105, pp. 691-706

[25] Chang, H.H., 1979b: Minimum stream power and river channel patterns. Journal of Hydrology, 41, pp. 303-327

[26] Chang, H.H., 1988 : Fluvial Processes in River Engineering. Wiley: New York

[27] Chang, H.H., 1980a: Stable alluvial canal design. Journal of the Hydraulics Division, ASCE, 106, pp. 873-891

[28] Chang, H.H., 1980b: Geometry of gravel streams. Journal of the Hydraulics Division, ASCE, 106, pp. 1443-1456

[29] Chang, H.H., 1986 : River channel changes: adjustments of equilibrium. Journal of Hydraulic Engineering, ASCE, 112, pp. 43-55

[30] Griffiths, G.A., 1984 : Extremal hypotheses for river regime: an illusion of progress. Water Resources Research, 20, pp. 113-118.

[31] Yang, C.T., 1987 : Energy dissipation rate approach in river mechanics. In Sediment Transport in Gravel-Bed Rivers, Thorne, C.R., Bathurst, J. C., Hey, R.D. (eds). Wiley: Chichester; pp. 735-758

Section 2

Reservoir Sedimentation and its Effects

Chapter 2

Bedload and Suspended Sediment of a Watershed Impacted by Dams

Jose Ramon B. Cantalice, Wagner Luis da Silva Souza,
Yuri Jacques Agra Bezerra Silva, Sergio M.S. Guerra, Alex Mauricio Araújo,
Douglas Monteiro Cavalcante and
Cinthia Maria Cordeiro Atanazio Cruz Silva

Additional information is available at the end of the chapter

http://dx.doi.org/10.5772/61478

Abstract

Sediment transport relates to suspended sediment and bedload. The suspended sediment plays the most important role on the land-ocen sediment flux. On the other hand, the bedload should be considered in order to assess the impacts of dams on sediment transport and sediment yield. Recent effects of dam construction have been widely reported. The sediment load has been reduced by more than 75% for major rives, such as Nilo, Orange, Volta, Indus, Ebro, Kizil Irmark, Colorado, and Rio Grande and more than 40% of its lux is trapped within large dams. In addition, the multiple trapping through sequential dams has impacted the sediment transfer from terrestrial to coastal zone, triggering the coastal erosion. In terms of sediment retention and transport, China stands out the most impacted country by dams, followed by United States, and continents such as Europe, Africa, and South America. Based on the foregoing, the impact of dams on sediment transport and yield of an important Brazilian watershed with multiple dams will be the focus of this chapter. Thus, a three years field sampling (2009-2011) was carried out to measure the sediment yield of Capibaribe Watershed, and also its contribution to coastal erosion. The ratio between QB and SSQ ranged from 0.12% to 27.3% with 76% of all values lower than 5%. Usually, the bedload transport rate of a river is about 5–25% of the suspended sediment transport. This ranging sheds light on the lack of bedload reaching the coastal zone and it is likely one of the reasons to yield coastal erosion. The low rates can be attributed to the presence of dams which have been admitted to have a strong effect on sediment transport. The sediment yield was equal to 3.69, 4.36, and 6.7 t km-2 ano-1 in 2009, 2010, and 2011, respectively. In comparison with bedload yield, the suspended sediment yield was higher than 95% for all studied years. Therefore, the limited bedload supply – mainly responsible for construction of coastal landform – is likely contributing to the coastal erosion along part of the northeast region, Brazil. The multiple dams along the Capibaribe River watershed produce a deficit in sediment flux to

coastal zone of Pernambuco State, Brazil, which relies on the low ratios between bedload and suspended sediment. As a result, it generates energy to coastal erosion of the Brazilian northeast.

Keywords: Capibaribe River, sediment yield, coastal processes

1. Introduction

Sediment transport relates to suspended sediment and bedload. The suspended sediment plays the most important role on the land–ocean sediment flux [1]. On the other hand, the bedload should be considered in order to assess the impacts of dams on sediment transport and sediment yield. Recent effects of dam construction have been reported by [1] and [2]. Based on data shown by [2], the sediment load was reduced by more than 75% for major rivers, such as Nilo, Orange, Volta, Indus, Ebro, Kizil Irmark, Colorado, and Rio Grande. The same author observed that more than 40% of sediment flux is trapped within large dams. In addition, the multiple trapping through sequential dams has impacted the sediment transfer from terrestrial to coastal zones [3].

According to [4], there is a correlation between dam construction and sediment supply (mainly sands) to coastal zone, triggering coastal erosion. In terms of sediment retention and transport, China stands out as the most impacted country by dams, followed by United States, and continents such as Europe, Africa, and South America. Based on the foregoing, a three-year field sampling (2009–2011) was carried out to measure the sediment yield of an important Brazilian watershed with multiple dams, and thus its contribution to coastal erosion.

Deforestation, uncontrolled grazing, and other destructive practices accelerate erosion with a concomitant increase in delivery of terrigenous sediments [5]. The sediment yield results from a complex interaction of several hydrogeological processes taking into account topography, soil characteristics, climate, land cover and use, catchment area, and dam-induced impacts [6]. In this sense, [7] says that after intense anthropogenic perturbations in the Changjiang (Yangtze) River basin, the riverine loads and compositions of materials into the Changjiang Estuary have greatly changed, resulting in dramatic deterioration in the Changjiang Estuary and adjacent sea environments and, even though water discharge has remained almost constant, the suspended sediment discharge was shown to be sharply decreased due to the construction of dams. Therefore, this chapter aims to assess the impact of dams on sediment transport and sediment yield of a Brazilian watershed.

2. Importance of sediment transport in watersheds

The sustainability of watersheds is strictly associated with sediment transport along their watercourses in which excessive sediment fluxes generated by extreme flows can destabilize river channels. As a result, sediment transport provokes damages to property and also public structure, narrows down the quality of water as well as increases flooding problems [8]. Comprehension regarding sediment transport in watersheds is useful for providing an

http://dx.doi.org/10.5772/61478

adequate management of streams and reservoirs. Data on amount of sediment which has been transported by rivers is essential in the planning of hydraulic structures, such as dams, irrigation channels, while the features and amount of sediment transported from the drainage basins provides information to predict stream changes [9].

Several cities originated on the banks of rivers, mainly because water resources contribute to the development of the area under its influence. Recife is one of these cities which had the formation and expansion influenced by the Capibaribe River, the major water resource of the city [10]. Moreover, this river has a historical and economic importance for Pernambuco State (Brazil), where has been developing activities associated with sugarcane industry.

There are several problems related with sediment transport in watersheds. For instance, it increases the cost of water treatment; modifies the size of channel; acts as a carrier of bacteria and viruses; increases the transport of pollutants, chiefly the suspended sediment; narrows down the flow depth, damaging sea transport and increasing the possibility of floods. On the other hand, there are also benefits associated with sediment transport; for example, it decreases the erosion action of water in river runoff; improves the quality of water due to reduction of some pollutants; allows the chemistry reactions on sediment surface; carries organic matter, improving the aquatic life for some microorganisms [11].

3. Suspended sediment and bedload transport

Sediment transport in watersheds is classified into two groups: suspended and bedload transport. Suspended sediment is a term applied to particles which are maintained suspended by the vertical component of velocity in turbulent flux while it is transported by the horizontal component of velocity in the same flux. Furthermore, the suspended sediment transport is chiefly governed by the flow velocity, whilst the coarsest sediments might move only occasionally and remain at rest much of the time [9].

It is essential to carry out an isokinetic and point-integrating suspended sediment sampling. The lack of accuracy and frequency in suspended sediment concentration measurements is usually associated with mistakes in suspended sediment flux estimates, chiefly because a large share of annual suspended sediment is transported in a short period of time, generally corresponding to a few flood events during the hydrological cycle [12]. Thus, high-intensity sampling associated with an adequate sampling is fundamental for evaluating the suspended sediment transport in watersheds. These details are essential because the suspended sediment concentration allows to calculate the suspended solid discharge, which in the most cases represents 95% of the total solid discharge, ranging in function of watercourse, flow velocity, flow depth, sediment grain-size, runoff type, cross section position, and so on [13, 14].

The bedload moves near the streambed, contrary to suspended sediment which predominantly moves in suspension. It is normal to observe these particles moving, rolling, and sliding in contact with the streambed, while a third sort of motion is known as saltation. Nevertheless, occurrences of high-intensity flows maintain momentarily the bedload in suspension [8],

usually ranging from 5 to 25% of suspended sediment transport [15]. In addition, the movement of coarser sediments is controlled by selective transport capacity, which indicates the concentration of different sizes of sediments in the cross section.

Frequently, to assess the life expectancy of Brazilian reservoirs, bedload flux has been estimated by using formulas (e.g., the Einstein equations) or by assuming that bedload represents a fixed percentage of the suspended load. In Brazil, as with most countries of South America, little information is available about suspended sediment flux, especially for smaller rivers. Information about bedload flux is extremely rare and, when it does exist, is limited to a few case studies [16]. In this sense, they observed in a step-pool stream representative of the conditions on the basalt scarps of southern Brazil that the bedload flux–streamflow relationship was adequately described by a potential mathematical function. When considering the bedload flux–streamflow relationship, the flux ranged from a minimum of 0.24 g m^{-1} s^{-1} for a streamflow of 0.53 m^3 s^{-1} to a maximum of 44 g m^{-1} s^{-1} for a streamflow of 1.3 m^3 s^{-1}. The percentage of bedload/suspended load varied between <1% and 60%, and this variation was strongly associated with peak flow.

[17], for a river from semiarid zone of Brazil, reported other such cases. They reported that suspended sediment and bedload discharges in sand-bed rivers shape semiarid landscapes and impact sediment delivery from these landscapes, but are still incompletely understood. Moreover, they also observed that the Exu River ratio of bedload/suspended sediment ranged from 4% to 12.72% and the highest values were noted in the period of largest flow rates during the rainy season.

4. The sediment flux from continent to the ocean

Land–ocean transfer of sediment by rivers is a key pathway for material transfer on earth [1], and according to [18], crucial to this understanding is knowledge of the ambient flux of sediment transported by rivers, as rivers contribute 95% of sediment entering the ocean.

According to [19], analysis of anthropogenic impoundment is important to both the earth sciences and their applications. These include emerging studies of global water resources which require an assessment of storage volumes available for flow stabilization, and also a global-scale understanding of the role of reservoirs also provides a key toward articulating the role of humans in riverine nutrients. Still reported by [19], estimation of the true global flux is also made difficult by insufficient treatment of the countervailing influences of increased sediment mobilization from anthropogenically induced soil erosion and of decreased delivery caused by flow diversion and sediment trapping in reservoirs.

Early attempts to generate estimates of the total flux of suspended sediment from the land to the oceans faced major problems in terms of lack of data for many major rivers and for extensive areas of the globe. Faced with this paucity of data, it was necessary to extrapolate existing information to ungauged areas. In the case of the work of Fournier in 1960, the overrepresentation of rivers with limited database resulted in a suspended sediment yield of 51.1 x 10^9 t, which was undoubtedly an overestimate [20].

http://dx.doi.org/10.5772/61478

Sediment flux to the coastal zone is conditioned by geomorphic and tectonic influences within the world's drainage basins, but also by geography of the basin (location and climate), geology, and human activities. These often counterbalancing factors have complicated our understanding of what controls sediment discharge to the global ocean [21]. Despite these complications, the importance of understanding fluvial delivery of sediment is beyond question. Understanding the redistribution of continental substrate through weathering and erosion is one of the fundamental goals of geological sciences [22-24].

[25] wrote that erosion and sediment dynamics play a key role in the functioning of the earth system and have important implications for human exploitation of the system and the sustainable use of its natural resources. They must therefore be seen as having a highly significant socioeconomic dimension. Soil erosion is integrally linked to land degradation, and excessive soil loss resulting from poor land management has important implications for crop productivity and food security and thus for the sustainable use of global soil resource. Against this background, changes in erosion rates and sediment transport by the world's rivers can have significant repercussions at a range of levels.

From a global perspective, changes in erosion rates have important implications for the global soil resource and its sustainable use for food production. Changes in land–ocean sediment transfer will result in changes in global biogeochemical cycles, particularly in the carbon cycle, since sediment plays an important role in the flux of many key elements and nutrients, including carbon. At the regional and local levels, changes in erosion rates can have important implications for the sustainability of agricultural production and food security. Equally, changes in the sediment load of a river can give rise to numerous problems. For example, increased sediment loads can result in accelerated rates of sedimentation in reservoirs, river channels, and water conveyance systems, causing problems for water resource development, and adverse impacts on aquatic habitats and ecosystems. Conversely, reduced sediment loads can result in the scouring of river channels and the erosion of delta shorelines as well as causing reduced nutrient inputs into aquatic and riparian ecosystems, particularly lakes, deltas, and coastal seas [26]. Because of their close links to land cover, land use, and the hydrology of a river basin, erosion and sediment transport processes are sensitive to changes in climate and land cover and to a wide range of human activities. These include forest cutting and land-clearance, the expansion of agriculture, land use practices, mineral extraction, urbanization and infrastructural development, sand mining, dam and reservoir construction, and programs for soil conservation and sediment control [27].

5. Impact of dams on trapping sediments

At the heart of the current debate on dams is the way choices are made, and the different opinions and perspectives that are expressed – or denied expression – in the process. The World Commission on Dams considers that the end of any dam project must be the sustainable improvement of human welfare. This means a significant advance of human development on a basis that is economically viable, socially equitable, and environmentally sustainable. If a

large dam is the best way to achieve this goal, it deserves our support. Where other options offer better solutions, we should favor them over large dams. Thus, the debate around dams challenges our view of how we develop and manage our water resources. Large dams have fragmented and transformed the world's rivers. The World Resources Institute (WRI) found that at least one large dam modifies 46% of the world's 106 primary watersheds. The extent to which river flows have been changed varies around the world. The United States and the European Union regulate the flow of 60–65% of the rivers in their territories, though the amount varies from basin to basin. Spain has 53 km^3 of storage behind large dams and regulates 40% of its river flow, varying from 71% in the Ebro River basin, to 11% in the basins on the Galicia coast. In Asia, just under half of the rivers that are regulated have more than one large dam [28].

[2] reported that globally, greater than 50% of basin-scale sediment flux in regulated basins is potentially trapped in artificial impoundments. If we consider both regulated and unregulated basins, the interception of global sediment flux by all registered reservoirs (≅45000) is conservatively placed at 4–5 Gt $year^{-1}$ or 25–30% of the total. There is an additional but unknown impact due to still smaller unregistered impoundments (≅800000). The [2] results demonstrate that river impoundment should now be considered explicitly in global elemental flux studies, such as for water, sediment, carbon, and nutrients. From a global change perspective, the long-term impact of such hydraulic engineering works on the world's coastal zone appears to be significant but has yet to be fully elucidated.

[1] reported the nonstationary nature of sediment flux to ocean. The sediment loads of many rivers are known to be changing in response to, for example, land clearance and land use change, which can cause increased sediment loads, and the construction of dams, which can trap sediment that would previously have been discharged to the oceans. They should, therefore, not be viewed as a static measure of the functioning of the system, but rather as providing a snapshot of the functioning of an ever-changing system. In the case of Nile River, for example, a near zero sediment load was observed owing to the situation after the construction of the Aswan High Dam. Other estimates of reduction in sediment discharge of some rivers impacted by dams are showed in Table 1.

In Brazil, also there is reduction in sediment load of Sao Francisco River, that drains ca. 8% of the territory of Brazil. The available data suggest that the construction of the Sobradinho Dam in 1978, which impounded a vast reservoir extending over 4220 km^2, and several other hydropower dams with a total generating capacity in excess of 10000 MW, reduced the annual sediment output from this large (645000 km^2) basin by about 80%, from ca. 11 Mt $year^{-1}$ to ca. 2 Mt $year^{-1}$ [1].

6. Sediment delivery in the shoreline and coastal erosion

Among the most important and dynamic natural environments worldwide, the approximately 440000 km long coastal area is one of a small group of systems where several human, animal,

River	Country	Reduction in sediment load (%)
Nile	Egypt	100
Orange	South Africa	81
Volta	Ghana	92
Indus	Pakistan	76
Don	Russia	64
Krishna	India	75
Ebro	Spain	92
Kizil Irmak	Turkey	98
Colorado	USA	100
Rio Grande	USA	96

Showed by [1] and based on data from [2].

Table 1. Estimates of sediment trapped by dams in some rivers of the world

vegetal, and geomorphologic activities interact. Its invaluable landscape and ecological richness make it a very desirable zone to develop social, industrial, and recreational infrastructure. On the other hand, coastal zones are attacked by different natural phenomena, mostly from hydro-meteorological origin, such as waves, wind, tides, and rainfall which can reach extraordinary magnitudes during the occurrence of events like hurricanes and tsunamis. The direct consequences of these extreme events are flooding (derived from mean sea level rise) and beach erosion (as a result of the increase in current velocities and wave energy); a combination of both of these causes land loss, damage to infrastructure and natural habitats, ecological imbalance, health problems in the population, and instability in economic activities. The phenomena mentioned above are commonly grouped under the generic term of "dangers," and the combination of these with the vulnerability of the natural and/or artificial elements found at the coast gives the risk of a specific coastal area. In the last decade, the interest shown in the assessment of risks comes from the evidence of an increase in the magnitude of natural dangers, added to the expansion of human activities in coastal zones which results in a higher level of risk [29].

The coastal zones of Latin America have many landforms and environments, including sedimentary cliffs, deeply incised estuaries, headlands, barrier coasts and low lying, muddy coastal plains. These forms will respond differently to the expected changes in climate and associated sea level rise, which may produce coastal erosion in the future. Considering the coasts of Latin America overall, erosion is not yet a serious threat, although it is widespread and it is severe in some parts [30].

[31] says that the coastal zones of Latin America feature a wide range of landforms. Expected climate change will bring about sea level rise and the different landforms will respond in different ways. Therefore, according to [30], it is necessary to explore the potential vulnerability of the distinct coastal types in response to climate change. Since risk to people is a key factor in vulnerability, the risk is greatest in the urbanized coasts, where the greatest impacts are expected to be caused by floods. However, the absence of long-term observations of oceano-

graphic data and detailed topo-bathymetric data presents a major difficulty for the evaluation of different risk scenarios at local level and consequently for the application of strategies aimed at minimizing these impacts on the population. In addition [30], tectonic subsidence is often a cause of regional vulnerability, as well as that which occurs in areas of permanent loss of sediments, owing to deforestation or to fragmentation of coastal ecosystems (e.g., sand dune vegetation, mangroves), to land use changes (mostly for agriculture and cattle ranching, and focal urban sprawl) and to sediment deficits caused by the presence of infrastructure (dams in the watersheds, jetties, and groynes).

Martínez et al. [32] presents an analysis of the erosion processes in Matanchén Bay located on the Pacific Coast of Nayarit State, Mexico. They said that at the beginning of the 1940s an unexplained growth in the beach at the northern tip of the bay was observed, while 40 years later, and up to date, erosion processes began adversely affecting small businesses in the area. The primary causes of the erosion are the anthropogenic modifications in the bay and its surroundings, which include the construction of a hydroelectric dam system, new transport infrastructure, tourist facilities, a harbor, and several dredging works in the existing port. In this paper, the evolution of the coastline at Matanchén Bay and its surroundings is analyzed for the first time and the actual coastline is compared to that predicted under the assumption that no countermeasures against the erosion are adopted.

[33], describing the northeast of Brazil, observed that the coastline is generally receding. This is noticeable along several stretches of the coast of Pernambuco, but is felt mostly in the area of the Recife metropolitan area. Here, as in many other places, urban encroachment and the construction of infrastructure along the coast, coupled with sea level rise processes, has led to a "coastal squeeze," which results in the loss of coastal habitats.

Still in Pernambuco State, Brazil, [34] showed the main processes that are involved in the erosion of Maria Farinha Beach, a beach of great ecological and socioeconomic importance and they observed that the erosion problem at Maria Farinha Beach is complex and difficult to solve, since the problem has multiple causes, including the construction of coastal defenses. As it affects several municipalities, the problem is exacerbated. Wave propagation simulations have shown that the combination of high spring tides and high waves significantly impact the coast of Maria Farinha. The comparison between the numerical model results and the profile data indicates that under these conditions the beach profile where erosion is observed is more exposed to wave energy than the beach profiles showing accretion. Three possible solutions are suggested – the construction of a submerged breakwater, the deployment of a sand bypassing system and the relocation of buildings on the beach front. Due to the diverse beach usage, the implementation of a sand bypassing system is recommended. The option of doing nothing would cause continued erosion in the critical area taking into account the presence of urbanized areas, often irregular, all along the beach. The case of Maria Farinha Beach indicates the necessity of better understanding coastal processes and thorough planning prior to coastal development. It is highlighted that, if preventive efforts had been made in the past, prior to development, such as establishing a buffer zone or a setback line, much of the erosion on Maria Farinha Beach would have been avoided.

According to [35], beaches are of great significance as recreational areas, but from a geological perspective, the beach has a value as a natural defense system for the coast, which is exposed to the constant risk of erosion due to the action of waves and tides. Problems of beach erosion

http://dx.doi.org/10.5772/61478

have become prevalent in northeast Brazil as a result of unplanned coastal development. Urbanization in conjunction with historic soil occupation and use, including the landfill of mangrove areas, the practice of soil sealing (which prevents drainage), combined with the local meteo-oceanographic characteristics, have caused a growing erosion problem and have contributed to a reduction in the resilience of the beaches. These authors using simulation methods to coastal erosion in Candeias Beach, in the southern area of the breakwater, observed that sediment transport to the south is even greater than if there was no protection to the coastline because there is no sediment source in the area that could replace the sediment that is being moved to the south. As a result, this could dramatically reduce the sediment availability in the area, leading to more beach erosion in the future. On the other hand, there is an improvement related to modifying the former breakwater. By opening up the gaps, wave-current transport was restored, thereby eliminating the sediment trap created by the installation of the original breakwater.

[36] presented the recent changes in sediment flux of the five largest rivers of East and Southeast Asia to Pacific Ocean and observed that the Yellow, Yangtze, Pearl, Red, and Mekong Rivers are important contributors of sediment to the western Pacific Ocean, and concluded that these rivers are of vital importance not only for providing water resources to more than 700 million people in six countries, but also for delivering large amounts of terrigenous sediment (~2000×10^9 kg/yr) to the coastal and shelf seas of the western Pacific Ocean, accounting for ~10% of the global sediment flux to the ocean. Freshwater, sediment, and nutrients discharged by these rivers play important roles in local and regional geomorphology and the biogeochemical cycle of the regional ocean. Although the rivers vary in their local geography, geology, and climate, human interventions of the past several decades have greatly modified the river systems. The present sediment flux from these five rivers has declined to ~600×10^9 kg/yr, equivalent to levels before widespread human interventions. Although the total freshwater discharge to the ocean remains almost unchanged, the stress on water resources for individual rivers continues to grow. Still, [36] reveals large anthropogenic changes in sediment flux from all five rivers to the western Pacific Ocean and summarizes their recent trends comparing the time-series data on water discharge and sediment flux to signals of climate oscillation and historical human activities. From this comparison it is concluded that the short-term variation (interannual scale) of sediment flux is dominated by climate oscillations such as the El Niño/La Niña cycle that affect the regional distribution of rainfall and thus the sediment yields from the river basins, and that the decrease in sediment flux on the decadal scale is controlled by human interventions including entrapment in reservoirs and human-influenced changes in soil erosion. The Yellow and Yangtze Rivers dominate the decline in sediment flux from both natural and anthropogenic impacts, as they are the largest contributors of sediment to the regional ocean. For the Mekong River, the sediment from the upper Mekong Basin is entrapped by reservoirs, and the increased sediment load in the lower Mekong arises from human interventions such as mismanaged land reclamation. As rapid development continues in East and Southeast Asia, human interventions in the large river systems will become still more intensive. Consequently, the continuing decline in river sediment flux to the ocean will put the mega-deltas at risk of destruction, adding to other severe challenges from regional environmental change.

7. Material and methods

The Capibaribe River watershed, 7557 km^2 in area, crosses from the end of semiarid area until the east coast. Climate in the portion located in the semiarid region is As' type, according to the Köppen classification, known as dry, with dry summer and the largest rainfall taking place between April and July, ranging from 550 mm to 700 mm annually. Toward the portion located in the east coast, the climate is classified as Ams' type with the largest rainfall taking place between May and July, ranging from 1700 mm to 2500 mm annually [37].

The amount of sediment supplied to the studied cross sections is influenced by nonconservationist agricultural activities, which trigger the erosion process, mainly represented by the occurrence of interrill and rill erosion. All these sources of sediment are affected by the dam's distribution along the Capibaribe River, which are predominantly located upstream of the studied cross section (Figure 1).

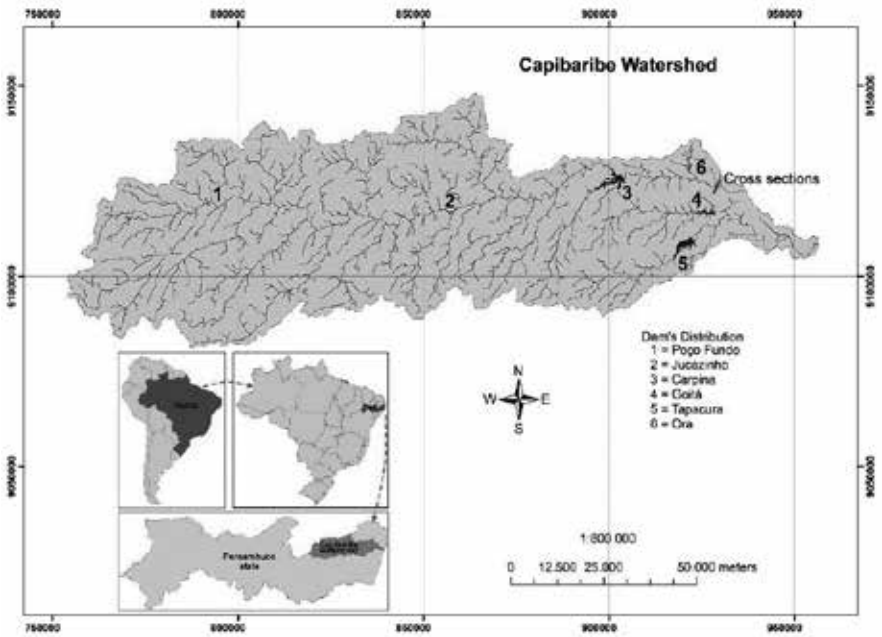

Figure 1. Location of Capibaribe watershed in the context of South America, dam's distribution and cross section in the studied river reach. Note: (Poço Fundo – Area = 854 km^2/volume = 27 x 10^6 m^3; Jucazinho – Area = 3918 km^2/volume = 327 x 10^6 m^3; Carpina – Area = 1828 km^2/volume = 270 x 10^6 m^3; Goitá – Area = 450 km^2/volume = 52.9 x 10^6 m^3; Tapacurá – Area = 360 km^2/volume = 94.2 x 10^6 m^3 and Ora (data not available).

8. Velocity measurement

During the campaigns in the Capibaribe River, the flow velocity was determined by rotating current meter (Figure 2), which is based on the proportionality between the angular velocity of the rotation device and the flow velocity.

http://dx.doi.org/10.5772/61478

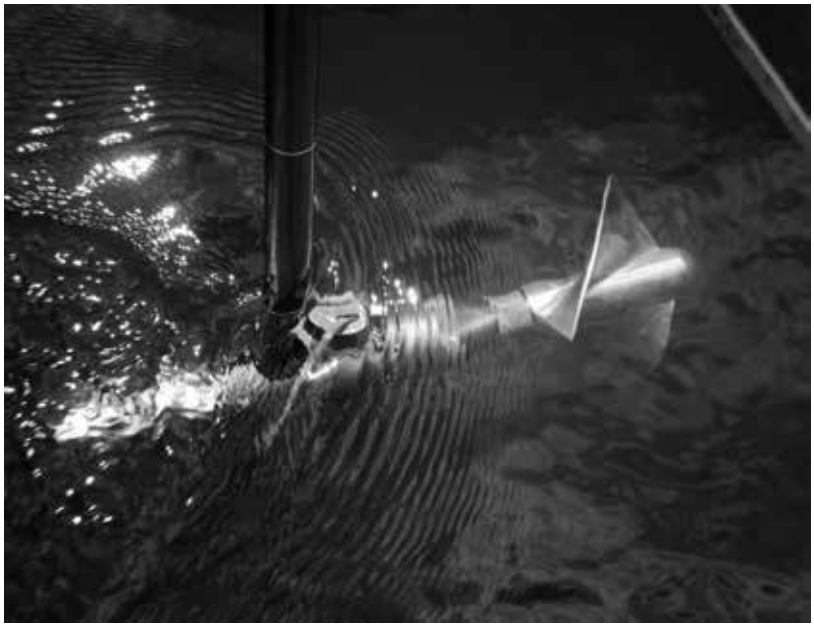

Figure 2. Rotating-element current meter used in the Capibaribe River.

The positions to which the rotating-element current meter was adjusted in each vertical in function of the flow depth are described in Table 2.

Positions	V (m s^{-1})	h (m)
0.6h	$V = V_{0.6h}$	< 0.6
0.2 and 0.8h	$V = (V_{0.2h} + V_{0.8h})/2$	0.6 - 1.2
0.2; 0.6 and 0.8h	$V = (V_{0.2h} + 2V_{0.6h} + V_{0.8h})/4$	1.2 - 2.0
0.2; 0.4; 0.6 and 0.8h	$V = (V_{0.2h} + 2V_{0.4h} + 2V_{0.6h} + V_{0.8h})/6$	2.0 - 4.0
s; 0.2h; 0.4h; 0.6h; 0.8h and b	$V = (V_s + 2(V_{0.2h} + V_{0.4h} + V_{0.6h} + V_{0.8h}) + V_b)/10$	> 4.0

s: surface; V_s: surface velocity and b: bottom of the river.

Table 2. Measurement of average flow velocity according to flow depth

In other words, the flow velocity was acquired by counting the number of revolutions of the propeller in a measured time interval, which was thirty seconds for all campaigns. The depth-average velocity was obtained in the cross section through a measurement velocity profile. In some campaigns, mainly during low water discharges, the Hidromec mini model was used due to low flow depth.

9. Water discharge measurement

At first, the width of the cross sections was measured by affixing a measuring tape parallel to the flow surface and transverse to the direction of flow from the left bank of the stream to the right bank and the flow depth of each vertical was obtained by specific measuring rule. The cross sections were divided into a series of vertical lines with the same width, varying according to the total width of the water flow at the moment of measuring, according to the equal-width-increment (EWI), method proposed by [9].

The water discharge was determined by computing the product of the mean flow velocity (m s^{-1}) and the area of influence (m^2) for each segment in the section and then summing these products over all segments (Equation 1).

$$Q = \sum Q_i = \sum A_i . V_i \tag{1}$$

where Q is the water discharge (m^3 s^{-1}), Q_i is the water discharge in each vertical segment (m^3 s^{-1}), A_i is the influence area of the vertical segment (m^2), and V_i is the average flow velocity in the influence area of each vertical segment (m s^{-1}).

10. Sampling of suspended sediment and bedload

Direct sampling was performed from 2009 to 2011 in the downstream cross section, which was divided into a series of 8–10 verticals with the same width. For suspended sediment sampling, the sampler US DH – 48 model (Figure 3) was used according to equal-width-increment (EWI), proposed by [38]. Furthermore, the US DH-48 sampler features a streamlined aluminum casting 13 inches long that partly encloses the sample container. The container, usually a glass milk bottle, is sealed against a gasket recessed in the head cavity of the sampler by a hand-operated, spring-tensioned, pull-rod assembly at the tail of the sampler. This instrument was calibrated with an intake nozzle, l/4 inch in diameter [11].

Moreover, during the sampling, the descending and ascending transit rate must be the same along the traverse of each vertical, resulting in a volume of water proportional to the flow in each vertical [9]. The transit rate depends on several features, such as sample volume collected, size of the nozzle in sampling equipment, depth of the sample taken, and flow velocity [39]. Thereby, according to [40], the transit rate was expressed as:

$$V_t = V_i . K \tag{2}$$

where V_t is the transit rate (m s^{-1}) and K is the constant of variable proportionality according to each different nozzle used, which was 0.4 for the ¼" nozzle of the sampler. Nevertheless, the information used during sampling was not the transit rate, but the time for the sampler to

http://dx.doi.org/10.5772/61478

Figure 3. Suspended sediment sampling (sampler - US DH-48) in the Capibaribe River.

descend to the streambed and return to the water surface, calculated by the expression proposed by [14, 40]:

$$t = \frac{2h}{V_t} \tag{3}$$

where t represents the minimum time of the suspended sediment sampling (s). A small distance was subtracted from the value of h to account for the fact that the equipment would not contact the streambed (10 or 15 cm).

All collected samples in each segment (vertical) of the cross sections in the Capibaribe River were individually preserved to determine the Suspended Sediment Concentration (SSC) in Soil Conservation Engineering Laboratory at UFRPE, which was determined through the ratio between the suspended sediment mass and liquid volume of the sample, according to evaporation method [38]. The concentration values in each vertical segment that made up the section were determined, and the suspended sediment discharge values (SSQ) were determined by the addition of the product of the suspended sediment concentration (SSC_i) and the respective water discharge (Q_i) from each vertical segment [42]:

$$SSQ = \sum \left(SSC_i Q_i \right) 0.0864 \tag{4}$$

where SSQ is the suspended solid discharge (t day^{-1}) and 0.0864 is a constant for unit adjustment. The bedload was obtained by means of the US BLH 84 sampler. For checking the accuracy of suspended sediment sampling, the Box Coefficient (BC) – ratio between average of suspended sediment concentration and suspended sediment concentration at each vertical – was calculated, following that proposed by [43]:

$$QB = \sum \frac{m}{wt_2} L_x 0.0864 \tag{5}$$

where QB is bedload discharge (t day^{-1}), m is the mass of sediment from bedload transport in each vertical (g), w is the width of nozzle which is considered 0.075 m, t_2 is the sampling time of bedload transport (30 s), and L_x is the distance among verticals (m). In addition, the sediment yield was calculated (t km^{-2} ano^{-1} or t ha^{-1} ano^{-1}).

11. Results and discussion

The rating curve relating water discharge (Q) and flow depth (h) provided a determination coefficient equal to 0.81, considering the direct measurements campaigns carried out with Q ranging from 0.25 to 11.60 m^3 s^{-1} (Figure 4). The reasonable adjustment was acquired due to the higher amplitude of Q evaluated. Thereby, the number of measurements and also the variation between minimum and maximum values improve the effectiveness of the rating curve [11].

The relation between suspended sediment concentration (SSC) and Q provided a low determination coefficient equal to 0.21 (data not shown), demonstrating the large complexity and variability associated with the SSC measurements. Furthermore, this behavior represents the effects of dams. In the same way, [44] working in the Capibaribe Watershed obtained low adjustment between SSC and Q discharge (R^2 equal to 0.14). Moreover, the high variability between SSC and Q was emphasized by [45], which obtained a high variability of regression coefficients. These results are associated with the dynamic relation between Q and SSC, becoming essential to keep manual sampling to decrease the mistakes linked with SSC estimation and improve the effectiveness of the rating curves [42].

On the other hand, the rating curve relating SSQ (dependent variable) and Q (independent variable) showed a good adjustment with determination coefficient equal to 0.86 (Figure 5). Nevertheless, this behavior cannot be understood as the same way of the rating curve which relates the Q and h due to the high complexity linked with suspended sediment transport. Indeed, it is possible to observe the momentary behavior of the SSQ instead obtaining this variable only with the Q even if a high number of measurements had been carried out. According to Horowitz [46], this approach is acceptable for a suspended sediment concentra-

http://dx.doi.org/10.5772/61478

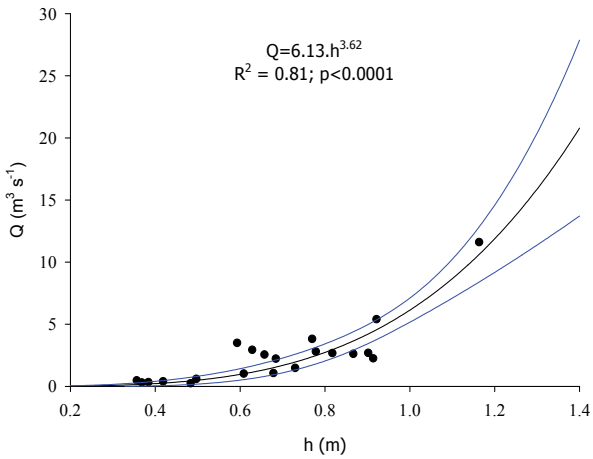

Figure 4. Rating curve of direct measurement campaigns performed under conditions in the Capibaribe River.

tion rating curve. Nonetheless, it is inadequate for a suspended solid discharge rating curve, chiefly because the Q is used for obtaining the SSQ. Accordingly, it is common to observe the increase in determination coefficient, but without increasing the importance of the rating curve relating Q and SSQ.

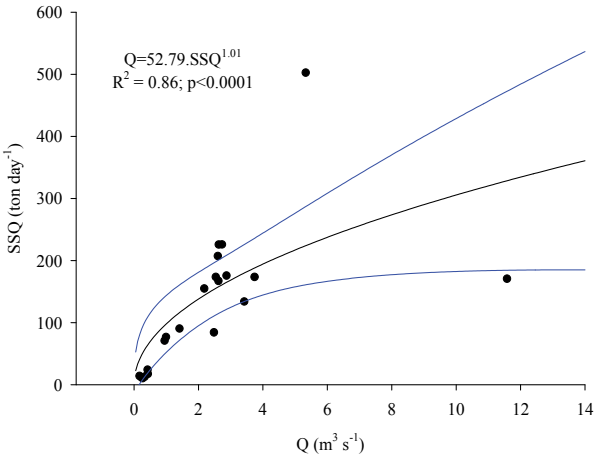

Figure 5. Suspended sediment rating curve of Capibaribe watershed.

A multimodal dominant discharge was observed, with peaks of suspended sediment concentration lagging behind, taking place at the same time as well as after extreme flow events (Figure 6). The first two trends of sediment concentration in relation to hydrograph are typical of semiarid environment and may be related to low flow or short distance of transport from erosion site. Despite being most common in the semiarid environment, the lag far behind the peak of suspended sediment concentration related to the flow might be linked to the flow

events provoked by high intensity rainfall, which resulted in more losses of soil particles in the downstream cross section [47].

In some instances, the low suspended sediment concentration may be linked to dilution effects provided by the high water discharge that was observed in the first peak (Figure 6). This behavior may be related to trapping sediments along Capibaribe River, due to dam effects. The mean suspended sediment concentration value, equal to 662 mg L^{-1}, is higher than values reported for other Brazilian rivers [48, 49] as well as world rivers under dam effect, such as Pérola and Yellow [7].

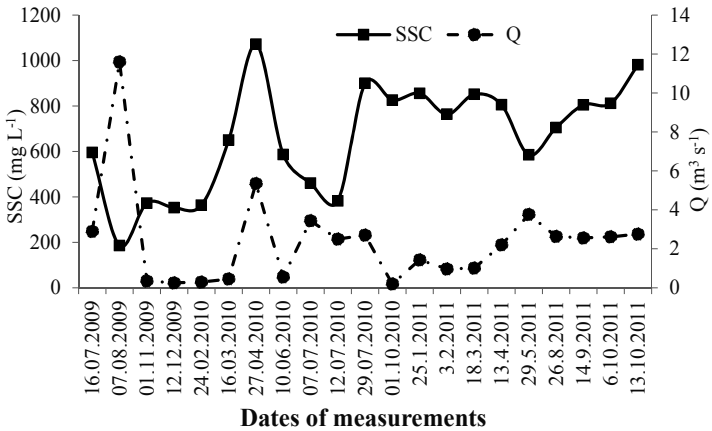

Figure 6. Hydrographs and sedigraphs at the studied site of the Capibaribe River.

Considerable variation of water discharge and sediment concentration values, ranging from 0.19 to 11.6 m^3 s^{-1} and 185.23 to 1071.55 mg L^{-1}, respectively, were observed; nevertheless, the values of individual suspended sediment samples showed adequate Box Coefficient (BC), ranging from 0.67 to 1.5 – acceptable limits suggested by [43]. Therefore, the sediment concentration samples from the Capibaribe River were considered sufficiently accurate. The SSQ ranged from 9.48 t day^{-1} to 501.56 t day^{-1} (Table 3).

The ratio between QB and SSQ ranged from 0.12% to 27.3% with 76% of all values lower than 5%. Usually, the bedload transport rate of a river is about 5–25% of the suspended sediment transport [15]. This ranging sheds light on the lack of bedload reaching the coastal zone and it is likely one of the reasons to yield coastal erosion. The low rates can be attributed to the presence of dams which have been admitted to have a strong effect on sediment transport, which evidenced the reduction on sediment supply at Reno River, but without quantifying this process due to the lack of assessment before dam construction. The presence of dams has been known to have a strong effect on sediment transport [50].

The sediment yield was equal to 3.69, 4.36, and 6.7 t km^{-2} ano^{-1} in 2009, 2010, and 2011, respectively. In comparison with bedload yield, the suspended sediment yield was higher than 95% for all studied years. According to [51], these values are low, but this behavior is in

agreement with that observed by [41]. Both national [52] and international studies [53] have shown the reduction of sediment yield due to dam construction. Therefore, the limited bedload supply – mainly responsible for construction of coastal landfor – is likeli contributing to the coastal erosion along part of the northeast region, Brazil.

Dates of measurements	SSC	BC	SSQ	QB	QB/SSQ
	(mg L^{-1})	(no dimensional)	(t day^{-1})	(t day^{-1})	(x100)
Jul-09	595	0.99–1.50	175	0.22	0.12
Aug-09	185	0.79–1.50	170	3.41	2.01
Nov-09	372	0.85–1.32	12	0.68	5.71
Dec-09	353	0.72–1.30	10	0.2	1.9
Feb-10	363	0.68–1.20	9	0.9	9.94
Mar-10	649	0.84–1.20	16	0.18	1.1
Apr-10	1071	0.90–1.10	501	7.76	1.55
Jun-10	586	0.87–1.30	23	0.22	0.93
Jul-10	460	0.97–1.43	133	9.77	7.35
Jul-10	382	0.92–1.50	83	9.46	11.37
Jul-10	899	0.67–1.37	225	3.44	1.53
Oct-10	826	0.85–1.29	13	2.53	27.3
Jan-11	855	0.86–13	89	0.19	0.21
Feb-11	764	0.86–1.40	70	0.18	0.26
Mar-11	851	0.93–1.25	76	0.14	0.18
Apr-11	805	0.83–1.18	154	0.57	0.37
May-11	585	0.74–1.36	172	2.14	1.24
Aug-11	705	0.67–1.13	166	5.82	3.51
Sep-11	805	0.85–1.08	172	2.97	1.72
Oct-11	811	1.05–1.26	206	5.32	2.58
Oct-11	981	0.86–1.12	225	3.85	1.71

Table 3. Suspended sediment concentration (SSC), suspended sediment discharge (SSQ), Box Coefficient (BC), and ratio between QB and SSQ of samples from the Capibaribe River in 2009, 2010, and 2011

12. Conclusions

The multiple dams along the Capibaribe River watershed produce a deficit in sediment flux to coastal zone of Pernambuco State, Brazil, which relies on the low ratios between bedload

and suspended sediment from Capibaribe River. As a result, it generates energy to coastal erosion of the Brazilian northeast.

Acknowledgements

The authors would like to acknowledge the financial support by Fundação de Amparo a Ciência e Tecnologia do Estado de Pernambuco (FACEPE), Edital FACEPE 12/2008 – ESTUDOS E PESQUISAS PARA POLÍTICAS PÚBLICAS ESTADUAIS EROSÃO COSTEIRA – SEGURANÇA PÚBLICA – DENGUE FACEPE/SECTMA/SEPLAG/SES.

Author details

Jose Ramon B. Cantalice[1*], Wagner Luis da Silva Souza[1], Yuri Jacques Agra Bezerra Silva[1], Sergio M.S. Guerra[2], Alex Mauricio Araújo[3], Douglas Monteiro Cavalcante[2] and Cinthia Maria Cordeiro Atanazio Cruz Silva[1]

*Address all correspondence to: cantalice21@hotmail.com

1 Agronomy Engineering Department, Soil Conservation Engineering Laboratory, Rural Federal of Pernambuco University (UFRPE) Brazil, Recife-PE, Brazil

2 Rural Technology Department, Rural Federal of Pernambuco University (UFRPE), Recife-PE, Brazil

3 Fluid Mechanics Laboratory, Federal of Pernambuco University (UFPE), Recife, PE, Brazil

References

[1] Walling, D.E. 2006. Human impact on land-ocean sediment transfer by the world's rivers. *Geomorphology*. 79(3), 192–216.

[2] Vörösmarty, C.J., Meybeckc, M., Feketea, B., Sharmad, K., Greena, P., Syvitski, J.P.M. 2003. Anthropogenic sediment retention: major global impact from registered river impoundments. *Global Planetary Change*. 39, 169–190.

[3] Zhang, Q., Xu, C.Y., Singh, V.P., Yang, T. 2009. Multiscale variability of sediment load and streamflow of the lower Yangtze River basin: Possible causes and implications. *J Hydrol*. 368, 96–104.

[4] Dias, A.J.M. 1993. Estudo de Avaliação da Situação Ambiental e Proposta de Medidas de Salvaguarda para a Faixa Costeira Portuguesa. *Geologia Costeira*. 26 p.

[5] Stender, Y., Jokiel, P.L., Rodgeres, K.S. 2014.Thirty years of coral reef change in relation to coastal construction and increased sedimentation at Pelekane Bay, Hawaii. *Peer J.* 2:e300, DOI 10.7717/peerj.300.

[6] Hovius, N. Controls on sediment supply by large rivers. In: *Relative Role of Eustasy, Climate, and Tectonism in Continental Rocks*. Society of Sedimentary Geology, Special Publication 59, 3-16. 1998.

[7] Dai, H., Du, J., Zhang, X., Su, N., Li, J. 2011. Variation of riverine material loads and environmental consequences on the Changjiang (Yangtze) estuary in recent decades (1955-2008). *Environ Sci Technol*. 45(1):223-7. doi: 10.1021/es103026a.

[8] Frey, P., Church, M. 2011. Bedload: a granular phenomenon. *Earth Surf Process Landforms*. 36, 58–69.

[9] Edwards, T.K., Glysson, G.D. 1999. Field methods for measurement of fluvial sediment. In: *Techniques of Water-Resources Investigations of the U.S. Geological Survey (USGS)*. Reston, Virginia, book 3, chapter C2. 97 p.

[10] Mayrinck, O.M.A. 2003. Paisagem do rio Capibaribe: um recorte de significados e representações (Tese de Doutorado), Instituto de Geociências/Universidade Federal do Rio de Janeiro. 273 p.

[11] Carvalho, N.O. 2008. *Hidrossedimentologia Prática*. Editora Interciência. Rio de Janeiro, RJ. 599 p.

[12] Meybeck, M., Laroche, L., Durr, H.H., Syvitski, J.P.M. 2003. Global variability of daily total suspended solids and their fluxes in Rivers. *Global Planet Change*. 39, 65–93.

[13] Carvalho, N.O. 1994. *Hidrossedimentologia Prática*. Rio de Janeiro: CPRM. 374 p.

[14] Carvalho, N.O., Júnior, N.P., Santos, P.M.C., Lima, J.F.E.W. 2000. *Guia de Práticas Sedimentométricas*. ANEEL, Brasília – DF, 154 p.

[15] Yang, T.C. 1996. *Sediment Transport Theory and Practice*. New York. McGraw-Hill companies. 395 p.

[16] Merten, G.H., Minella, J.P.G. 2014. Bedload flux in southern Brazilian basalt scarp. *Sediment Dynamics from the Summit to the Sea* (Proceedings of a symposium held in New Orleans, Louisiana, USA, 11–14 December 2014) (IAHS Publ. 367, 2014). doi: 10.5194/piahs-367-185-2015.

[17] Cantalice, J.R.B., Filho, M.C., Stosic, B.D., Piscoya, V.C., Guerra, S.M.S., Singh, V.P. 2013. Relationship between bedload and suspended sediment in the sand-bed Exu River, in the semi-arid region of Brazil. *Hydrologic Sci J*. doi: 10.1080/02626667.2013.839875.

[18] Syvitski, J.P.M., Peckham, S.D., Thierry, R., Hilberman, M. 2003. Predicting the terrestrial flux of sediment to the global ocean: a planetary perspective. *Sediment Geol*. 162, 5–24.

[19] Vorosmarty, C.J., Meybeckc, M., Feketea, B., Sharmad, K., Greena, P., Syvitski, J.P.M. 2003. Anthropogenic sediment retention: major global impact from registered river impoundments. *Global Planet Change*. 39, 169–190.

[20] Walling, D.E., Webbe, B.W. 1996. *Erosion and Sediment Yield: Global and Regional Perspectives*. IAHS Publ. n 236, 1–19.

[21] Hay, W.W. 1994. Pleistocene-holocene fluxes are not the Earth's norm. In: *Material Fluxes on the Surface of the Earth* (Ed. by Panel on Global Surficial Geofluxes) Studies in Geophysics, National Academy Press, Washington, DC, pp. 15-27.

[22] Milliman, J.D., Meade, R.H. 1983. World-wide delivery of river sediment to the oceans. *J Geol*, 91, 1-21.

[23] Milliman, J.D. 2001. Delivery and fate of fluvial water and sediment to the sea: a marine geologist's view of European rivers. *Sci Marina*. 65 (Suppl. 2), 121-132.

[24] Syvitiski, J.P.M., Milliman, J.D. 2007. Geology, geography and humans battle for dominance over the delivery of fluvial sediment to the coastal ocean. *J Geol*. 115, 1-19.

[25] Montgomery, D.R. 2007. Soil erosion and agricultural sustainability. *Proc Natl Acad Sci*. Vol. 04, n 13. Washington D.C., PNAS, pp. 268–272.

[26] Walling, D.E. 2009. The impact of global change on erosion and sediment transport by rivers: Current progress and future challenges. The United Nations World Water Assessment Programme. The United Nations World Water Development Report 3, *Water in a Changing World*, UNESCO, Paris, 29 p.

[27] Walling, D.E. 2005. Human impact on land–ocean sediment transfer by the world's rivers. *Geomorphology*. Vol. 79. Amsterdam, Elsevier, pp. 192–216.

[28] World Commission on Dams (WCD). 2000. *Dams and Development: A new Framework for Decision-Making*. Thanet Press, USA, 399 p.

[29] Castillo, M.E., Baldwin, E.M., Casarin, R.F., Vanegas, G.P., Juaréz, M.A. 2012. Characterization of Risks in Coastal Zones: A Review Clean – Soil, Air, Water. 40(9), 894–905.

[30] Silva, R., Martínez, M.L., Hesp, P., Catalan, P., Osorio, A.F., Martell, R., Fossati, M., Miot da Silva, G., Mariño-Tapia, I., Pereira, P., Cienfuegos, R., Klein, A., and Govaere, G. 2014. Present and future challenges of coastal erosion in Latin America. In: Silva, R. and Strusińska-Correia, A. (eds.), Coastal Erosion and Management along Developing Coasts: Selected Cases. *J Coastal Res*, Special Issue, 71, 1–16. Coconut Creek (Florida), ISSN 0749-0208.

[31] Muehe, D. 2010. Brazilian coastal vulnerability to climate change. *Pan-Am J Aquatic Sci–Electron Peer-Rev Sci J*. 5(2), 173-183.

[32] Martínez, R., Silva, R., and Mendoza, E. 2014. Identification of coastal erosion causes in Matanchén Bay, San Blas, Nayarit, Mexico. In: Silva, R., and Strusińska-Correia, A.

(eds.), Coastal Erosion and Management along Developing Coasts: Selected Cases. *J Coast Res*, Special Issue, 71, 93–99. Coconut Creek (Florida), ISSN 0749-0208.

[33] Dominguez, J.M.L. 2009. The coastal zone of Brazil. In: Dillenburg, S., Hesp, P.A. (eds). 2009. *Geology and Geomorphology of Holocene Coastal Barriers in Brazil*. Springer-Verlag Lecture Notes in Earth Sciences. 107, 17-51.

[34] Mallmann, D.L.B., Pereira, P.S. 2014. Coastal erosion at Maria Farinha Beach, Pernambuco, Brazil: Possible causes and alternatives for shoreline protection. In: Silva, R. and Strusińska-Correia, A. (eds.), Coastal Erosion and Management along Developing Coasts: Selected Cases. *J Coast Res*, Special Issue, No. 71, 24–29. Coconut Creek (Florida), ISSN 0749-0208.

[35] Gomes, G., Silva, A.C. 2014. Coastal erosion case at Candeias Beach (NE-Brazil). In: Silva, R. and Strusińska-Correia, A. (eds.), Coastal Erosion and Management along Developing Coasts: Selected Cases. *J Coast Res*, Special Issue, 71, 30-40. Coconut Creek (Florida), ISSN 0749-0208.

[36] Wang, H., Saito, Y., Zhang, Y., Bi, N., Sun, X., Yang, Z. 2011. Recent changes of sediment flux to the western Pacific Ocean from major rivers in East and Southeast Asia. *Earth-Sci Rev*. 108, 80–100.

[37] SUDENE, 1990. Dados pluviométricos mensais do Nordeste. Estação de Pernambuco: Recife, 363 p.

[38] USGS – United States Geological Survey. 2005. Techniques of Water Resources Investigation. Washington, book 9, chaps. A1-A9, available online at http://pubs.water.usgs.gov/twri9A.

[39] Wilde, F.D., Radke, D.B. 1998. Field Measurements. In: *National Field Manual for Collection of Water – Quality Data*. U.S. Geological Survey. Techniques of Water Resources Investigations, Book 9, chap A4, 7–99.

[40] USGS – United States Geological Survey. 1973. Techniques of Water Resources Investigations. Washington. 20 p.

[41] Merten, G.H., Poleto, C. 2006. Qualidade dos Sedimentos. Associação Brasileira de Recursos Hídricos – ABRH. Porto Alegre, RS. 397 p.

[42] Horowitz, A.J. 2003. An evaluation of sediment rating curves for estimating suspended sediment concentrations for subsequent flux calculations. *Hydrol Process*, 17, 3387–3409.

[43] Gray, J.R. 2005. Sediment data collection techniques. U.S. Geological Survey Training Course. CD-ROM.

[44] Souza, W.L.S. 2011. Produção de Sedimento da Bacia Hidrográfica do Rio Capibaribe para Zona Costeira da Região Metopolitana do Recife. Dissertação, Programa de Pós-

Graduação em Ciência do Solo da Universidade Federal Rural de Pernambuco, 137 p.

[45] Saeidi, P., Tabatabaei, J., Saedi, T. 2011. Effective discharge for suspended sediment transportation in Ghohruod watershed. *Afri J Agric Res*. 6(23), 5360-5366.

[46] Horowitz, A.J., Elrick, K.A., Smith, J.J. 2008. Monitoring urban impacts on suspended sediment, trace element, and nutrient fluxes within the City of Atlanta, Georgia, U.S.A.: program design, methodological considerations and initial results. *Hydrol Process*. 22, 1473–1496.

[47] Colby, B.R.. 1963. Fluvial sediments-a summary of source, transportation, deposition and measurement of sediment discharge: *US Geol Survey Bull*. 118l–A, 47 p.

[48] Lima, J.E.F.W., Santos, P.M.C., Carvalho, N.O., Vieira, N.O., Silva, E.M. 2005. Suspended sediment fluxes in the large river basins of Brazil. In: VII Congresso Científico da IAHS. Foz do Iguaçu, RS. 291. pp. 355-364.

[49] Guyot, J.L., Filizola, N.P., Laraque, A. 2005. Régime et bilan du flux sédimentaire de l'Amazone à Óbidos (Pará, Brésil) de 1995 à 2003. In: *Sediment Budgets 1.* Walling, D.E., Chorowitz, A.J. IAHS Publication. 291. pp. 347-354.

[50] Meade, R. H., Moody, J. A. 2008. Changes in the discharge of sediment through the Missouri- Mississippi river system, 1940–2007. In: VIII Encontro Nacional de Engenharia de Sedimentos. Campo Grande, Brazil, 2-8 November 2008, Proceedings, 27 p.

[51] WMO – World Meteorological Organization. 2003. Manual on sediment management and measurement. Operational Hydrology Report, n. 47. Ed. Xiaoquing, Yang. Geneva, Switzerland. 176 p.

[52] Medeiros, P.R.P., Knoppers, B.A., Santos Júnior, R.C. 2007. Aporte fluvial e dispersão de matéria particulada em suspensão na zona costeira do Rio São Francisco (SE/AL). *Geochimica Brasiliensis*. 21(2), 212–231.

[53] Jiao, J., Wang W., Li, J. 2003. Silting land and sediment blocking benefit of check-dams in hilly and gully region on the Loess Plateau. In: Transact Chinese Soc Agric Engin. 19(6), 302–306.

Chapter 3

Simulation of Reservoir Siltation with a Process-based Soil Loss and Deposition Model

Marcus Schindewolf, Constanze Bornkampf, Michael von Werner and Jürgen Schmidt

Additional information is available at the end of the chapter

http://dx.doi.org/10.5772/61576

Abstract

Soil erosion on arable land is the key driver of reservoir siltation in the German loess belt. In this regard, the Baderitz Reservoir suffers from deleterious sediment inputs and resulting siltation processes. In order to estimate the reservoir lifespan, the event-based soil erosion and deposition model EROSION 3D was applied. Simulations of sediment input and sediment deposition processes within the reservoir were realized using a typical crop rotation and a normal heavy rainfall year of the region. Model parameterization was enabled by existing data based on a large number of artificial rainfall simulations. Yearly soil losses of approximately 12 t/ha correspond to sediment inputs of nearly 8800 t. The mean annual increase of the reservoir bottom of 9 cm causes a 13% loss of reservoir storage in only 10 years. The model results are plausible and could be used for planning and dimensioning of mitigation measures.

Keywords: soil esoil erosion modelling, loess belt, water conservation, hydraulic engineering

1. Introduction

Soil erosion, as one of the main triggers of land degradation, seriously threatens the sustainability of cropping systems in many parts of the world. Soil erosion leads to both on-site and off-site damages. On arable land, on-site effects lead to a reduction of soil fertility, often less regarded. More attention is given to the off-site damages if sediments and/or attached nutrients are entering settlements, traffic lanes or stream networks. Since siltation and eutrophication may cause enormous costs on national economy, the latter is of special public interest. In this

regard, active and passive soil conservation measures become important in order to decrease sediment inputs into surface waters.

Since soil erosion is strictly a non-continuous process, the main soil loss and sediment delivery into stream network is caused by single, extreme rainfall events [1]. Due to the highly complex nature of the physical processes involved, monitoring and surveying of soil erosion processes is associated with many difficulties. In order to overcome these problems, mathematical simulation models have been developed starting with the Universal Soil Loss Equation (USLE) by [2]. However, the USLE was derived by correlating empirical data resulting in a limited transferability of this model. Examples for successful USLE-based applications are given by [3-6]. Although such approaches fullfil their aims of sediment input calculations, they are less suitable for event-based planning purposes. Since USLE-based approaches only generate annual mean soil losses, the highly non-continuous nature of erosion processes is neglected. This renders the application of these model types for planning and dimensioning of passive mitigation measures, impossible.

A younger erosion model generation makes use of physical principles as mass and energy balances, which allow adequate representation and quantitative estimation of soil detachment, transport, and deposition processes. In this regard, only process-based models are able to focus on the challenge of planning and dimensioning of mitigation measures. As a result of high data demands and difficult parameterization procedures, only few examples are found in literature [7].

In this context, the EROSION 3D model might be a suitable tool for the estimation of soil loss, deposition and sediment input into surface waters. Since the model is physically-based, it can be applied for all types of soils and climate regions.

2. Materials and methods

2.1. Site description

The research area is located within the German loess belt (51°09′47 N, 13°10′12 E). The catchment (20 km^2) is a part of the Jahna Catchment, a tributary of the Elbe River. The dominant regional soil type is the Luvisol with high silt content. In this regard, soils are characterized by a high water-holding capacity and fertility, but vice versa highly endangered by erosion caused by low aggregate stabilities.

After [8], the study area is located in a warm oceanic Cfb-climate with 624 mm annual rainfall and 8.1 °C mean annual temperature (Figure 1). Most rainfall events occur between May and September, mainly as convective rains.

Due to low plant covers at the beginning and end of the crop year, the most intense erosion events occur between May and June (corn, sugar beet) and in September (rape, winter grains). The Baderitz Reservoir was constructed between 1985 and 1987 for purposes of flood control and irrigation. With an area of 0.1 km^2 and a mean depth of approximately 6 m, the whole

http://dx.doi.org/10.5772/61576

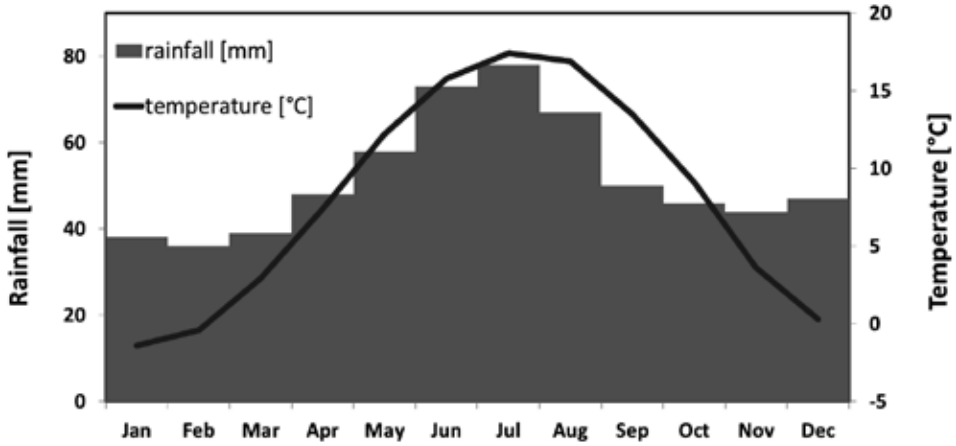

Figure 1. Climate chart of the study region.

retaining capacity amounts to 676,000 m^3, whereas 300,000 m^3 are common and 70,000 m^3 are uncommon flood retention. The dam is 9.7 m high and 180 m long. Since the last 27 years, the reservoir suffered from deleterious sediment inputs. Only between 1997 and 2006 the delta of the Jana Creek rose more than 150 m in length to an area of at least 0.02 km^2 within the reservoir (Figure 2).

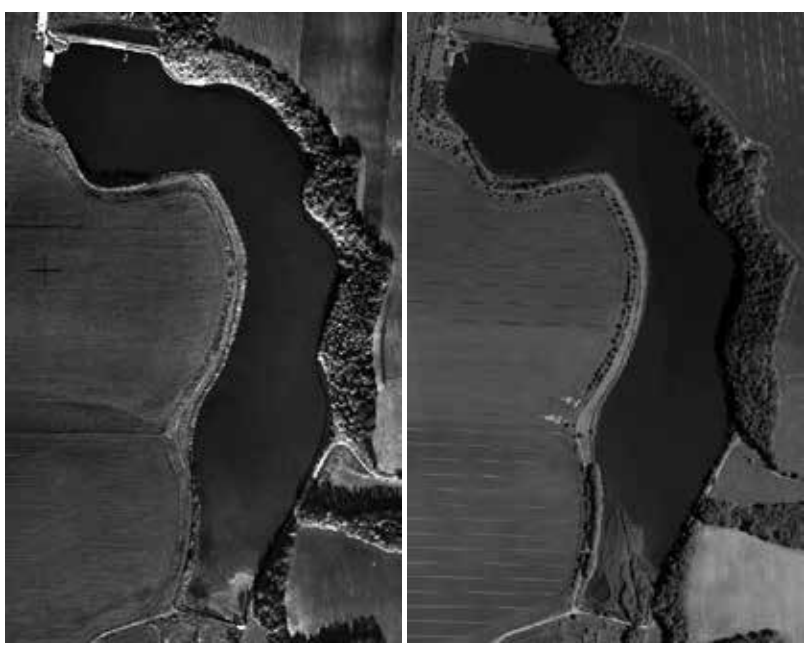

Figure 2. Development of the creek delta at the inlet of Baderitz Reservoir between 1997 and 2006.

Jahna Creek is draining the catchment with a mean discharge of 0.15 m^3/s. Peak flows are mostly related to heavy rainfall events.

As a result of the high soil fertility, more than 75% of the catchment area are used by croplands. Typical crops are winter wheat, rape, sugar beet, and corn. Grassland is limited to narrow stripes on the valley bottoms. Settlements cover 5%, whereas forest is limited to small isles (Figure 3).

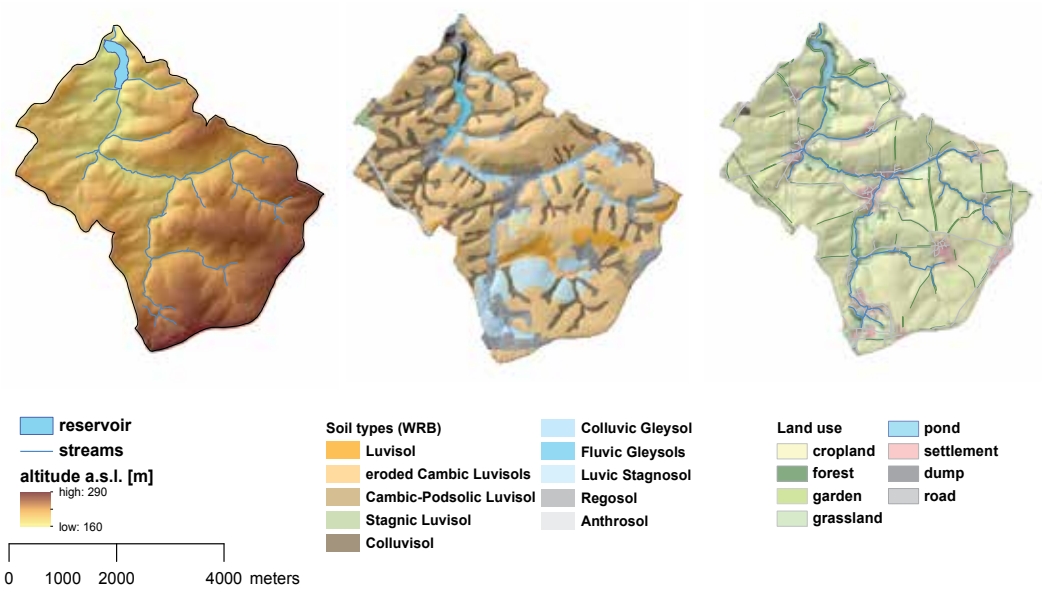

Figure 3. Relief, soil types, and land use of the Baderitz Reservoir catchment.

2.2. The soil loss simulation model EROSION 3D

EROSION 3D [9-11] is a field-tested, physically-based soil erosion model to estimate the spatio-temporal distribution of erosion and deposition, as well as the delivery of suspended soil material into surface water courses [10]. Since more than 20 years, the model was continuously improved and extensively validated using plot- and catchment-based soil erosion data [12-14].

The theoretical concept of the model is based on the momentum flux approach. The erosive impact of overland flow and rainfall droplets is proportional to the momentum flux exerted by the flow and falling droplets, respectively [9-10, 15]. In detail, the model covers rainfall infiltration, excess rainfall and subsequent generation of surface runoff, detachment of soil particles by raindrop impact and surface runoff, transport of detached soil particles by surface runoff, routing of surface runoff, and sediment transport through the catchment.

Since the model is raster-based, EROSION 3D demands a grid-cell parameter representation of the catchment. Using internal parameter transfer functions, EROSION 3D only needs few

http://dx.doi.org/10.5772/61576

input soil parameters compared to other process-based erosion models as EUROSEM [16], WEPP [17] and LISEM [18], which allows application for research as well as planning purposes.

Overland flow routing is generated by applying a multiple flow algorithm FD8 [19-20]. After reaching a critical source area of runoff generation [m^2], multiple flow is converged to single flow (D8) [21] equivalent to channel flow. Once the runoff and transported sediments are entering the channel network, sediments are routed outside the catchment, disregarding deposition processes (Figure 4).

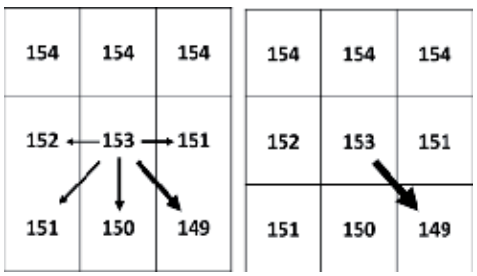

Figure 4. Multi-direction flow (FD8, left) and single direction flow (D8, right).

Regarding parameter identification, the interactive software tool DPROC was developed to enable the semiautomatic generation of model input data by using available relief, land use, and soil data sets. Model parameters (Table 1) are derived as functions of land use, soil characteristics, and simulations date, using an extensive database deducted from numerous rainfall experiment simulations on test plots in the mid-nineties [22-24] Experiments cover a broad range of different soil, crop, and tillage types, as well as special soil characteristics and crop phenology stages.

Input parameter	Unit	Method
Altitude (DEM)	[m]	Airborne laserscan
Rainfall intensity per time step	[mm/min]	Statistical analysis of the German Weather Service
Grain size distribution	[%]	Derived via sum curves of available soil map
Bulk density	[kg/m^3]	Databases*
SOC	[%]	Databases*
Surface roughness	[$s/m^{1/3}$]	Databases*
Initial soil moisture	[Vol.%]	Databases*
Skinfactor	[−]	Databases*
Resistance to erosion	[N/m^2]	Databases*
*[22-24, 27],		

Table 1. Input parameters of the EROSION 3D simulation model.

2.3. Data preprocessing and parameterization

GIS data preprocessing of land use, soil type, relief, and rainfall information was accomplished according to [24]. Land use maps were applied from available sources in a scale of 1:25,000, soil maps in a 1:50,000 scale. Since soil erosion is a complex process, highly influenced by local morphology, the DEM of 20 m cell size was interpolated to a 5 m grid according to [25].

2.3.1. Digital elevation model

Considering the morphological shape of the reservoir bottom, no digital information was available from official sources. Consequently, the resulting shape of the reservoir bottom is a more or less flat surface. Isolines of a historical topographic map [26] were digitized, interpolated, and merged with the existing DEM. This map of 1935 represents the land surface prior to the construction of the reservoir and so the assumed underwater relief. Finally, the dam of 9 m height was attached (Figure 5).

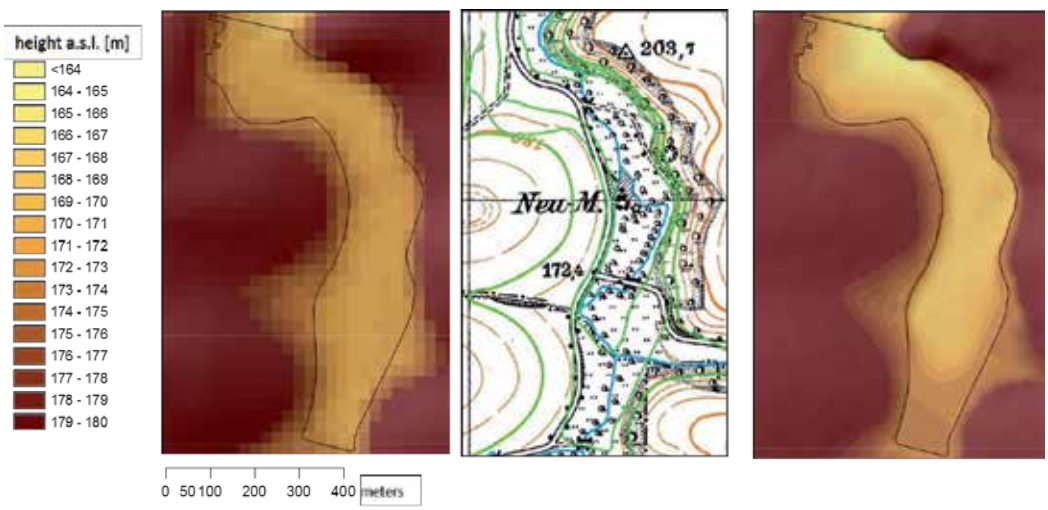

Figure 5. Original DEM in a 20 m cell size (left), digitized contour lines of a historical map of 1935 (center), and modified DEM of 5 m cell size with the elevated dam.

2.3.2. Representation of water bodies in the EROSION 3D model

Since the EROSION 3D model was originally developed for runoff and deposition processes on arable land, complex hydrodynamic 2D or 3D flow algorithms for water bodies are not included. Considering a critical source area of concentrated flow in the study region of approximately 0.08 km^2, the reservoir is among the channel network, only permitting single direction flow. Since hydrodynamic conditions in stand water are different to those in a turbulent stream, single flow calculations need to be disabled within the reservoir body. Additionally, hydraulic roughness needs to be increased on that area to enable sedimentation processes as they take place in water bodies.

http://dx.doi.org/10.5772/61576

2.3.3. Parameterization of the worst-case scenario

As a first step of model application, a worst-case scenario is simulated in order to identify the most important sediment delivery areas, as well as the sediment pass over points into surface waters. In this regard, all croplands are assumed to be under seedbed conditions related to conventional tillage with the moldboard plough. This implies no soil cover of plants or plant residues, low hydraulic roughness due to the fine soil management, and high soil moisture contents (field capacity).

2.3.4. Parameterization of normal heavy rainfall years

Since the model is capable to process single storms as well as storm sequences, annual soil losses and sediment input into the stream network can be simulated. For this purpose, the model demands single events of a normal heavy rainfall year (Figure 6), which was generated by the [27].

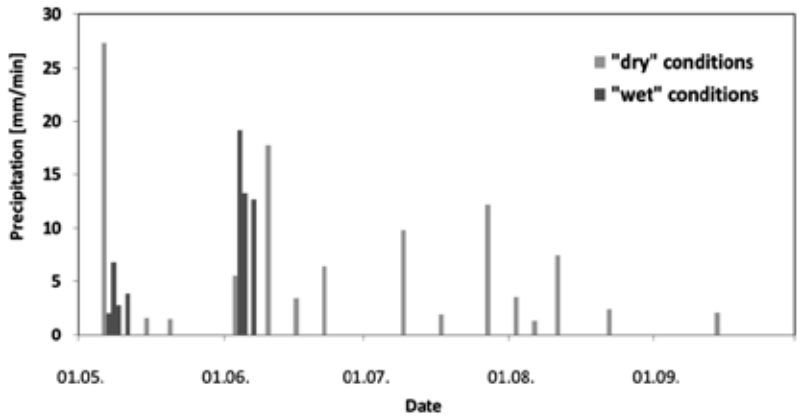

Figure 6. Normal heavy rainfall year of the study region.

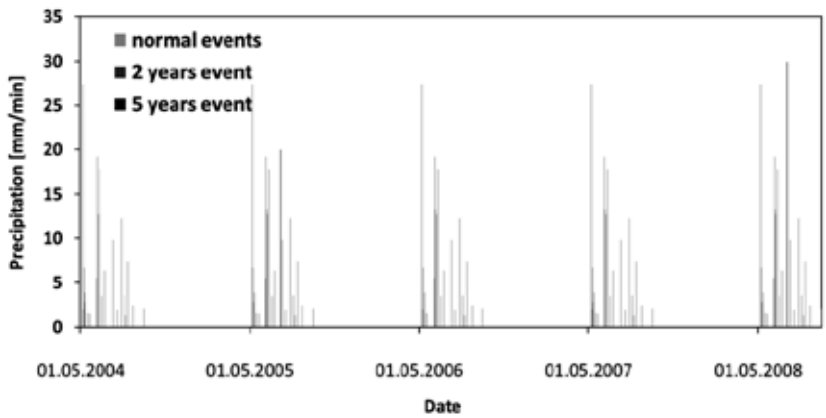

Figure 7. Five-year rainfall sequence with normal heavy rains and statistical extreme events.

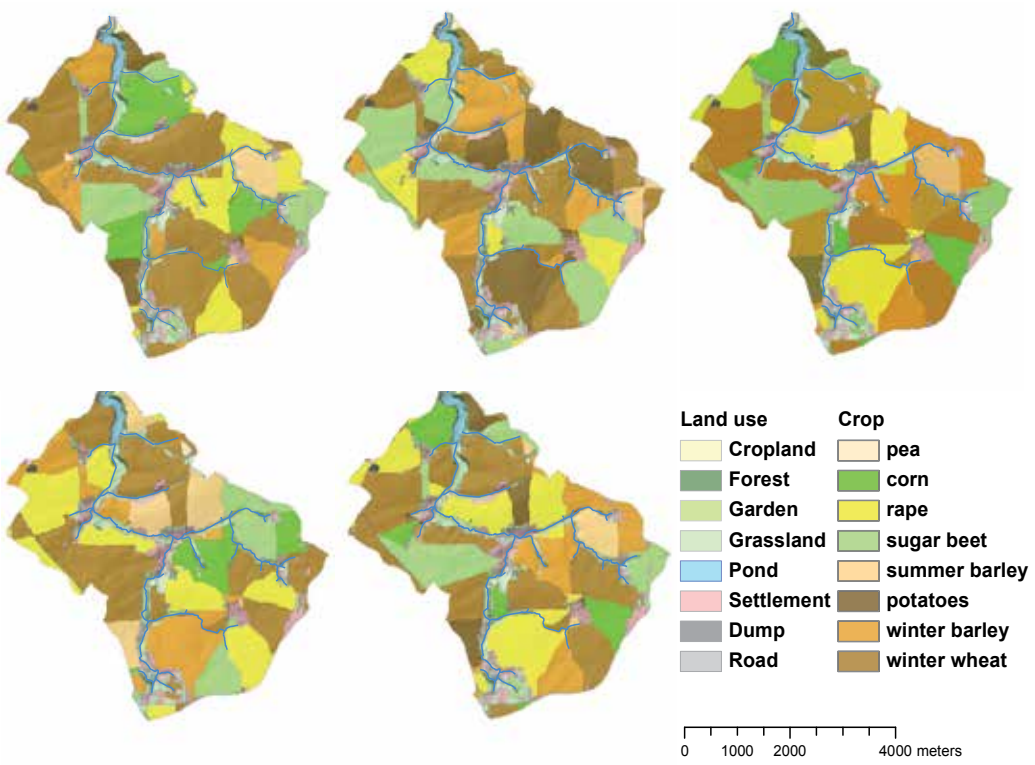

Figure 8. Crop type distribution in five crop years (start 2004).

In order to simulate a ten-year rainfall sequence, rainfall events of the normal years have to be combined with statistical extremes as it is compiled in Figure 7.

By applying land use and crop type maps from 2004 to 2009 (Figure 8), initial conditions of all rainfall occurrence dates were parameterized with the software DPROC. Considering dynamic moisture conditions, all events with previous rainfall events, less than 24 h ago, were set to high soil moisture contents (field capacity, Figure 6). Land use and soil parameters were derived from the database of DPROC. After the harvest of grains and rape in August and September, a stubble cover was assumed and the planting of rape was supposed to early September.

3. Results

3.1. Soil loss and sediment flux for the worst-case scenario

The Baderitz Reservoir catchment is highly endangered by soil losses. All croplands tend to deliver considerable amounts of sediments. Since all soil types are characterized by high silt contents, soil erosion is mainly controlled by slope length and slope steepness. Highest soil

http://dx.doi.org/10.5772/61576

loss rates are reached in thalwegs (Figure 9), where surface runoff concentration allows highest transport capacities and related sediment concentrations.

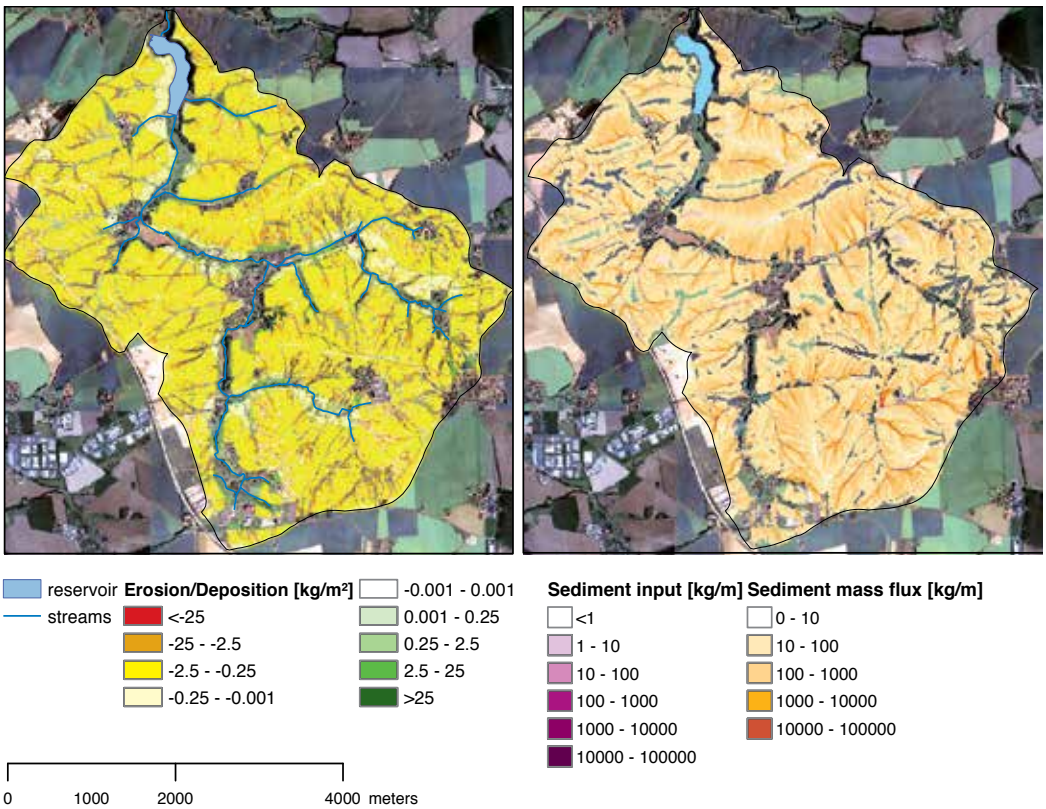

Figure 9. Sediment budget, sediment flux, and sediment input into surface waters for the worst-case scenario.

Mean soil loss amounts to 9.8 t/ha. All croplands are endangered by soil erosion, whereas grasslands, hedges, and woods act as buffers, where sediments are deposited (Figure 9). In this regard, all streams with insufficient buffers are affected by high sediment inputs.

3.2. Soil loss and sediment flux in the catchment during long-term simulations

The overall soil loss for the first reference year is 12.3 t/ha in the reservoir catchment.

Comparable to the worst-case scenario, all croplands are endangered by erosion. A distinct relation to the applied crop is visible (Figure 10).

Compared to prior simulations, croplands reveal high soil loss values, buffer stripes act as important retention areas. As overall trapping efficiency of this buffer is insufficient, effect of crop rotation becomes more important with the 10-year estimation compared to single events or single years (Figure 11). The mean soil loss after the 10-year simulation is about 193 t/ha. A distinct pattern of high endangered croplands of different categories is visible. Nearly

comprehensive values of red pixels (<−25 kg/m^2), mixed of orange and red values (−2.5–25 and <−25), and a third class with red pixels only in areas of runoff concentration (Figure 11) are simulated.

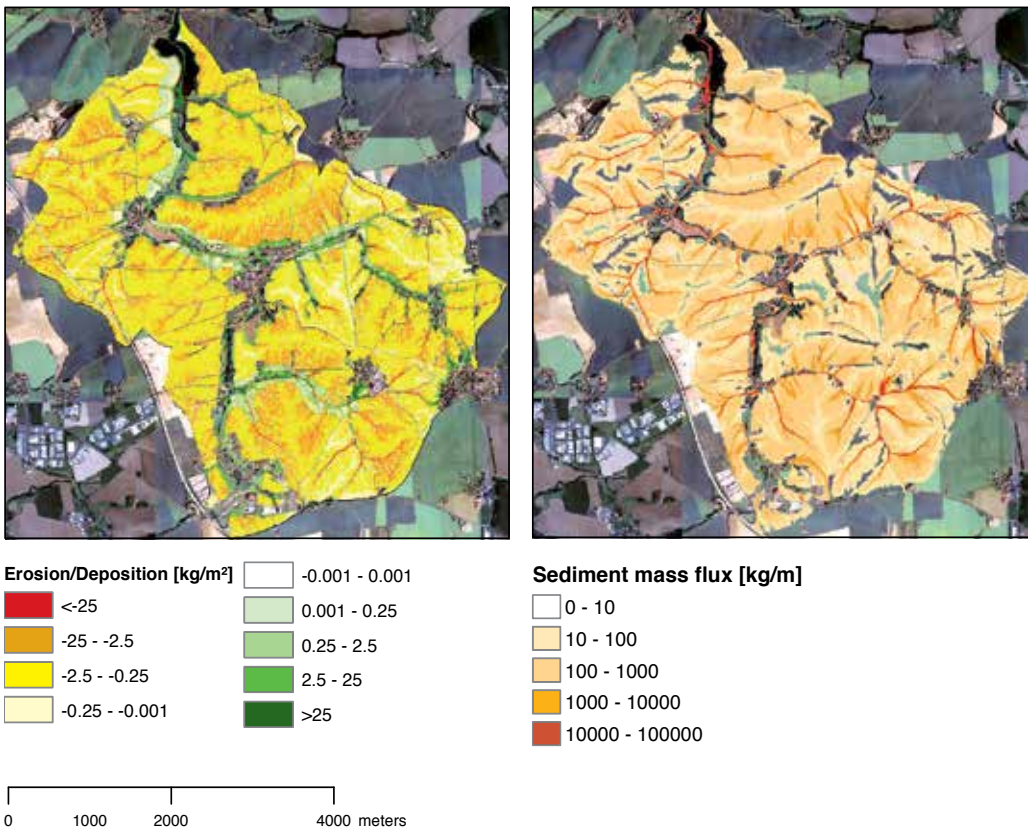

Figure 10. Sediment budget and sediment flux for the first reference year.

3.3. Sediment inputs into Baderitz Reservoir during long-term simulation.

During all simulation steps (1 year, 5 years, and 10 years) maximum sediment deposition can be identified at the water entrance area of the reservoir (Figure 12), which can be explained by the abrupt change in runoff velocity when water enters the reservoir. Additionally, sediments are deposited along the natural channel as shown in Figure 12.

Consequently, the bottom level is increasing due to sediment deposition after each erosive event. In a long-term simulation run, the EROSION 3D model adjusts the surface relief according to the amount of erosion and deposition. The changes are compiled in Figure 13, with an increasing reservoir bottom level and a resulting decreasing expanse of the water surface.

http://dx.doi.org/10.5772/61576

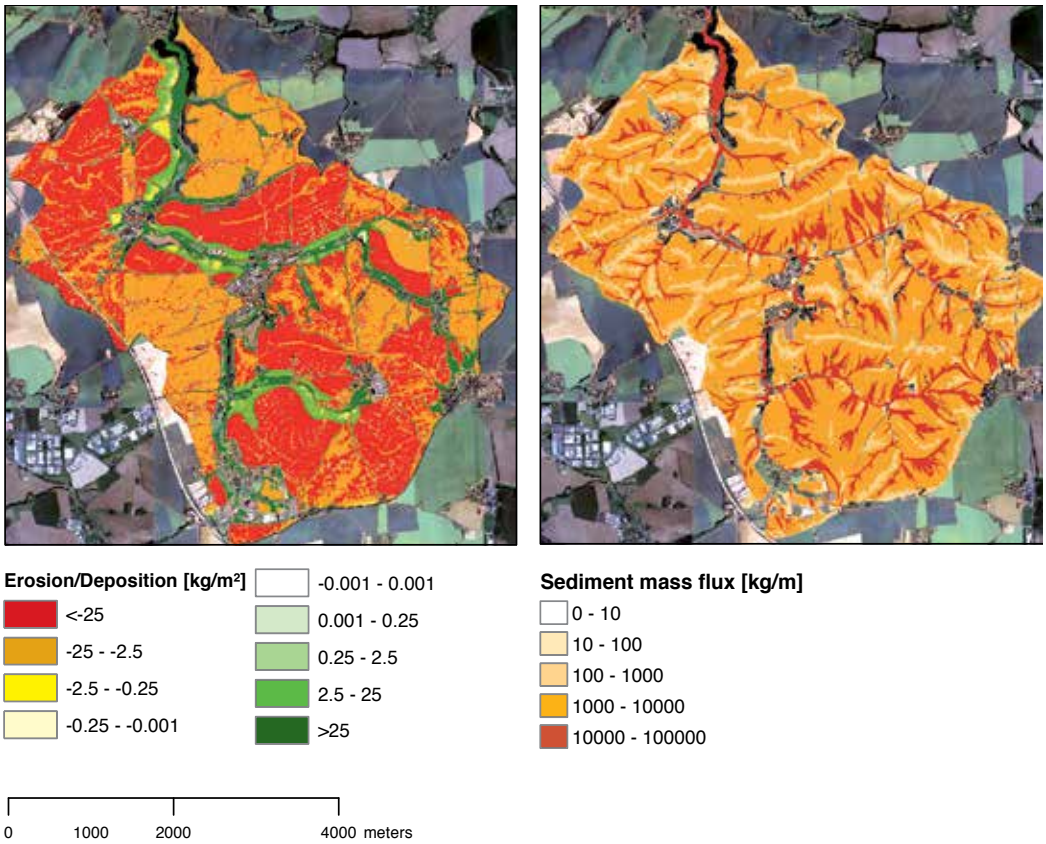

Figure 11. Sediment budget and sediment flux for ten reference years.

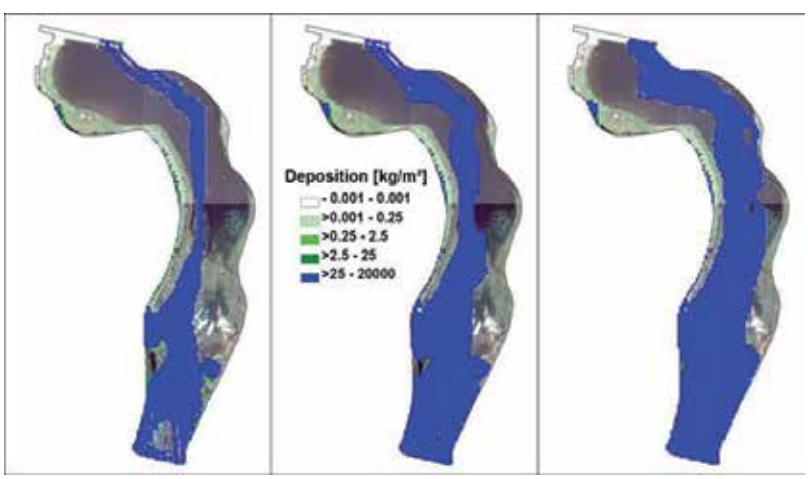

Figure 12. Siltation of the Baderitz Reservoir. Growing deposition areas after 1, 5, and 10 years.

Figure 13. Siltation of the Baderitz Reservoir.

After the first year, inputs of 7943 t sediment or 5673 m^3 (estimated bulk density of 1.4 g/cm^3) were computed. This means, approximately 1% of retention reduction during the first year after installing the dam. After 10 years long-term simulation, inputs in the reservoir amounted to 124,470 t, which corresponds to 88,910 m^3 and a loss of 13% retention volume and a total elimination of the uncommon flood retention (Figure 14). On average, the reservoir bottom is heightened by about 0.9 m, with an increase of 16,900 m^2 in land surface.

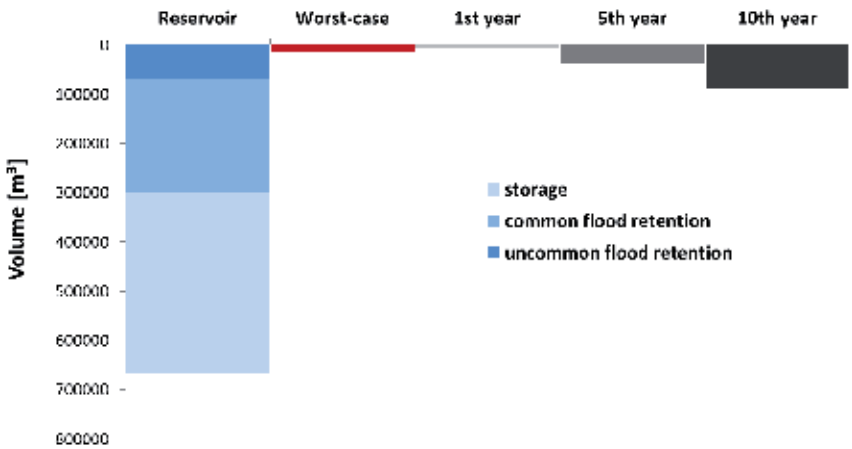

Figure 14. Siltation of the Baderitz Reservoir.

4. Discussion

Erosion and sedimentation processes are driven by temporal dynamic characteristics as land use, crop types and crop rotation, and relative constant catchment characteristics such as slope morphology and soil type.

http://dx.doi.org/10.5772/61576

Since most endangered rainfalls and "high" moisture conditions occur in late spring, crops with low plant cover reveal high losses of <–2.5 kg/ha after the first simulation year. Although winter wheat has a comparable high plant cover in May, high soil bulk densities decrease infiltration rates and water storage capacities of the soil. As most of the precipitation is runoff, protection value of plant cover is obsolete.

Croplands with phenologically dependent high plant covers in the most endangered spring season (e.g., rape, Figure 8) are less affected.

Considering long-term simulation, especially croplands with a high amount of winter wheat and rape are overall less endangered. As the two extreme events statistically occur during July, crops with low cover in this month reveal high soil losses.

Compared to the worst-case scenario, sediment delivery ratio (SDR), described as throughflow in Figure 15 for one-year or ten-year long-term simulation, is much smaller. This means that the retention efficiency of sediment buffers is increasing with decreasing sediment fluxes. During high fluxes as simulated with the worst-case run, two-third of the sediments are routed into the water network and only 6% are remaining within the reservoir.

Decreasing SDR with increasing simulation year is caused by a cumulative bank up and resulting trapping efficiency of deposition areas. Between 70 and 75% of the sediments are deposited in the morphology of the catchment and between 12 and 15% are remaining in the reservoir (Figure 15).

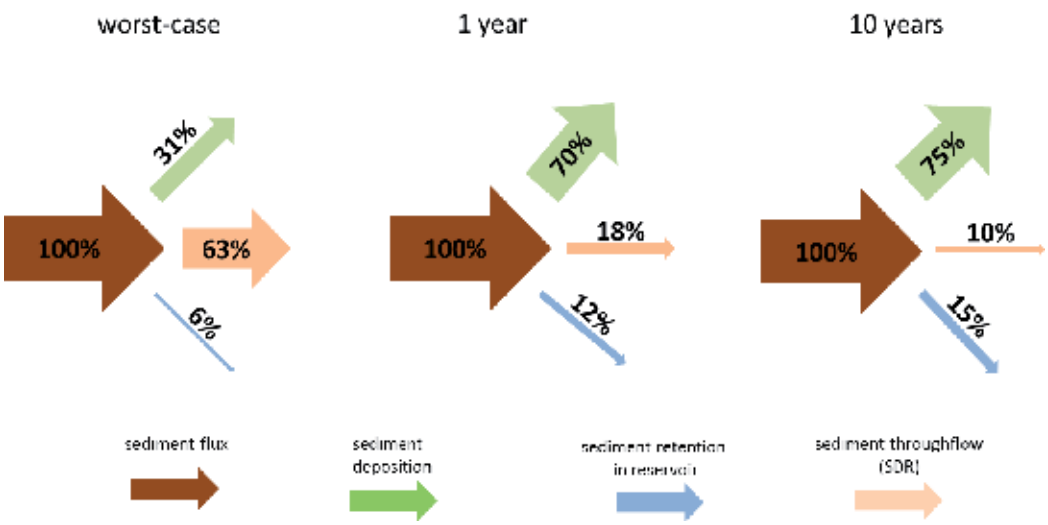

Figure 15. Sediment budgets for worst-case and long-term simulation, changed after [3].

Since bathymetric data is lacking so far, sediment inputs only can be plausibly tested by comparisons with ortho-photos (Figure 16).

The picture was taken in 2009 after the reservoir was drained and reflooded. The water level is 3 m below the original level. Simulation results for a 20 year long-term run reveal an almost identical extent and shape. As this project was simulated with standard pre-calibrated database values, the results reveal high model quality, which makes further application for reservoir siltation even on larger scales possible.

Figure 16. Comparison of observed and simulated sediment fan.

5. Conclusion

The process-based EROSION 3D model was successfully applied to simulate reservoir siltation in a meso-scaled German loess catchment. The simulation results in a progressive siltation of the reservoir, which is seriously impairing the primary purposes of the reservoir. Reservoir live span as flood retention is halved after 20 years, which immediately makes a sediment disposal essential.

To avoid excessive siltation, soil conservation measures should be implemented within the catchment. The EROSION 3D-based soil loss prediction maps could help to identify the most erosion-sensitive areas within the catchment, as well as the points of sediment transfer into surface water bodies. Further studies should focus on modelling and implementing of soil loss mitigation in the catchment. Both, local authorities and farmers will be made aware to take appropriate and effective actions to reduce soil loss.

Author details

Marcus Schindewolf*, Constanze Bornkampf, Michael von Werner and Jürgen Schmidt

*Address all correspondence to: marcus.schindewolf@tbt.tu-freiberg.de

Soil and Water Conservation Unit, Technical University of Freiberg, Freiberg, Germany

References

[1] Schmidt, R : Beobachtung, Messung und Kartierung der Wassererosion. In: G. Richter (ed.): Bodenerosion: Analyse und Bilanz eines Umweltproblems. Wissenschaftliche Buchgesellschaft, Darmstadt, 110–121. 1998

[2] Wischmeier W H, Smith H: Predicting rainfall erosion losses—A guide to conservation planning. U.S. Dep. of Agriculture. Washington. 1978

[3] Bronstert A, de Araújo JD, Batalla RJ, Cunha Costa A, Delgado JM, Francke T, Foerster S, Guentner A, López-Tarazón JA, Leite Mamede G, Medeiros PH, Mueller E, Vericat D: Process-based modelling of erosion, sediment transport and reservoir siltation in mesoscale semi-arid catchments. *J Soils Sediments. 2014;*14: 2001–2018. DOI 10.1007/s11368-014–0994–1

[4] Kovacs AS, Fulop B, Honti M :Detection of hot spots of soil erosion and reservoir siltation in ungauged Mediterranean catchments. *Energy Procedia*. 2012;18: 934–943

[5] Krasa J, Dostal T, van Rompaey A, Vaska J, Vrana K:Reservoirs' siltation measurments and sediment transport assessment in the Czech Republic, the Vrchlice catchment study. *CATENA. 2005;*64: 348–362. DOI:10.1016/j.catena.2005.08.015

[6] Alatorre LC, Beguería S, García-Ruiz JM: Regional scale modelling of hillslope sediment delivery: A case study in the Barasona Reservoir watershed (Spain) using WATEM/SEDEM. *Journal of Hydrology.* 2010;391: 109–123. DOI:10.1016/j.jhydrol. 2010.07.010

[7] Lo KFA.:Quantifying Soil Erosion for the Shihmen Reservoir Watershed, Taiwan. *Agricultural Systems. 1994;*45: 105–116

[8] Köppen W, Geiger G (1939): Handbuch der Klimatologie. 5 Bände, Berlin.1939

[9] Schmidt J: A Mathematical Model to Simulate Rainfall Erosion. In: H.-R. Bork, J. de Ploey and A. Schick (eds.): Erosion, Transport and Deposition Processes—theories and models, Bd. 19, *CATENA Supplement*, 101–109. 1991

[10] Schmidt J: Entwicklung und Anwendung eines physikalisch begründeten Simulationsmodells für die Erosion geneigter landwirtschaftlicher Nutzflächen. *Berliner Geografische Abhandlungen 61.* Berlin: Freie Universität. 1996

[11] von Werner MGIS-orientierte Methoden der digitalen Reliefanalyse zur Modellierung von Bodenerosion in kleinen Einzugsgebieten. *Dissertation*. Berlin, Freie Universität. Berlin. 1995

[12] Jetten V, de Roo APJ, Favis-Mortlock D :Evaluation of field-scale and catchment-scale soil erosion models. *CATENA.1999;*37 (3–4): 521–541

[13] Defersha MB, Melesse AM:Field-scale investigation of the effect of land use on sediment yield and runoff using runoff plot data and models in the Mara River basin, Kenya. *CATENA. 2012;*89 (1): 54–64. DOI: 10.1016/j.catena.2011.07.010

[14] Starkloff T, Stolte J: Applied comparison of the erosion risk models EROSION 3D and LISEM for a small catchment in Norway. *CATENA. 2014;*118: 154–167. DOI: 10.1016/j.catena.2014.02.004

[15] Schmidt J : Modelling long term soil loss and landform change. In: A. Abrahams and A. Parson (eds.): Overland Flow—Hydraulics and Erosion Mechanics, University College London Press, London, 409–433. 1992

[16] Morgan R, Quinton J, Smith R, Govers G, Poesen J, Auerswald K, Chisci C, Torri D, Styczen ME: The European soil erosion model (EUROSEM)—a process-based approach for predicting sediment transport from fields and small catchments. *Earth Surface Processes and Landforms. 1998;* 23: 527–544

[17] Laflen JM, Elliot WJ, Flanagan DC, Meyer CR, Nearing MA: WEPP-predicting water erosion using a process-based model. *Journal of Soil and Water Conservation. 1997;*52: 96–102

[18] De Roo APJ, Wesseling CG, Ritsema CJ): LISEM: A single event physically based hydrological and soil erosion model for drainage basins. I: Theory, input and output. *Hydrological Processes. 1996;*10: 1107–1117

[19] Freeman GT Calculating catchment area with divergent flow based on a regular grid. *Computers and Geosciences. 1991;*17: 413–22

[20] Quinn PF, Beven KJ, Chevallier P, Planchon O: The prediction of hillslope flow paths for distributed hydrological modelling using digital terrain models. *Hydrological Processes. 1991;*5: 59–79

[21] O'Callaghan JF, Mark DM: The extraction of drainage networks from digital elevation data. Computer Vision. *Graphics and Image Processing. 1984;*28: 323–344.

[22] Michael A: Anwendung des physikalisch begründeten Erosionsprognosemodells EROSION 2D/3D - Empirische Ansätze zur Ableitung der Modellparameter. *Disserta-*

tion. Freiberg: Fakultät für Geowissenschaften, Geotechnik und Bergbau der TU Bergakademie Freiberg. 2000

[23] Seibert S, Auerswald K, Fiender P, Disse M, Martin W, Haider J, Michael H, Gerlinger K: Surface runoff from arable land—a homogenized data base of 726 rainfall simulation experiments. 2002;DOI: 10.1594/GFZ.TR32.2

[24] Schindewolf M, Schmidt J, von Werner M: Modelling Soil Erosion and Resulting Sediment Transport into Surface Water Courses on Regional Scale. *Zeitschrift für Geomorphologie*. 2012;157–175. DOI: 10.1127/0372–8854/2012/S00087

[25] Hutchinson M: A new precedure for gridding elevation and stream line data with automatic removal of spurious pits. *Journal of Hydrology. 1989;*106: 211–232

[26] Landesvermessungsamt Sachsen:Messtischblatt 1:25,000. Sachsen. 1935

[27] German Weather Service: *Expertise.* Zentralstelle für Hydrometeorologische Entwicklungen und Anwendungen, Abteilung Klimatologie. Offenbach: DWD, 1994

Chapter 4

Assessment of Reservoir Sedimentation Effect on Coastal Erosion and Evaluation of Sediment Removal Techniques for Its Reduction — The Case of Nestos River, Greece

Manolia Andredaki, Anastasios Georgoulas, Vlassios Hrissanthou and Nikolaos Kotsovinos

Additional information is available at the end of the chapter

http://dx.doi.org/10.5772/61459

Abstract

Nestos is one of the most important transboundary rivers flowing through Bulgaria and Greece. In the Greek part of the river, two reservoirs, the Thisavros Reservoir and the Platanovrysi Reservoir, have already been constructed and started operating in 1997 and 1999, respectively. In the first part of the chapter, the reservoir sedimentation effect on the coastal erosion is investigated, for the case of the Nestos River delta and the adjacent shorelines, through a combination of mathematical modeling, modern remote sensing techniques, and field surveying, while in the second part, the mechanical removal as well as the flushing of sediment from the reservoir of Platanovrysi and its disposal in the subbasin downstream of the Platanovrysi Dam up to the Nestos River delta are investigated as potential treatment methods of reducing coastal erosion, using a modification of the same mathematical model that is utilized in the first part of the chapter. The overall findings and conclusions arising from the work presented and discussed in the present chapter contribute to the overall need to thoroughly understand the direct effect of dam construction on coastal erosion, as well as to examine the effectiveness of potential sediment management treatments.

Keywords: Sediment transport/management, reservoir, mathematical modeling, coastal erosion, shoreline change monitoring, Nestos River

1. Introduction

Coastal erosion constitutes a major environmental problem in many parts of the world. Especially in deltaic regions, the construction of dams in the river basin acts as an artificial barrier to the sediment supply to the river mouths and therefore the rates of shoreline retreat and sea level rise may exceed the corresponding rates of vertical shoreline accretion, resulting in the increase and in many cases the predomination of deltaic and coastal erosion. Over the last decades, many investigations have been directly or indirectly focused on the assessment of reservoir sedimentation and its effect on sediment yield reduction and coastal erosion, in the wider coastal regions of various rivers worldwide, using different investigation methodologies and techniques (e.g., [1]-[8]).

Nestos constitutes an important transboundary river, characterized by its great biodiversity. It flows through two European countries, Bulgaria and Greece, discharging into the Aegean Sea. It originates from Mount Rila (2716 m) in South Bulgaria, where Nestos River is known as Mesta. Its total length reaches 234 km and the river basin covers an area of 5749 km^2, 130 km (<56%) and 2280 km^2 (<40%) of which lies in Greek territory [9].

In the Greek part of the river, two hydroelectric dams, the Thisavros Dam and the Platanovrysi Dam, have already been constructed and started operating in 1997 and 1999, respectively. This implies a reduction of sediment yield at the outlet of the Nestos River basin and a corresponding disturbance of the sediment balance in the basin in general, which can result in coastal erosion. However, the reduction of the sediment yield at the outlet of the considered river due to the construction of these two reservoirs as well as the increase in the coastal erosion of the deltaic and the adjacent coastal regions have never been evaluated and correlated previously.

According to the authors' best knowledge, the work that is presented in the first part of this chapter constitutes one of the first assessments of reservoir sedimentation effect on the coastal erosion for the case of the Nestos River delta and the adjacent shorelines, utilizing mathematical modeling, remote sensing techniques, and field surveying [10]. The main objectives are to evaluate the overall reduction of the sediment yield at the outlet of the river due to the construction of the two dams and to examine the resulting erosion/accretion response of the deltaic as well as the adjacent shorelines. For this purpose, the sediment yield at the outlet of the Nestos River basin before and after the construction of the two dams is calculated, through the application of a mathematical simulation model (RUNERSET – RUNoff ERosion SEdiment Transport). The model is initially tested against appropriate field measurements that are available in the literature. Moreover, a shoreline change monitoring methodology for the coastal region of the Nestos River delta and the adjacent shorelines is proposed, tested, and applied for the digital and detailed extraction of the shoreline position with respect to time, aiming to determine the erosion/accretion shoreline balance for two time periods that correspond to the periods before and after the construction of the dams. Finally, the mathematically calculated reduction of the sediment yield at the outlet of the river is correlated with the results from the application of the shoreline change monitoring methodology and some valuable conclusions and recommendations are drawn. The considered mathematical simulation model (RUNERSET) calculates the mean annual value of sediment yield, due to rainfall and runoff.

http://dx.doi.org/10.5772/61459

The proposed model consists of three submodels: a rainfall-runoff submodel, a soil erosion submodel and a sediment transport submodel for streams. The coastal erosion/accretion monitoring data that were used in order to determine the shoreline evolution consist of remote sensing data from high-resolution satellite images (year 2002, considered period of construction/operation of the dams) and aerial photographs (year 1945, period before the construction/operation of the dams/reservoirs) as well as from high-resolution DGPS (Differential Global Positioning System) field measurements (year 2007, period after the construction/operation of the dams/reservoirs). It is calculated that the construction and operation of the considered dams have caused a dramatic decrease (about 83%) in the sediments supplied directly to the basin outlet and indirectly to the neighboring coast, and that this fact has almost inversed the erosion/accretion balance in the deltaic as well as the adjacent shorelines. Before the construction of the reservoirs, in the entire pilot study region, accretion predominated erosion by 25.36%, while just within 5 years of the construction/operation of the reservoirs, erosion predominates accretion by 21.26% [10]. Moreover, in the same part of this chapter, aiming to quantitatively investigate the dynamic evolution of erosion in the considered coastal region, a more recent shoreline (2013) was also extracted. For this purpose, additional DGPS field measurements were performed, following the same methodology and time period (spring) with the corresponding field measurements of the year 2007. Recording this more recent state of the coastline (2013) and comparing with the previous shorelines up to the perceived period of the construction and operation of the dams (2002) showed that erosion, in relation to the deposition/accretion that has been observed in the period 2002-2007, shows an increasing trend.

It has been estimated that every year almost 2% of the effective volume of reservoirs worldwide is lost due to sedimentation. This is an unavoidable fact, which however can be reduced, quantified, and incorporated into the design and operation of a reservoir [11]. The sediment management methods in reservoirs can be classified into three main categories: a) methods that minimize the inflow of sediment into the reservoirs, b) methods that minimize the accumulation of sediment in the upstream part of the reservoir and c) methods that maximize the overall sediment discharge that passes downstream of the reservoirs. The application of this last class of methods could serve as a possible treatment for the reduction of shoreline erosion, which has been mainly caused by the construction of the above-mentioned dams in the case of Nestos River. Two of the most widely applied methods of sediment removal from reservoirs are the processes of mechanical removal or dredging [11] and flushing [12]. In the work that is presented in the second part of this chapter, the dredging as well as the flushing of sediment from the reservoir of Platanovrysi, and its disposal in the subbasin downstream of the Platanovrysi Dam up to the Nestos River delta, are investigated as potential treatment methods of reducing coastal erosion ([13], [14]). For this purpose, the considered mathematical model (RUNERSET) was accordingly modified in order to incorporate these effects, and various scenarios of sediment management in the Platanovrysi Reservoir were simulated, while an assessment of the most effective and consistent month of the year for sediment flushing or dredging, as well as of the maximum transport quantity of the removed material was conducted. Finally, a comparison of the two methods takes place, concerning the maximum sediment quantities that reach the basin outlet, at the optimal for each method month of the year.

The overall findings and conclusions, arising from the work presented and discussed in this chapter, contribute to the need to thoroughly understand the direct effect of dam construction on coastal erosion. More specifically, the presented work constitutes one of the first attempts to quantify the disruption of the sediment balance in the delta of Nestos River due to the construction and operation of the Thisavros and Platanovrysi Reservoirs, considering simultaneously the impact of this disturbance on the erosion/accretion balance both at the river delta and the adjacent shorelines. Moreover, for the first time, an effort is made for the evaluation of the optimum periods and sediment management methods, aiming to increase the annual sediment that reaches the outlet of the Nestos River basin, and consequently to reduce erosion in the delta of the river and the adjacent shorelines. Finally, it is evident that the overall research methodology applied may constitute a quite useful tool for the further investigation of the effect of dam construction on the coastal erosion for other pilot application areas, throughout the world.

2. Assessment of reservoir sedimentation effect on coastal erosion

2.1. Description of the mathematical simulation model

As mentioned previously in the introduction section of this chapter, the considered mathematical simulation model (RUNERSET) calculates the mean annual value of sediment yield, due to rainfall and runoff, and it consists of three submodels: a rainfall-runoff submodel, a soil erosion submodel, and a sediment transport submodel for streams.

By means of the rainfall-runoff submodel, the runoff depth for a certain rainfall depth is computed. It is a simplified water balance model [15], in which the variation of soil moisture due to rainfall, evapotranspiration, deep percolation, and runoff is considered. The basic balancing equation is:

$$S_n' = S_{n-1} + N_n - E_{pn} \tag{1}$$

where S_{n-1} is the available soil moisture for the time step $n-1$ (mm); N_n is the rainfall depth for the time step n (mm); E_{pn} is the potential evapotranspiration for the time step n (mm); and S_n' is an auxiliary variable (mm).

The direct runoff depth h_{on} (mm) and the deep percolation IN_n (mm) for the time step n can be evaluated by comparing S_n' with the maximum available soil moisture S_{max} (mm), which is estimated by the following relationship of the US Soil Conservation Service [16]:

$$S_{\max} = 25.4[(1000/CN) - 10] \tag{2}$$

where CN is the curve number depending on the soil cover, the hydrologic soil group, and the antecedent soil moisture conditions ($0 < CN < 100$).

http://dx.doi.org/10.5772/61459

In the present study, two different methods were used for the estimation of the potential evapotranspiration E_p : the radiation method improved by Doorenbos and Pruitt [17] was used for the Greek part of the Nestos River basin, while the Thornthwaite method [18] was used for the Bulgarian part of the Nestos River basin.

The following meteorological data are required for the application of the radiation method: mean daily temperature (°C), sunlight hours per day (hr/day), mean daily relative humidity (%), and mean daily wind velocity (m/s). These data were available in the Greek part of Nestos River basin. For the application of the Thornthwaite method, only mean daily temperature data (°C) are required, which were available in the Bulgarian part of the Nestos River basin.

According to the equations given above, apart from the meteorological data, the input data for the rainfall-runoff submodel are: monthly rainfall depth, altitude, latitude, soil cover – land use, and hydrologic soil group.

The soil erosion submodel is based on the assumption that the impact of droplets on the soil surface and the surface runoff are proportional to the momentum flux contained in the droplets and the runoff, respectively [19].

The momentum flux exerted by the falling droplets, ϕ_r(kg m/s^2), is given by:

$$\phi_r = Cr\rho Au_r \sin a \tag{3}$$

where C is the soil cover factor; $r$is the rainfall intensity (m/s); $\rho$is the water density (kg/m^3); $A$is the subbasin area (m^2); u_r is the mean fall velocity of the droplets (m/s); and α is the mean slope angle of the soil surface (°).

The original relationship of Schmidt for the momentum flux exerted by the droplets is valid for bare soils. Therefore, an additional factor is necessary to express the decrease of the momentum flux because of the vegetation. It is believed that the dimensionless crop and management factor C of the USLE (Universal Soil Loss Equation) is appropriate to express the vegetation influence.

The momentum flux exerted by the runoff, ϕ_f (kg m/s^2), is given by:

$$\phi_f = q\rho bu \tag{4}$$

where q is the direct runoff rate per unit width [m^3/(s m)]; $b$is the width of the subbasin area (m); and u is the mean flow velocity (m/s).

The available sediment discharge per unit width, q_{rf} [(kg/(m s)], due to rainfall and runoff, in the subbasin considered is given by [19]:

$$q_{rf} = (1.7E - 1.7)10^{-4} \tag{5}$$

where

$$E = (\phi_r + \phi_f) / \phi_{cr} \quad (E > 1) \tag{6}$$

and ϕ_{cr} is the critical momentum flux (kg m/s^2).

The critical momentum flux ϕ_{cr}, which designates the soil erodibility, can be calculated from:

$$\phi_{cr} = q_{cr} \rho b u \tag{7}$$

where q_{cr} [m^3/(s m)] is the direct runoff rate per unit width at initial erosion.

The critical runoff rate q_{cr} is determined from the critical erosion velocity depending on soil roughness.

Equation (6) suggests the concept of critical situation characterizing the initiation of sediment motion on the soil surface.

The sediment supply *ES* [(kg/(s m)] to the main stream of the subbasin considered is estimated by means of a comparison between the available sediment discharge q_{rf} in the subbasin and the sediment transport capacity by overland flow per unit width, q_t[kg/(s m)], which is computed as follows [19]:

$$q_t = c_{\max} \rho_s q \tag{8}$$

where c_{max} is the concentration of suspended particles at transport capacity (m^3/m^3); $\rho_s$is the sediment density (kg/m^3).

The additional input data for the soil erosion submodel, with reference to the rainfall-runoff submodel, are: mean slope angle of soil surface, subbasin area, soil cover factor, length of the main stream of the subbasins, roughness coefficient of soil surface, critical erosion velocity, water, and sediment density.

The sediment yield at the outlet of the main stream of the subbasin considered can be computed by the concept of sediment transport capacity by the stream flow. The following relationships are used to compute sediment transport capacity by the stream flow [20]:

$$\begin{aligned} \log c_t &= 5.435 - 0.286 \log \frac{w D_{50}}{\nu} - 0.457 \log \frac{u_*}{w} + \\ &+ (1.799 - 0.409 \log \frac{w D_{50}}{\nu} - 0.314 \log \frac{u_*}{w}) \log (\frac{us}{w} - \frac{u_{cr} s}{w}) \end{aligned} \tag{9}$$

http://dx.doi.org/10.5772/61459

$$\frac{u_{cr}}{w} = \frac{2.5}{\log(u_* D_{50} / \nu) - 0.66}, \text{ if } 1.2 < u_* D_{50} / \nu < 70 \quad (10)$$

$$\frac{u_{cr}}{w} = 2.05, \text{ if } \frac{u_* D_{50}}{\nu} \geq 70 \quad (11)$$

where c_t is the total sediment concentration by weight (ppm); $w$is the terminal fall velocity of suspended particles (m/s); $D_{50}$is the median grain diameter of the bed material (m); $\nu$is the kinematic viscosity of the water (m^2/s); $u_*$is the shear velocity (m/s); $u$is the mean flow velocity (m/s); $u_{cr}$is the critical mean flow velocity (m/s); and s is the energy slope.

Equation (9) was determined from the concept of unit stream power (rate of potential energy expenditure per unit weight of water,us) and dimensional analysis. The variable u_{cr} in Equation (9) suggests that a critical situation is considered at the beginning of sediment particle motion, as in most sediment transport equations.

The sediment yield *FLO* [kg/(s m)] at the outlet of the main stream of the subbasin considered can be estimated by comparing the available sediment in the stream, *ESI* [kg/(s m)], with the transport capacity by the stream flow, q_{ts}[kg/(s m)], resulting from the total sediment concentrationc_t.

It is implied from the above relationships that only the main stream of each subbasin is considered, because numerous unavailable data for the geometry and hydraulics of the entire stream system would otherwise be required. Therefore, the additional input data for the stream sediment transport submodel, with reference to the foregoing submodels, concern the main stream of the subbasins: base flow, bottom slope, bottom width, bed roughness, diameter of suspended particles, grain diameter of bed material, and kinematic viscosity of water.

Finally, a sediment routing plan is necessary in order to specify the sediment motion from subbasin to subbasin.

2.2. Application of the simulation model

2.2.1. Available data and maps for Nestos River basin

For more precise calculations, the Nestos River basin was divided into 60 subbasins. In more detail, the basin of the Thisavros Reservoir (Bulgarian and Greek parts) was divided into 31 subbasins, the basin of the Platanovrysi Reservoir (Greece) into nine subbasins and the basin downstream of the Platanovrysi Reservoir into 20 subbasins. The outlet of the last basin is known as Toxotes outlet.

Available meteorological data (monthly rainfall data and mean monthly temperature data) from 22 meteorological stations in Greece and Bulgaria were used as input data for the

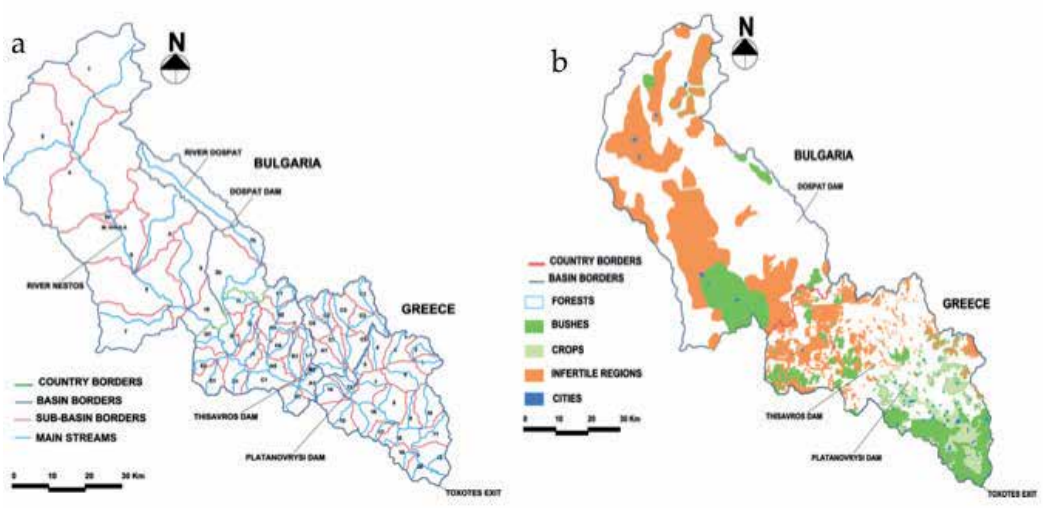

Figure 1. Subbasins/main streams map and soil cover map of the Nestos River basin

simulation model. Various digital thematic maps were constructed from georeferenced background maps, for the accurate computation of the required input parameters. Indicatively, the subbasins and main streams map as well as the soil cover map are depicted in Figure 1.

However, other kind of thematic maps were also constructed and used such as a Thiessen polygons map and a geological map. The calculations were performed on a monthly time basis for each subbasin.

2.2.2. Model testing

In order to validate the mathematical model predictions, sediment measurements (suspended load) for 53 years (1937-1989) that were available for the location "Momina Koula" [21] in the Bulgarian part of Nestos River (Figure 1), were utilized. According to the measurements, the mean annual suspended sediment yield for the considered time period is 202 t/km^2 [21]. Bed load measurements were not available and therefore, the following assumption [10] was made: the ratio of bed load to suspended load at the outlet of a basin on an annual basis amounts approximately to 0.25. According to this assumption, the measured mean annual sediment yield at "Momina Koula" is 252.5 t/km^2.

The mathematical model described in the previous section was applied to the basin corresponding to this location for the same time period [10]. The basin area is 1511 km^2, which is about 30% of the entire basin area of the Nestos River. The results of the model application for the different years are given in Table 1.

The mean annual value of sediment yield at the basin outlet, according to Table 1, is 315 000 t or 207.9 t/km^2. This means that the mathematical model underestimates the measured mean annual sediment yield by about 18%. However, taking into account the overall assumptions

http://dx.doi.org/10.5772/61459

Year	Annual sediment yield (t)	Year	Annual sediment yield (t)	Year	Annual sediment yield (t)	Year	Annual sediment yield (t)
1937	366 000	1950	278 500	1964	91 000	1977	85 500
1938	300 500	1951	428 500	1965	276 500	1978	280 500
1939	271 500	1952	374 000	1966	475 500	1979	315 000
1940	447 500	1953	359 000	1967	107 500	1980	314 000
1941	144 500	1954	786 000	1968	252 500	1981	200 500
1942	313 500	1955	381 000	1969	634 500	1982	209 500
1943	36 000	1956	458 000	1970	152 500	1983	68 500
1944	327 000	1958	413 000	1971	511 500	1984	185 000
1945	485 000	1959	274 000	1972	179 000	1985	239 000
1946	338 000	1960	555 500	1973	318 000	1986	511 000
1947	517 500	1961	160 500	1974	225 000	1987	288 500
1948	72 000	1962	798 500	1975	55 500	1988	253 000
1949	230 500	1963	705 500	1976	319 500	1989	7 500

Table 1. Computational results of sediment yield for the location "Momina Koula"

of the mathematical model as well as the complexity of the simulated process, these arithmetic predictions can be considered to be acceptable.

The relatively low deviation between computation and measurement results for the mean annual sediment yield at the location "Momina Koula" was an encouraging indication for the further application of the simulation model to other parts of the Nestos River basin. The following calculations were therefore performed for a time period of 11 years (1980-1990), which corresponds to the period before the construction and operation of the considered reservoirs:

- Calculation of mean annual sediment amount inflowing into the Thisavros Reservoir from the Bulgarian part (3052 km^2) and from the Greek part (804 km^2) of the Nestos River basin ([10]; [22])
- Calculation of mean annual sediment amount inflowing into the Platanovrysi Reservoir from the corresponding basin (405 km^2, Greece) [23]

In a previous study [24], the mean annual value of sediment yield at the outlet of the Nestos River basin (Toxotes) was calculated. Due to the construction and operation of the considered reservoirs, the sediment yield originates mainly from the part of the Nestos River basin which lies downstream of the Platanovrysi Reservoir (840 km^2, Greece).

The calculated values of the annual sediment yield for different years at certain locations of the Nestos River basin (Thisavros Reservoir, Platanovrysi Reservoir, and Toxotes) are summarized in Table 2.

Year	Basin of Thisavros Reservoir (Bulgarian part) (t)	Basin of Thisavros Reservoir (Greek part) (t)	Basin downstream of Dospat Reservoir (t)	Basin of Platanovrysi Reservoir (t)	Basin downstream of Platanovrysi Reservoir (t)	Entire basin of Nestos River (t)
1980	1 084 000	184 000	154 500	366 000	278 000	2 066 500
1981	968 000	128 000	128 500	344 000	588 000	2 156 500
1982	850 000	312 500	112 500	409 000	426 000	2 110 000
1983	309 500	114 000	32 500	99 500	73 000	628 500
1984	678 500	360 500	107 500	277 000	494 000	1 917 500
1985	991 000	94 500	127 500	54 500	131 000	1 398 500
1986	1 495 500	613 000	162 000	303 500	198 000	2 772 500
1987	1 021 000	875 500	131 500	761 500	673 000	3 462 500
1988	884 000	357 500	130 000	241 000	383 000	1 995 500
1989	73 500	121 000	xx	192 500	207 000	594 000
1990	545 500	552 500	46 500	289 500	64 000	1 498 000
Mean value	809 000	337 500	113 000	314 500	331 000	1 873 000

Table 2. Computational results of sediment yield at various locations of the Nestos River basin

2.2.3. Main computations of sediment yield for the Nestos River Basin

For these calculations, the major assumption is that all sediments inflowing into the reservoirs are deposited in the reservoirs, which represents the most unfavorable case regarding coastal erosion. According to Table 2, the mean annual value of sediment yield at the outlet of the Nestos River basin before the construction of the dams (mean annual value of sediment yield at the outlet of the entire Nestos River basin) is about 1.9×10^6 t, while after the construction of the dams (mean annual value of sediment yield at the outlet of basin downstream of the Platanovrysi Reservoir) this amounts to 0.33×10^6 t. Therefore, it is evident that the construction and operation of the considered reservoirs has caused a dramatic decrease, of about 83%, in the sediments supplied directly to the basin outlet and indirectly to the neighboring coast. Since Nestos River constitutes one of the main sediment supply sources for the west and east parts of the coastal region in the vicinity of its delta, it is expected that the calculated reduction in the sediment yield that reaches the Nestos River mouth will influence the seashore sediment balance, and it may result in a considerable increase in the erosion rates of the Nestos River mouth and the adjacent shorelines.

http://dx.doi.org/10.5772/61459

2.3. Description and testing of adopted methodology for shoreline change monitoring

2.3.1. Overview

The adopted shoreline change monitoring methodology for the Nestos River delta and the adjacent shorelines was the use of available high-resolution satellite images from the Quick-Bird (QB) satellite archive and aerial photographs from the Hellenic Military Geographical Service (HMGS), in conjunction with high-resolution GPS field measurements of the region [10]. In more detail:

- Use of ortho-rectified/georeferenced satellite images that were available in the QB archive for the extraction of the shoreline in the year 2002. The spatial resolution of these satellite images is 0.6 m per pixel. The proposed year was selected, as it was more close to the years 1997 and 1999 of the construction and operation of the considered reservoirs.
- Use of high-resolution DGPS field measurements for the extraction of the shoreline in the year 2007, in order to obtain the shoreline state approximately a decade after the operation of the considered reservoirs. The accuracy of these field measurements can reach the order of few centimeters.
- Comparison of the extracted shorelines between these 2 years in order to access a short-term shoreline evolution of the region that can be considered to be the period after the construction of the dams.
- Ortho-rectification/georeferencing of available, old aerial photographs of the region from the year 1945 from the HMGS and extraction of an old shoreline, approximately 50 years before the construction and operation of the reservoirs.
- Comparison of the extracted shorelines between the years 1945 and 2002 in order to access a long-term shoreline evolution of the region that can be considered to be the period before the construction of the dams.

In order to test the accuracy of the adopted shoreline change monitoring methodology, this was first applied to a small part of the total pilot study region (Figure 2). The proposed test part is composed by the mainland shoreline at the west of Nestos River delta extending from the Akroneri Cape until the Keramoti Bay.

The main steps of the utilized methodology are outlined in the following subsections.

2.3.2. Creation of common working background

In order to use a common working subbase, an ortho-rectified background of the wider geographical region was created using various available topographic maps from the HMGS. The merging and ortho-rectification of the proposed maps was conducted in ArcMap software from the ArcGIS 9 package, using as Ground Control Points (GCPs) a wide number of known, benchmark trigonometric points of the region that were available by the HMGS.

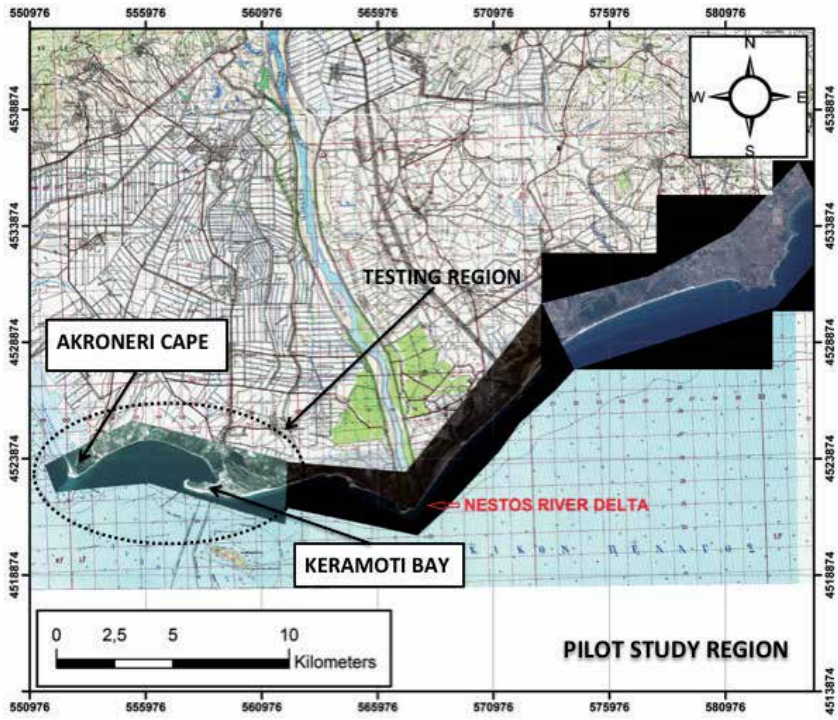

Figure 2. Pilot study region for shoreline change monitoring and selected region for testing the accuracy and effectiveness of the adopted shoreline change monitoring methodology

2.3.3. Ortho-rectification of aerial photographs and extraction of digital shoreline

The ortho-rectification of the available old aerial photographs of the region and the digital extraction of the corresponding shoreline was conducted with the ArcMap software of the ArcGIS 9 package. The basic stages of the proposed procedure are summarized below:

- The aerial photographs were scanned and digitally imported into the ArcMap database in order to be ortho-rectified in the EGSA 87 coordinate system, using as GCPs points that were both visible in the aerial photographs as well as in the ortho-rectified map background. A total number of 6-8 GCPs were used for each aerial photograph.
- A surface analysis was then performed in the aerial photographs and automatic contours were generated.
- The contour that corresponded to the dividing line between land and sea pixels was manually selected by visual inspection and digitally extracted as the shoreline position in the year 1945.

Figure 3 (a) illustrates the digitally extracted shoreline for the testing region (year 1945) superimposed on the corresponding aerial photograph where the adequate accuracy and the validity of the extraction method described above can be clearly seen.

http://dx.doi.org/10.5772/61459

2.3.4. Step 3 – Ortho-rectification of high-resolution satellite images and extraction of digital shoreline

The digital shoreline extraction from the ortho-rectified, high-resolution, satellite images of the region was also conducted using the ArcMap software of the ArcGIS 9 package. The basic stages are summarized below:

- Ortho-rectified, QB satellite images of the pilot study region were selected and ordered from the archive database of GEOMED LTD, one of the authorized resellers of these images, in Greece.
- The proposed 4-band satellite images were then imported into the ArcMap database in the EGSA 87 coordinate system and adjusted to the infrared channel.
- The well-known "Natural Breaks (Jenks)" pixel classification method was then applied on the images, from the "spatial analyst" tool of the ArcMap software, in order to separate sea and land pixels.
- Then a contour line was automatically inserted at the interface of the classified sea and land pixels and digitally extracted as the shoreline.
- Figure 3 (b) illustrates the digitally extracted shoreline for the testing region (year 2002) superimposed on the corresponding satellite image, where the adequate accuracy and the validity of the extraction method described above can be clearly seen.

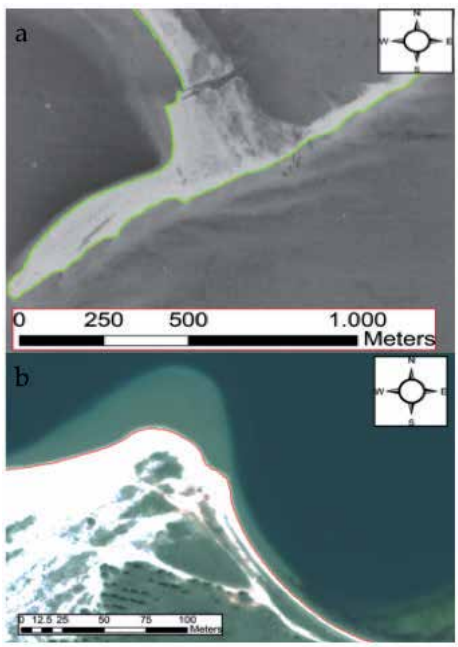

Figure 3. (a) Digitally extracted shoreline from the aerial photograph that corresponds to the test region (year 1945), superimposed on the aerial photograph. (b) Digitally extracted shoreline from the high-resolution satellite images that correspond to the test region (year 2002), superimposed on the satellite image

2.3.5. Step 4 – DGPS field measurements and extraction of digital shoreline

The DGPS field measurements were conducted using a high-resolution DGPS system that consists of two GPS receivers. A static receiver that was installed at various, known, benchmark trigonometric points of the region that were preinstalled by the HMGS and a rover (mobile) receiver which was used for the surveying of the shoreline in the field. The recorded data points from the rover receiver along the shoreline were then postprocessed and extracted in AutoCAD files in the EGSA 87 coordinate system and finally imported superimposed at the ArcMap database. The accuracy of the DGPS measurements according to the specifications of the proposed equipment was of the order of few centimetres. However, this was double-checked and verified using GCPs with known coordinates.

2.4. Quantitative and qualitative results from the application of the selected shoreline change monitoring methodology at the entire pilot study area

2.4.1. General

In the present subsection, quantitative and qualitative results from the application of the proposed methodology to the entire pilot study region are presented and discussed in detail. Figure 4 illustrates indicatively some stages of the application for the entire pilot study area.

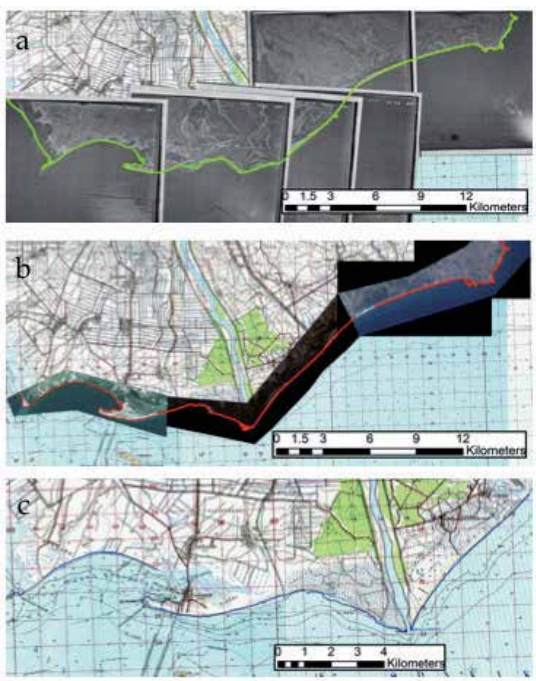

Figure 4. (a) Digitally extracted shoreline from aerial photographs (year 1945) for the entire pilot study region, superimposed on the aerial photographs. (b) Digitally extracted shoreline from satellite images (year 2002) for the entire pilot study region, superimposed on the satellite images. (c) Digitally extracted shoreline from DGPS measurements (year 2007) for the entire pilot study region, superimposed on the common working background

http://dx.doi.org/10.5772/61459

2.4.2. Calculation of erosion/accretion balance for the region of the Nestos River delta and the adjacent shorelines, before and after the construction of the dams

In order to investigate the erosion/accretion balance between the years 1945 and 2002 (time period before the construction of the dams) and the years 2002 to 2007 (time period after the construction of the dams), polygons that represent eroded and accreted areas were extracted from the ArcMap database. These are illustrated in Figure 5 for the two different time periods, respectively. The boundaries of these polygons are defined by the nonintersecting parts of the two digitally extracted shorelines in each of the examined time periods.

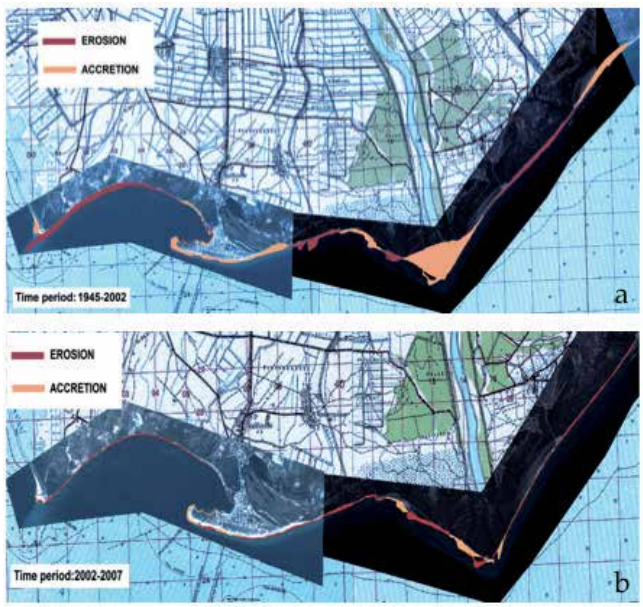

Figure 5. Eroded/accreted areas for the time periods 1945-2002 and 2002-2007

The resulting erosion/accretion balance expressed in m^2 as well as in percentages relative to the total area, is summarized in Table 3.

1945-2002	
Erosion area (m^2)	Accretion area (m^2)
1335027.90	2242207.82
Erosion percentage (%)	Accretion percentage (%)
37.32	62.68
2002-2007	
Erosion area (m^2)	Accretion area (m^2)
374892.96	243453.14
Erosion percentage (%)	Accretion percentage (%)
60.63	39.37

Table 3. Areas of erosion and accretion in the pilot study region, for the time periods 1945-2002 and 2002-2007

As it can be observed, from the year 1945 up to the year 2002 and for the considered shoreline (total length of 25 km), the erosion was about 1335028 m^2 (23421 m^2 per year) and the accretion 2242208 m^2 (39337 m^2 per year), i.e., the overall balance of the eroded/accreted areas from 1945 to 2002, indicates that accretion is the dominant mechanism covering a total area almost 1.7 times bigger than the corresponding area of the eroded parts. In other words, accretion dominates erosion by 25.36%. On the other hand, examining the same shoreline region from 2002 to 2007, the erosion was about 374893 m^2 (74979 m^2 per year) and the accretion 243453 m^2 (48691 m^2 per year), i.e., the erosion mechanism dominates accretion by approximately 21.26%. Therefore, it can be concluded that the dramatic decrease in the sediments supplied directly to the Nestos River basin outlet and indirectly to the neighboring coast, due to the construction and operation of the considered reservoirs, has almost inversed the previous state regarding the erosion/accretion balance in the considered region, just within 5 years of the construction of the dams. This finding evaluates the direct effect of the construction of the Thisavros and Platanovrysi Dams, to the erosion increase in the coastal region of the Nestos River delta and the adjacent shorelines.

2.5. New shoreline

As mentioned previously, for the purposes of the present investigation it was deemed appropriate to also extract a more recent shoreline (year 2013), in order to perform a comparison with the shorelines of the years 2002 and 2007, aiming at the quantitative investigation of the dynamic evolution of the examined coastal region, from the shoreline erosion point of view [14].

For this purpose, additional DGPS field measurements were conducted, following the same methodology and time period (spring) with the corresponding field measurements that were conducted in the year 2007. This more recent shoreline (2013) consists of three subregions: the Akroneri Cape region, the Keramoti Bay region and the region in the vicinity of the Nestos River delta.

The erosion/accretion balance between the shorelines of 2002-2007, 2007-2013, and 2002-2013 is illustrated in detail for these three subregions (Akroneri Cape in Figure 6, Keramoti Bay in Figure 7, and Nestos River delta in Figure 8).

As it can be macroscopically observed from Figure 6, in Akroneri Cape region, the eroded areas (red color) dominate the accreted areas (green color) in each one of the examined time periods. Examining both the subsequent periods 2002-2007 and 2007-2013 as well as in total the period from 2002 (considered period for reservoir construction and operation) to 2013 (most recent situation), in comparison with the initially examined period (2002-2007), it is characteristic that as years are passing, areas that in the first period were under relatively severe accretion are suffering in the subsequent periods from quite noticeable erosion.

Almost the same trend is also observed in the region of Keramoti Bay, as it can be concluded by comparing the same time periods as previously (Figure 7). In more detail, while in the initial

http://dx.doi.org/10.5772/61459

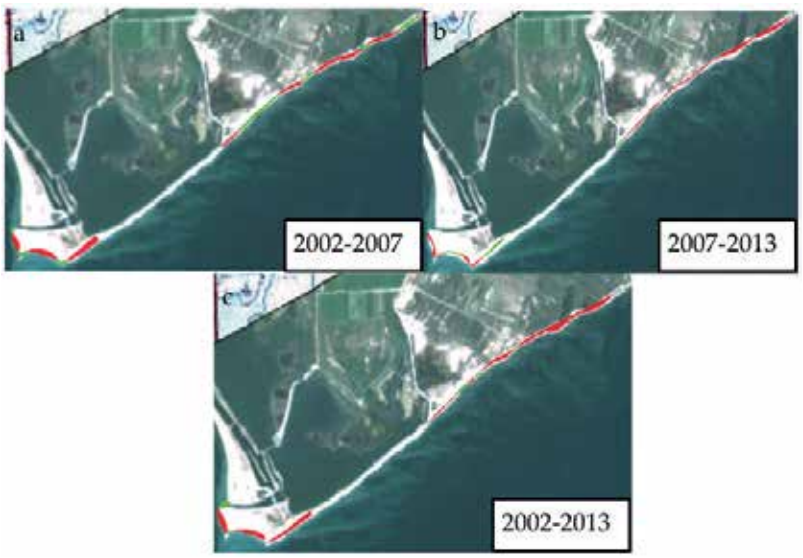

Figure 6. Erosion (red color) /Accretion (green color) balance at Akroneri Cape region

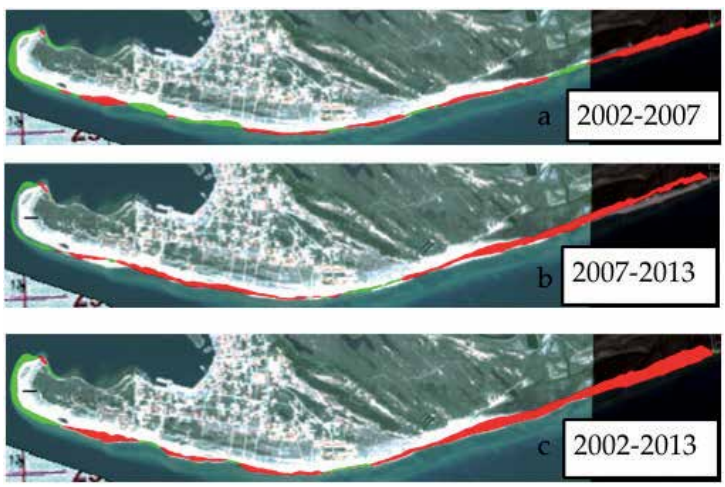

Figure 7. Erosion (red color) /accretion (green color) balance at Keramoti Bay region

time period quite big areas of erosion as well as accretion can be traced, in the subsequent time period the areas that were initially under severe accretion, are now subjected to light accretion or even under considerable erosion. Accordingly, the areas that were initially subjected to considerable erosion, present now a more intense shoreline retreat.

Regarding the region in the vicinity of the Nestos River delta, despite the fact that the shoreline presents a more intense and dynamic evolution, also in this case the initially presented

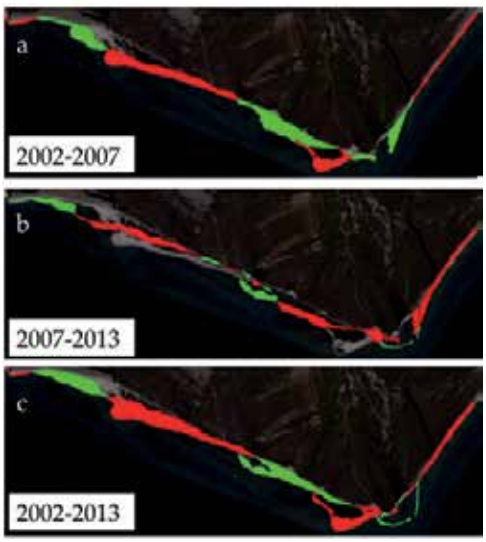

Figure 8. Erosion/accretion balance in the region of the Nestos River delta

(2002-2007) erosion/accretion balance in the subsequent time period (2007-2013) has been disturbed, indicating an increasing trend in the areas that are subjected to erosion with respect to the areas that are subjected to accretion.

All the above macroscopic observations are quantitatively summarized in Figure 9, where the percentages of erosion and accretion for the two subsequent time periods as well as for the entire examination period are depicted for each one of the examined regions.

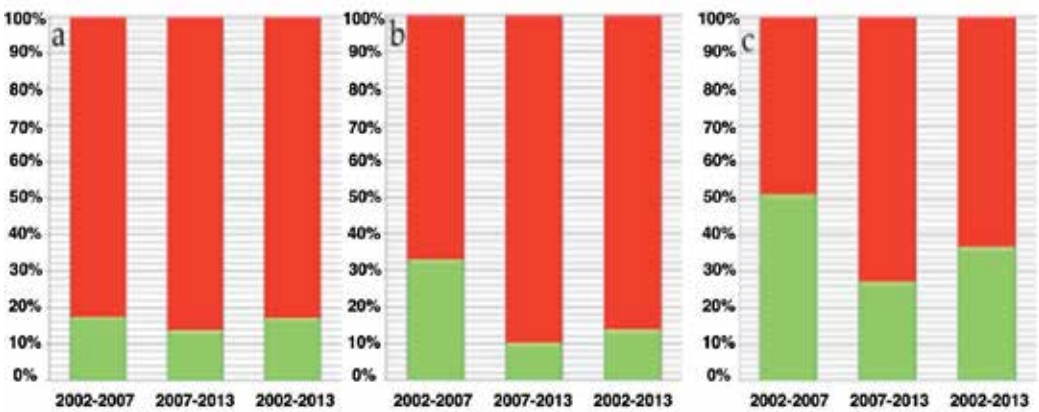

Figure 9. Erosion (red color) /accretion (green color) percentages for the considered time periods, at Akroneri Cape region (a), at Keramoti Bay region (b) and the Nestos River delta region (c)

http://dx.doi.org/10.5772/61459

As it can be observed in all three considered regions, the erosion percentage in the time period 2007-2013 shows a significant increase in comparison with the previous time period (2002-2007). At Akroneri Cape region, an increase in the areas subjected to erosion by just 4% is observed. On the other hand, in the regions of Keramoti Bay and Nestos River delta, the corresponding increase reaches 23% and 24%, respectively, within just 6 years. It is also characteristic that in the case of the Nestos River delta, while in the time period 2002-2007 an erosion/accretion balance is observed, in the subsequent time period erosion predominates accretion by a considerable percentage. All the above quantitative observations can lead to the conclusion that the predomination of erosion with respect to accretion, after the construction and operation of the two reservoirs (year 2002), shows a continuously increasing trend.

3. Evaluation of sediment management techniques for coastal erosion reduction

3.1. Overview

In this third part of the present chapter, the effect of sediment removal by dredging and flushing from the Platanovrysi Reservoir downstream is investigated, in order to evaluate the increase in the sediment budget that reaches the outlet basin, as this increase can contribute to the reduction of shoreline erosion. For this purpose, the previously validated and applied mathematical model (RUNERSET - RUNoff ERosion SEdiment Transport) is modified accordingly in order to take into account sediment dredging and flushing applications. The proposed modifications involve the addition of different amounts of eroded material (sediment) in the subbasin that lies directly downstream of the Platanovrysi Reservoir for dredging processes as well as the inclusion of a flushing discharge. In more detail, a parametric investigation is conducted using a wide series of simulated scenarios, aiming to identify the optimum periods that dredging and flushing can be applied in order to maximize the increase of the sediment that is transported and reach the basin outlet [13].

3.2. Application of sediment dredging technique to Platanovrysi Reservoir

In order to investigate the possible contribution of the mechanical removal (dredging) of sediment from the Platanovrysi Reservoir, and its deposition in the subbasin downstream of the Platanovrysi Dam, the mathematical model RUNERSET [10] was accordingly modified. In more detail, the proposed modification involves the addition of different, eroded sediment amounts in Subbasin 7 (Figure 1) for specific months of each year, for the time period 1980-1990.

A total number of 888 simulations were conducted for the years 1980-1990 assuming the following scenarios: application of dredging in each month of each year and for various amounts of sediment removal. Initially, diagrams of the total annual amount of sediment that reaches the basin outlet, versus the amount of sediment that was removed by dredging from the Platanovrysi Reservoir, were constructed. Figure 10 illustrates indicatively these diagrams for two of the considered years.

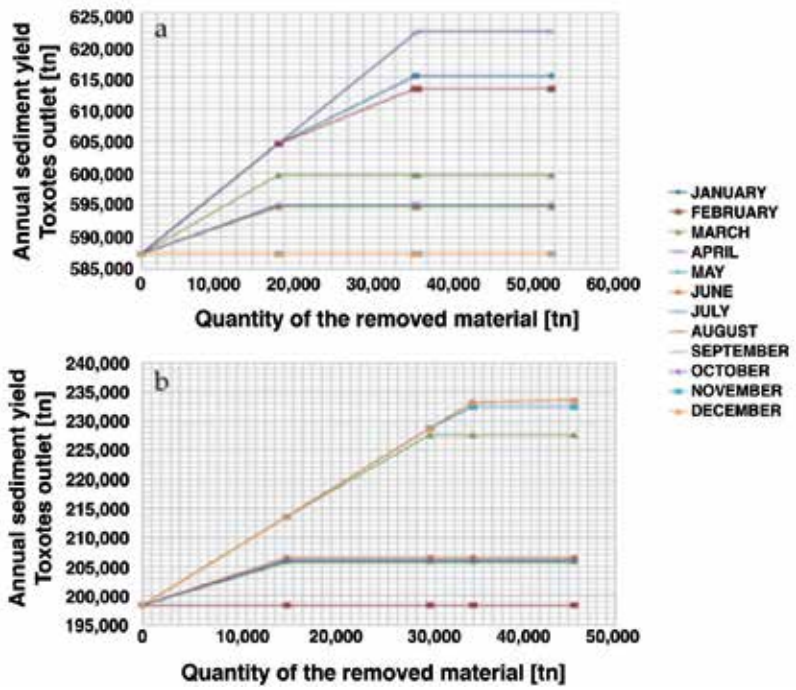

Figure 10. Indicative results from simulated dredging scenarios for the years 1981 (a) and 1986 (b)

From these diagrams it is obvious that for dredging scenarios in specific months of the year, the total annual sediment amount that reaches the basin outlet is higher than the corresponding amount in the rest of the months. Therefore, the months of the year can be clearly classified as "effective" and "ineffective" for a dredging application. In more detail, from the overall analysis of the simulation results, it can be concluded that January, February, March, April, November, and December can be, in general, characterized as "effective" months, while for the time period from May to October (ineffective months), a potential dredging application would not alter significantly the annual sediment amount that reaches the outlet of the river. The month classification in "effective" and "ineffective" is summarized schematically in Figure 11 (a), where the additional annual amount of dredged sediment that reaches Toxotes outlet of the river (Figure 1), is plotted against the amount of sediment that was removed in the specific month of the year in each case, for the overall simulated scenarios.

It has also to be mentioned that for amounts of sediment removal up to 35000 tn and for dredging scenarios in the effective months of the year, the ratio of the additional sediment amount that reaches Toxotes outlet, to the removed sediment amount, is equal to unity. This indicates that, generally, up to a limiting value of 35000 tn of dredged sediment from the Platanovrysi Reservoir, in an effective month, all of this removed amount of sediment will reach Toxotes outlet. Moreover, from a certain amount of removed sediment and above, there is not any change in the amount of sediment that reaches the basin outlet. This indicates that there is a maximum transport quantity of dredged material that the Nestos River can transport

http://dx.doi.org/10.5772/61459

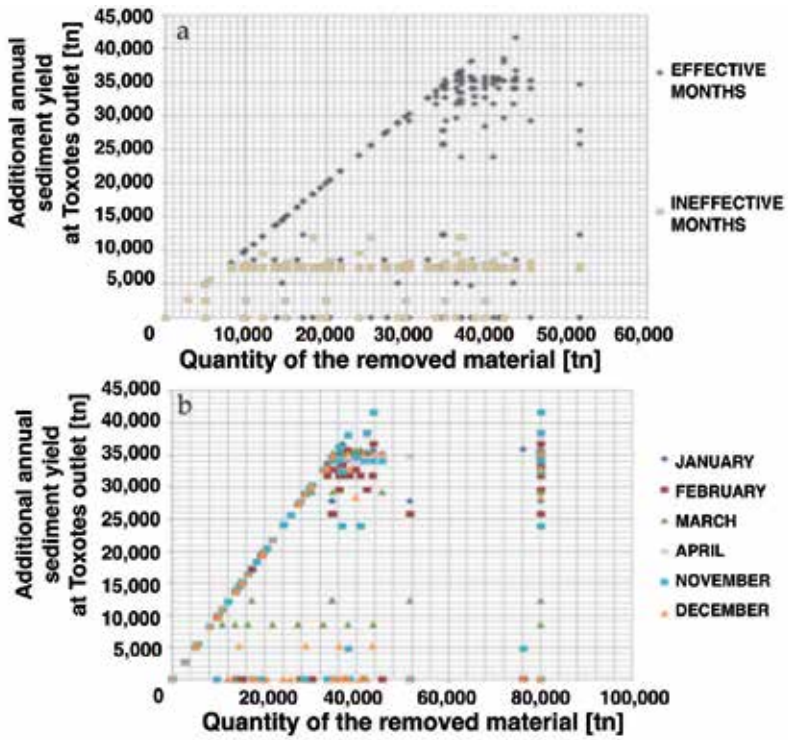

Figure 11. (a) Effective and ineffective months for dredging application, (b) Result of dredging application during the effective months of the year (the data points represent the overall simulated scenarios)

up to the basin outlet. This limiting amount varies accordingly for each month. Therefore, it is vital to define the month of the year in which this sediment transport quantity is maximized. Figure 11 (b) indicates that the maximum value of sediment surplus that reaches the basin outlet, takes place if dredging is applied in November.

However, for November there are also a lot of simulations that resulted in a zero sediment surplus at the basin outlet (in some of the overall simulated years). This means that while the Nestos River can transport the maximum amount of sediment that reaches the basin outlet, if the dredging application is performed during November for a certain year, it is also possible in a different year that no sediment at all reaches the outlet. Therefore, an additional classification of the "effective" months to "consistent" and "inconsistent" must be conducted. According to the diagram of Figure 11 (b), the months January and April can be characterized as "consistent," while February, March, November, and December can be characterized as "inconsistent."

In order now to investigate the most "effective" and "consistent" month of the year for applying sediment dredging, between January and April, a direct comparison of these two months was conducted. For this purpose, the overall results from all the simulated years (1980-1990) and for all the amounts of dredged sediment were collected, for January and April.

The quantitative analysis of the proposed simulation results indicated that the overall sediment dredging performance of these two months could be classified into three distinct parts. The first part refers to dredging scenarios with sediment removal up to 34400 tn, in which the performance of each month with respect to the amount of sediment surplus that reaches the basin outlet is the same, having a value of 100%. The second and third parts consist of dredging scenarios with sediment removal from 34400 tn up to 36150 tn and greater than 36150 tn, respectively. In these last two parts of the collected data, the performance of each month is different, having values also lower than 100%. Taking into account the fact that the Nestos River cannot in general transport to the basin outlet dredged sediment amounts greater than 35000 tn, the third part of the resulting data was neglected from the comparison process. For the proposed comparison, the mean value of the dredged sediment amount that did not reach the basin outlet was taken as the effectiveness criterion, while the corresponding standard deviation was used as the criterion for consistency. The overall analysis from the comparison between January and April is summarized in Table 4. It is obvious that April can be assumed as the most suitable month of the year for a dredging application to the Platanovrysi Reservoir. It is also worth mentioning that the sediment amount of 35000 tn, that is, the maximum amount of dredged sediment that can reach the outlet of the Nestos River, is equal to 2.46% of the mean annual sediment yield of the river at its outlet, before the construction of the considered dams, and the 10.95% of the mean annual yield of the river after the construction and operation of the reservoirs. Finally, this sediment amount also constitutes the 11.53% of the mean annual sediment yield that reaches the Platanovrysi Reservoir.

	Quantity of removed material [tn]	**Additional annual sediment yield at Toxotes outlet [tn]**			
		JANUARY	**Nondelivered sediment quantity [tn]**	**APRIL**	**Nondelivered sediment quantity [tn]**
34400	27806	6594	34400	0	
34625	34626	-1	34625	0	
34744	27806	6938	34744	0	
34825	34825	0	34102	723	
34903	34902	1	34101	802	
36150	35238	912	36150	0	
Mean value	34941.17	32533.83		34687	
Mean attribution [%]	–	93.11		99.27	
		Mean value	2407.33	Mean value	254.17
		Standard deviation	3396.38	Standard deviation	394.55

Table 4. Comparison of effectiveness and consistency between January and March for dredging application

http://dx.doi.org/10.5772/61459

3.3. Application of sediment flushing to Platanovrysi Reservoir

In order to investigate the possibility of minimizing shoreline erosion due to the construction of the proposed dams, with the application of flushing, the mathematical model RUNERSET was accordingly modified, in order to take into account the corresponding flushing discharge. Also in these series of simulations, the model was applied for the years 1980–1990. For the calculation of the flushing discharge, Equation (12) was used assuming that the sediment flushing discharge is known [11]:

$$Q_f = \left(\frac{Q_s}{3,5 \cdot 10^{-3} \cdot \left(S \cdot 10^4 \right)^{1,8}} \right)^{1/1,2} \quad Q_f = \left(\frac{Q_s}{3,5 \cdot 10^{-3} \cdot \left(S \cdot 10^4 \right)^{1,8}} \right)^{1/1,2} \quad Q_f = \left(\frac{Q_s}{3,5 \cdot 10^{-3} \cdot \left(S \cdot 10^4 \right)^{1,8}} \right)^{1/1,2} \tag{12}$$

where Qs is the removed sediment discharge from the reservoir during a flushing event (tn/s); S is the bottom slope along the flushing channel, assuming that the flow is uniform and therefore the slope of the energy line and the flow line coincide; and Q_f: is the flushing discharge (m^3/s).

In order to determine the optimum month of the year for the application of flushing in the Platanovrysi Reservoir, a series of simulations were performed with a sediment flushing discharge of 0.0135 tn/s (that corresponds to the value of 35000 tn) and for flushing events occurring in different months. The results are summarized in Table 5.

	PERCENTAGE OF FLUSHED SEDIMENT THAT REACHES TOXOTES OUTLET [%]										
1980	**1981**	**1982**	**1983**	**1984**	**1985**	**1986**	**1987**	**1988**	**1989**	**1990**	
JAN	**99.99**	**79.50**	**100.00**	**100.00**	**100.00**	**99.99**	**99.88**	**99.99**	**99.91**	**100.00**	**100.00**
FEB	95.71	73.78	90.94	93.72	0.00	99.99	0.00	0.00	84.48	90.86	90.97
MAR	99.99	35,20	100.00	100.00	0.00	24.55	83.59	99.99	0.00	100.00	100.00
APR	**99.99**	**99,22**	**99.22**	**97.44**	**100.00**	**97.42**	**97.59**	**0.00**	**99.91**	**97.43**	**97.45**
MAY	34.26	21.77	24.06	22,88	21.46	21.98	21.58	22.54	27.61	21.70	21.55
JUN	20.83	20.91	20.92	0.00	20.89	20.83	23.58	23.68	0.00	20.84	20.86
JUL	21.40	21.48	21,78	7.45	21.46	21.69	22.43	21.68	21.61	21.70	21.55
AUG	21.40	21.48	21.49	21.56	21.46	21.69	21.58	21.68	21.61	21.70	21.55
SEP	20.83	20.91	20.92	20.85	20.89	20.83	20.72	20.82	20.75	20.84	20.86
OCT	21.40	21.48	21.49	21.56	21.46	21.69	21.58	21.68	20.75	0.00	21.55
NOV	92.56	0.00	68.36	99.15	97.48	99.99	97.59	13.68	99.91	0.00	97.45
DEC	0.00	0.00	0.00	81.18	100.00	99,99	99.88	0.00	0.00	94.00	14.58

Table 5. Results from simulations of flushing scenarios for different months of the year

It is obvious that the optimum month for the application of a flushing event, in order to maximize the overall flushed sediment amount that reaches the basin outlet, and therefore decreases the indirect shoreline erosion, is January and not April (as in the corresponding investigation for the application of dredging). However, April is found to be the second most effective month. In the literature it is stated that in order to maximize the amount of sediment that is removed from a reservoir and therefore restore its storing capacity, a flushing event will be more effective if it occurs at the beginning of the ice melting period [11]. Therefore, from this point of view, April could be characterized as the optimum month of the year for the application of a flushing event.

In order to calculate the river's maximum transport quantity of flushed sediment at the outlet of its basin, additional scenarios of continuous through each year flushing events were simulated. For this purpose, the mathematical model RUNERSET was further modified in order to take into account sediment flushing discharge equal to 0.1 tn/s, a value much greater than the previously identified critical value of 0.0135 tn/s. From the analysis of the results it is found that the Nestos River could transport to the basin outlet approximately 200000 tn of additional sediment, if the flushing of sediment was applied continuously during the whole year. It is worth mentioning that this amount constitutes the 62% of the mean annual sediment yield today.

Taking into account that the application of flushing could be more effective, at least from the point of view of limiting shoreline erosion, during certain months of the year (time period from November to April), additional continuous flushing scenarios were simulated for the period of the six more effective months of the year for each of the considered years (1980-1990). The overall results are summarized in Figure 12.

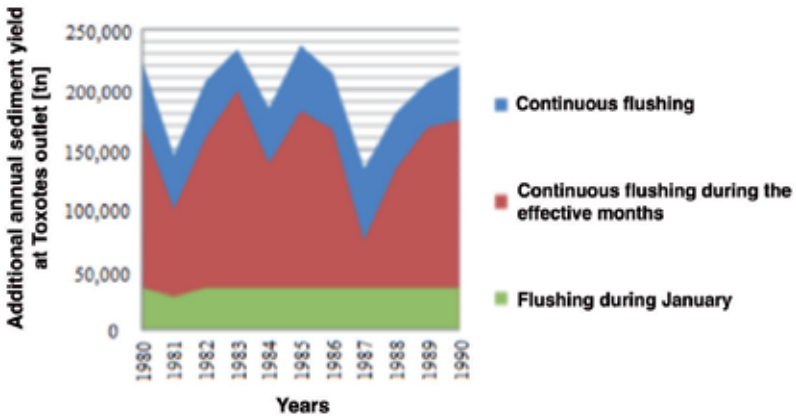

Figure 12. Results from simulated flushing scenarios

Examining Figure 12, it can be concluded that in the case that the continuous flushing event happens during the six of the most effective months of the year, the amount of sediment that reaches the basin outlet of the Nestos River reaches the 76.5% of the corresponding amount in

http://dx.doi.org/10.5772/61459

the case of continuous flushing throughout the whole year. Moreover, in the case that the sediment flushing event is applied only during January the amount of sediment that reaches the outlet constitutes the 17.35% of the maximum possible amount (continuous flushing throughout the year). This amount is also equal to the 73.5% of the amount that would reach Toxotes outlet, in the case of a continuous flushing event during the noneffective months of the year (period from May to October).

3.4. Comparison of the considered sediment removal methods

In order to select the optimum of the two examined methods, a comparison was conducted by collecting the maximum amount of sediment that reaches the basin outlet of the Nestos River, that are attributed, if each method is applied in its optimum identified month of the year; April for the application of mechanical sediment removal, and January for the application of sediment flushing.

In order to calculate these quantities, a sediment discharge (dredging/flushing) greater than the previously used values of 35000 tn for the case of dredging and 0.0135 tn/s for the case of flushing was assumed. In more detail, the mathematical model was further modified in order to take into account a sediment discharge of Q_s=289200 tn and q_{sf}=0,1 tn/s, since it was proven that for values generally above 35000 tn (approximately 0.0135 tn/s for the case of a flushing event with a duration of 30 days), the results of the simulations did not change. The results of the proposed comparison are summarized diagrammatically in Figure 13.

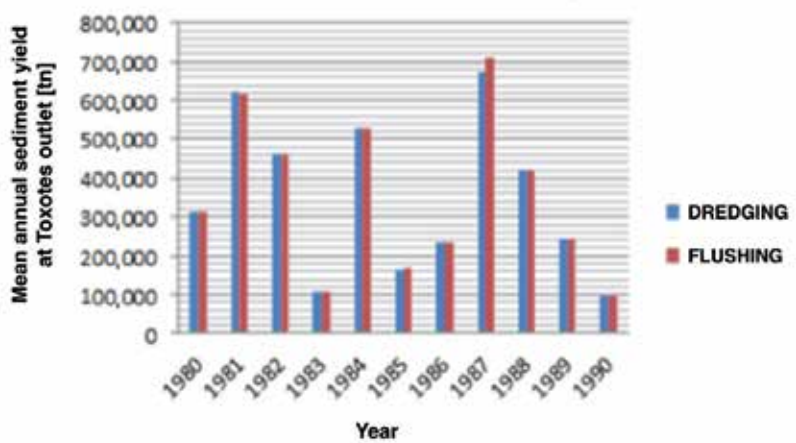

Figure 13. Comparison between dredging and flushing

It can be seen that flushing seems to perform slightly better than dredging but in a degree that cannot be chosen as the optimum method. Therefore, in order to choose the optimal method for the aim of the present investigation, other criteria such as technical difficulties in their application as well as cost of application should be taken into consideration.

4. Conclusions

Coastal erosion that is generated by the reduction of the annual sediment yield at river outlets due to the construction of dams constitutes one of the main environmental problems in many parts of the world. Nestos is one of the most important transboundary rivers, characterized by its great biodiversity. The Nestos River flows through two European countries, Bulgaria and Greece, and discharges its water into the Aegean Sea. In the Greek part of the river, two dams, the Thisavros Dam and the Platanovrysi Dam, have already been constructed and started operating in 1997 and 1999, respectively. The construction of the dams implies a reduction of sediment yield at the outlet of the Nestos River basin and the alteration of the sediment balance of the basin in general, which results in coastal erosion.

The present chapter deals with the assessment of reservoir sedimentation effect on the coastal erosion for the case of the Nestos River delta and the adjacent shorelines, through mathematical modeling, remote sensing techniques, and field surveying. The mathematical model is applied for the estimation of the sediment yield reduction at the outlet of the river due to the subsequent sediment accumulation within the reservoirs, while a shoreline change monitoring methodology is applied for the estimation of the alteration of the erosion/accretion balance in the wider coastal region of the Nestos River delta, examining the proposed balance in two different time periods, before and after the construction of the dams.

The mathematical model results indicate that the construction of the considered dams has caused a dramatic decrease (about 83%) in the sediments supplied directly to the basin outlet (delta) and indirectly to the neighboring coast. Comparing the overall balance of the eroded and accreted areas in the region, before and after the construction and operation of the reservoirs, it can be concluded that the decrease in the sediments supplied directly to the Nestos River basin outlet and indirectly to the neighboring coast, has almost inversed the previous situation (where accretion predomin;ated erosion by 25.36%), just within 5 years of the construction of the reservoirs, with erosion now predominating accretion by 21.26%. The extraction of a more recent shoreline and the corresponding comparison with the previously identified shoreline states clearly indicates a continuously increasing trend in the predomination of erosion in relation to accretion.

Based on the above, it emerges that the construction and operation of the Thisavros and Platanovrysi Reservoirs have significantly increased coastal erosion in the Nestos River delta and the adjacent shorelines. This fact, together with the anticipated rise of sea level, may pose a great problem to the coastal area resources, threatening the local communities and ecosystems of the considered region. Therefore, it is necessary to further investigate the sediment budget within the estuarine and the adjacent coastal systems and to further monitor erosion/accretion trends of the region for the coming decades.

In the present chapter also, a previously validated and applied mathematical model is modified accordingly in order to take into account the application of sediment dredging and flushing in a reservoir of river hydrological basin. The modified model is applied for the case of the Nestos River (Greece) in order to identify the optimum sediment removal scenario in a

http://dx.doi.org/10.5772/61459

certain reservoir (Platanovrysi Reservoir) upstream of the considered river outlet (Toxotes outlet), in order to maximize the amount of sediment that reaches the delta of the river. In more detail, a wide series of parametric simulation scenarios is performed, aiming to identify the optimum periods that the dredging and flushing can be applied. From the overall analysis of the simulation results, a definite classification of the months into "effective" and "ineffective" as well as into "consistent" and "inconsistent" with respect to the total amount of removed sediment that reaches the basin outlet is made. It is also found that the considered river has a maximum transport capacity of the removed material, regardless of the further increase of the dredged and/or flushed sediment capacity from the identified limiting value. A comparison between the two considered methods identified flushing to be slightly more effective than dredging.

Finally, the overall results of the present investigation indicate that the proposed modified mathematical model can serve as a quite effective and useful tool that can be applied for similar investigations at various river basins worldwide and it could also be incorporated into the early design stages of new reservoirs that are going to be constructed, estimating the amount of sediment discharge that needs to pass through the reservoir in the downstream part of the river basin in order to minimize the unavoidable deltaic and adjacent shoreline erosion.

Acknowledgements

The authors would like to acknowledge the financial support from the Research Project, INTEREG IIIC BEACHMED-e, "Strategic management of beach protection for sustainable development of Mediterranean coastal zones."

Author details

Manolia Andredaki[1], Anastasios Georgoulas[2*], Vlassios Hrissanthou[1] and Nikolaos Kotsovinos[1]

*Address all correspondence to: anastasios.georgoulas@gmail.com

1 Department of Civil Engineering, Democritus University of Thrace, Xanthi, Greece

2 Department of Engineering, University of Bergamo, Dalmine (BG), Italy

References

[1] Ly C.K. 1980, The role of the Akosombo Reservoir on the Volta river in causing coastal erosion in central and eastern Ghana (West Africa), *Mar Geol*, Vol. 37, pp. 323-332.

[2] Chen X. and Zong Y. 1998, Coastal erosion along the Changjiang deltaic shoreline, China: history and prospective, *Estuar Coast Self Sci*, Vol. 46, pp. 733-742.

[3] El-Raey M., Sharaf El-Din S.H, Khafagy A.A. and Abo Zed A.I. 1999, Remote sensing of beach erosion/accretion patterns along Reservoirietta-Port Said shoreline, Egypt, *Int J Remote Sensing*, Vol. 20, No. 6, pp. 1087-1106.

[4] Malini B.M. and Rao K.N. 2004, Coastal erosion and habitat loss along the Godavari delta front – a fallout of reservoir construction (?), *Curr Sci*, Vol. 87, No. 9, pp. 1232-1236.

[5] Chen X., Yan Y., Fu R., Dou X. and Zhang E. 2008, Sediment transport from the Yangtze River, China, into the sea over the Post-Three Gorge Reservoir Period: A discussion, *Quater Int*, Vol. 186, pp. 55-64.

[6] Liu C., Sui J. and Wang Z. 2008, Sediment load reduction in Chinese rivers, *Int J Sed Res*, Vol. 23, pp. 44-55.

[7] Huang G. 2011, Time lag between reduction of sediment supply and coastal erosion, *Int J Sed Res*, Vol. 26, pp. 27-35.

[8] Zhang W., Mu S., Zhang Y. and Chen K. 2011, Temporal variation of suspended sediment load in the Pearl River due to human activities, *Int J Sed Res*, Vol. 26, pp. 487-497.

[9] Samaras A.G. and Koutitas C.G. 2008, Modelling the impact on coastal morphology of the water management in transboundary river basins: The case of River Nestos, *Manag Environ Qual: Int J*, Vol. 10, No. 4, pp. 455-466.

[10] Andredaki M., Georgoulas A., Hrissanthou V. and Kotsovinos N. 2014, Assessment of reservoir sedimentation effect on coastal erosion in the case of Nestos River, Greece, *Int J Sed Res*, Vol. 29, pp. 34-48.

[11] Morris G.L. and Fan J. 1998, *Reservoir Sedimentation Handbook*. New York: McGraw-Hill Book Co.

[12] Basson G. and Rooseboom A. 1997, Dealing with reservoir sedimentation. South African Water Research Commission.

[13] Andredaki M., Georgoulas A. and Hrissanthou V. 2014, Sediment management in reservoirs in order to reduce shoreline erosion: The case of Nestos River, Greece, 4th International Symposium on Sediment Management, 14-16 September, Ferrara, Italy (Paper ref. no. 112).

[14] Andredaki M. 2014, Effect of reservoir sedimentation on shoreline erosion – The example of Nestos River, PhD Thesis, Sector of Hydraulic Structures, Department of Civil Engineering, Democritus University of Thrace, Xanthi, Greece.

http://dx.doi.org/10.5772/61459

[15] Giakoumakis S., Tsakiris G. and Efremides D. 1991, On the rainfall-runoff modeling in a Mediterranean island environment. In: *Advances in Water Resources Technology*, ed. by G. Tsakiris, Balkema, Rotterdam, pp. 137-148.

[16] SCS (Soil Conservation Service) 1972, *National Engineering Handbook*. Section of Hydrology, SCS, Washington DC, USA.

[17] Doorenbos J. and Pruitt W. O. 1977, Crop water requirements. FAO, Irrigation and Drainage Paper 24 (revised). FAO, Rome, Italy.

[18] Thornthwaite C. W. 1948, An approach towards a rational classification of climate. *Geographic Rev*, Vol. 38, pp. 55-94.

[19] Schmidt J. 1992, Predicting the sediment yield from agricultural land using a new soil erosion model. Proceedings 5th International Symposium on River Sedimentation, ed. by P. Larsen and N. Eisenhauer, Karlsruhe, Germany, pp. 1045-1051.

[20] Yang C. T. 1973, Incipient motion and sediment transport. *J Hydraul Div*, ASCE, Vol. 99, No. 10, pp. 1679-1704.

[21] Gergov G. 1996, Suspended sediment load of Bulgarian rivers. *GeoJournal*, Vol. 40, No. 4, pp. 387-396.

[22] Kapona E. and Tona E. 2003, Computation of the inflowing sediments into Thisavros Reservoir of Nestos River. Diploma Thesis, Department of Civil Engineering, Democritus University of Thrace, Xanthi, Greece (in Greek).

[23] Klisiari A. 2002, Computation of the inflowing sediments into Platanovrysi Reservoir of Nestos River. Diploma Thesis, Department of Civil Engineering, Democritus University of Thrace, Xanthi, Greece (in Greek).

[24] Hrissanthou V. 2002, Comparative application of two erosion models to a basin. *Hydrol Sci J*, Vol. 47, No. 2, pp. 279-292.

Local Scour

Chapter 5

The Impact of Ice Cover and Sediment Nonuniformity on Erosion Around Hydraulic Structures

Peng Wu, Jueyi Sui and Ram Balachandar

Additional information is available at the end of the chapter

http://dx.doi.org/10.5772/61468

Abstract

Based on two case studies, the impact of ice cover on local scour around bridge piers is presented in this chapter. Bed material with different grain sizes is used and ice covers with different roughness is used to study the scour characteristics. The impact of nonuniformity of sediment is also investigated. Results show that with the increase in densimetric Froude number, there is a corresponding increase in the dimensionless scour depth. For nonuniform sediment, due to the formation of an armor layer, less maximum scour depth was noted around bridge foundation structures compared to uniformly distributed sediment. The increase in ice cover roughness results in a larger scour depth and geometry. The results indicate that it is imperative to pay attention to the impact of ice cover on the scour around hydraulic structures.

Keywords: ice cover, local scour, non-uniform sand, bridge abutment

1. Introduction

1.1. Sediment transport around hydraulic structures

Sediment transport embodies the processes of erosion, entrainment, movement, and deposition. In nature, these processes are always present. Although there are many types of sediment, fluvial sediment is one of the most common. It comprises sediment accumulated by the erosion of rock and mineral particles that are transported by flowing water. The process of erosion is complex and plays a vital role in the formation of different landscapes of the world we live in.

Statistics show that thirteen of the large rivers in the world carry sediment loads in excess of 5.8 billion tons annually [5]. In addition to producing large quantities of sediment, erosion also causes other problems such as the pollution of water body and altering the runoff conditions.

Additionally, from the perspective of hydraulic engineering, sediment transport can result in serious on-site damage to hydraulic structures such as bridge abutments, bridge piers, spur dikes, etc.

The presence of a hydraulic structure in a river introduces the phenomenon of local scour. The interaction between flow and structures has been an actively researched topic in the past decade. Reynolds stress is an important parameter to quantify the suspended load of sediment transport, while the bed shear stress is pertinent to determine the bed load of sediment transport. Kuhnle et al. [14] examined the three-dimensional flow field around a submerged spur dike. An amplification factor of bed shear stress 3 was found. Duan et al. [7] measured the flow and turbulence around an experimental spur dike in a flat and scour bed. Differences of mean velocity, turbulent intensity, and Reynolds stresses between those two flow fields were analyzed. The bed shear stress calculated from the Reynolds stresses was 2-3 times that of the incoming flow. Since the abutment and spur dike have similar contraction impact on the flow, all the three studies showed similar amplification factor of bed shear stress in open channel flow.

1.2. Impact of ice cover

Extensive studies have been conducted to study the local scour around structures in the past few decades. However, most of the previous studies were focused on flow in open channels. The impact of ice cover on local scour has not been well understood. For many regions in the northern hemisphere, winter may last up to six months. Figure 1 shows the ice cover around Ambassador Bridge, Windsor, Canada, which is located on the Detroit River. It can be seen from Figure 1 that the region around the pier is completely covered by ice. The presence of the ice cover affects the flow characteristics of the river. Hence, further research on the impact of ice cover on the local scour around bridge piers becomes important.

As pointed out by Morse and Hicks [21], fundamental problems of ice engineering are primarily related to ice jams, floods, and transportation over ice. River ice hydrology has been an implicit part in ice engineering. Some studies on ice engineering research can be found in the references [1,12,22,9,21,23,26,30,32]. To date, the mechanism of local scour around bridge abutments and piers under ice cover is still not well understood.

Lau and Krishnappan [15] used the k-ε turbulence model to numerically determine the velocity distribution and suspended load transport under ice cover. The assumption was that the ice covered flow can be treated as two-layer flow which is divided at the location of maximum velocity. Based on the assumption that the mechanics of bed-form formation is the same for open and ice covered channels, Smith and Ettema [27] developed a method from flume data for estimating the flow resistance in ice covered channels. Ettema et al. [8] proposed a different approach to estimate the sediment transport under ice cover by using the procedures from open channel flow. The variation of ice cover roughness and flow cross sections under ice cover can limit the accuracy of this method. Ettema and Daly [9] conducted a series of flume experiments on the sediment transport under ice cover. Since the flow distribution is substantially modified by ice cover, the sediment transport under ice cover is hard to estimate. Sui et al. [26] conducted a series of flume experiments for the incipient motion under different flow

http://dx.doi.org/10.5772/61468

and boundary conditions. The influence of ice cover roughness has been assessed. They found that the slope of ice cover has a great impact on the critical dimensionless shear stress for the river sediment motion.

Figure 1. The ice cover around bridge piers (Ambassador Bridge, Windsor, ON, Canada, 2015)

1.3. Impact of nonuniformity of sediment

Incipient motion of the particles is an important criterion that determines the motion of the sediment particles. When the flow attains or exceeds the criteria for incipient motion, sediment particles along the alluvial channel start to move. As defined by Yang [33], if the motion is rolling, sliding, or jumping along the bed, it is called bed load transport. If the particle is supported by the upward components of turbulent currents and stays in suspension, it is called suspended load transport.

For nonuniform sediment, no single critical grain diameter can be determined to distinguish which size of sediment moves and which does not for any specific conditions. Therefore, the incipient motion of bed material is also the beginning of armor process of the bed surface [5]. With the development of an armor layer, further sediment transport is inhibited. Since nonuniform sediment makes up the typical bed composition in natural rivers, the study of the impact of nonuniformity has to be considered with the formation of armor layer.

The forces acting on a sediment particle at the bottom of the scour hole under ice cover are shown in Figure 2. In natural rivers, the velocity profile is similar to the one shown in Figure 2, which exaggerates the impact of ice cover. Herein, the figure is used to show the impact of ice cover on velocity profile around bridge piers and abutments.

For most natural rivers, the river slopes are small enough that the component of gravitational force acting on the particle in the direction of flow can be neglected. As shown in Figure 2, the forces to be considered related to the incipient motion are the drag force F_D, lift force F_L, submerged weight W, and the resistance force F_R. The angle of the scour hole with vertical abutment is α.

A sediment particle is at a state of incipient motion when the following conditions have been satisfied:

$$\begin{cases} F_D = F_R \sin\alpha \\ W = F_L + F_R \cos\alpha \end{cases} \tag{1}$$

From existing literature it is apparent that studies on local scour around hydraulic structures under ice covered conditions with nonuniform sediments are limited. The effects of ice cover and nonuniformity have to be considered in the analysis of local scour. In this chapter, Equation (1) and Figure 2 are used as the basis for analysis of incipient motion under ice cover. The force analysis of a particle under ice cover is conducted by introducing the armor layer particle size. At the end, dimensionless shear stress is calculated by using ADV (Acoustic Doppler Velocimetry) data.

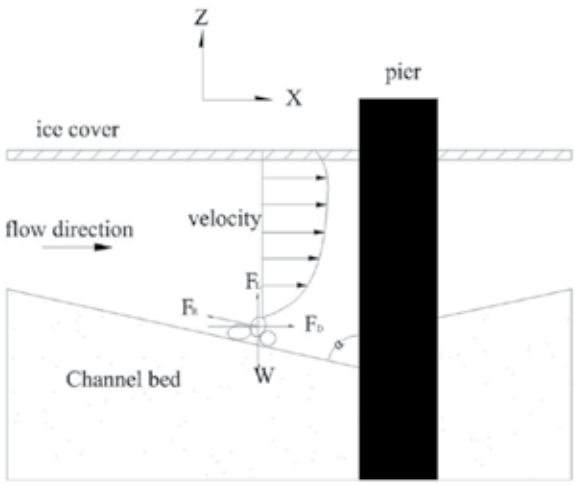

Figure 2. Incipient motion in the scour hole under ice cover (modified by [30])

2. Case studies

2.1. Experimental setup and measurement

The first case study was conducted in a 40-m long, 2-m wide, and 1.3-m deep flume with two sand boxes. The flume is a large-scale flume located at Quesnel River Research Center, BC, Canada. The aim of this case study was to investigate the ice cover impact on bridge abutment with nonuniform sediment. Smooth and rough ice covers were used. Styrofoam is commonly used to simulate ice cover in both case studies. Two different nonuniform sediments were used with D_{50} of 0.58 mm and 0.47 mm, respectively. The geometric standard deviations (σ_g) were

http://dx.doi.org/10.5772/61468

all larger than 1.4 for the sediments, hence they can be treated as nonuniform sediment. The D_{90} of the two sediments was 2.57 mm and 1.19 mm, respectively. The sieve analysis of sediments can be found in Figure 3. Square and round abutment models were made with an equivalent diameter of 200 mm. A constant blockage of 10% was used for all experiments. Table 1 summarizes the running conditions. In all, 36 experiments were conducted.

Abutment type	Cover condition	D_{50} (mm)	Water depth (m)	Approaching velocity (m/s)
Square	Open	0.58	0.07	0.26
Square	Open	0.58	0.07	0.21
Square	Open	0.58	0.19	0.21
Round	Open	0.58	0.07	0.21
Round	Open	0.58	0.19	0.23
Round	Open	0.58	0.07	0.26
Round	Smooth	0.58	0.07	0.23
Round	Smooth	0.58	0.19	0.20
Round	Smooth	0.58	0.07	0.20
Square	Smooth	0.58	0.07	0.20
Square	Smooth	0.58	0.19	0.16
Square	Smooth	0.58	0.07	0.23
Square	Rough	0.58	0.07	0.22
Square	Rough	0.58	0.07	0.20
Square	Rough	0.58	0.19	0.14
Round	Rough	0.58	0.07	0.20
Round	Rough	0.58	0.19	0.20
Round	Rough	0.58	0.07	0.22
Square	Open	0.47	0.07	0.26
Square	Open	0.47	0.07	0.21
Square	Open	0.47	0.19	0.21
Round	Open	0.47	0.07	0.21
Round	Open	0.47	0.19	0.23
Round	Open	0.47	0.07	0.26
Round	Smooth	0.47	0.07	0.23
Round	Smooth	0.47	0.19	0.20
Round	Smooth	0.47	0.07	0.20

Abutment type	Cover condition	D_{50} (mm)	Water depth (m)	Approaching velocity (m/s)
Square	Smooth	0.47	0.07	0.20
Square	Smooth	0.47	0.19	0.16
Square	Smooth	0.47	0.07	0.23
Square	Rough	0.47	0.07	0.2
Square	Rough	0.47	0.07	0.20
Square	Rough	0.47	0.19	0.14
Round	Rough	0.47	0.07	0.20
Round	Rough	0.47	0.19	0.20
Round	Rough	0.47	0.07	0.22

Table 1. Summary of Case 1

H (mm)	Surface condition	Test Number	D (mm)	H/D	D/D_{50}
108	Open channel	A1	16	6.8	31
		A2	30	3.6	59
		A3	42	2.6	82
		A4	90	1.2	176
	Ice cover	B1	16	6.8	31
		B2	30	3.6	59
		B3	42	2.6	82
		B4	90	1.2	176

Table 2. Summary of Case 2 (H represents flow depth; D is the pier diameter)

In each experiment, a 10 MHz SonTek ADV was used to measure the 3D flow velocity in the vicinity of abutments. For the ADV measurement, two values were used to ensure the measurements can provide an accurate representation of the flow velocity: signal-to-noise ratio (SNR) larger than 15 db and the correlation (COR) between 70% and 100%. Then, the data were analyzed by WinADV (Wahl, 2000). However, due to the limitations of ADV, the velocity profile close to the ice cover could not be measured.

The second case study was conducted at the Sedimentation and Scour Study Laboratory at the University of Windsor. The flume has a dimension of 12 m long, 1.2 m wide. The aim of this study was to investigate the ice cover impact on scour around a bridge pier. Only one type of ice cover and one uniform sediment with D_{50} of 0.51 mm was used. The sieve analysis of

http://dx.doi.org/10.5772/61468

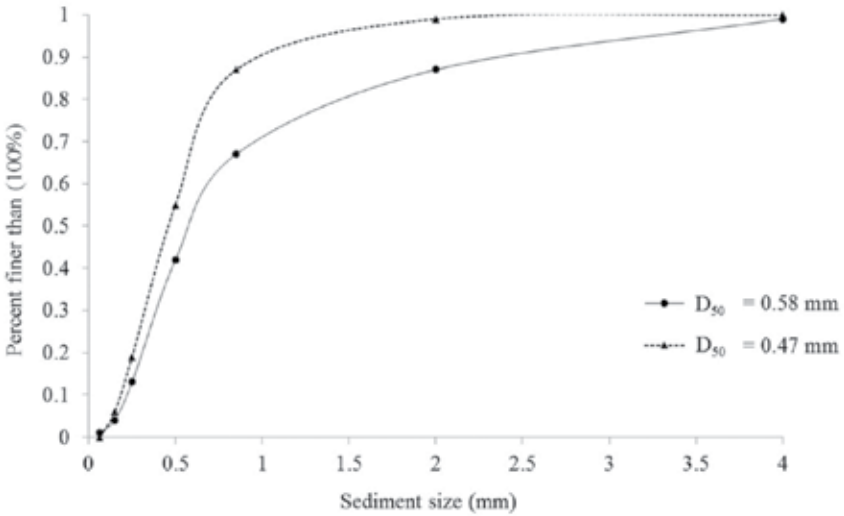

Figure 3. Sieve analysis of sediments used in Case 1

sediment is presented in Figure 4. Four pier diameters and one water depth was selected for comparison. In all, 8 experiments were conducted. Table 2 summarizes the test conditions in the case study. This study aims to investigate the ice cover impact around bridge piers with uniform sediment. A test period of 48 hours was selected to achieve near-equilibrium conditions. After each experiment, the scour profile and scour pattern were measured by using a laser point gauge.

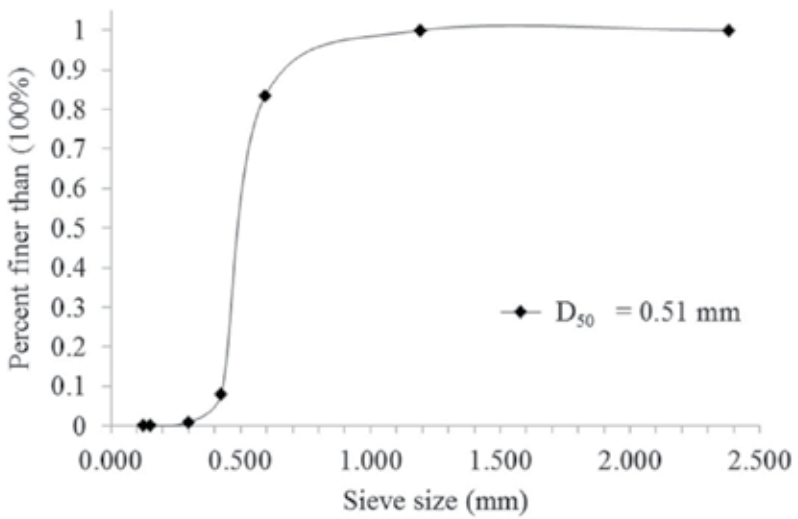

Figure 4. Sieve analysis of sediments used in Case 2

2.2. Results and analysis

2.2.1. Case 1

Figure 5 shows the scour pattern around abutments with nonuniform sediment. As shown in the figure, armor layer can be clearly noted on top of the scouring region around abutments. In both upstream and downstream of the abutment, coarse sediments were distributed equally around the scouring area. From experimental observation, the formation of armor layer greatly affects the maximum scour depth. Due to armor layer, the time needed to reach maximum scour depth is less than 24 hours.

Typical scour patterns around square and round abutments under different covered conditions were mapped. Figure 6 shows the contours around round abutment under both smooth cover and rough cover in the same flow conditions. Under both the covered conditions, the maximum scour depth is located at 60–70 degrees facing upstream. Additionally, rough cover can yield a relative larger scour compared to that from smooth cover as shown in Figure 6.

In all, 36 maximum scour depths are plotted in Figure 7, in which 18 are from a square abutment and 18 from a round abutment. Figure 7 shows the difference in maximum scour depth between the two types of abutments under different flow conditions. Based on Melville [19], the shape factor for square abutment in open channels is assumed as 1.0, while for the abutment with a round head, the value is assumed as 0.75. Figure 7 indicates that under both open channel and ice-covered conditions, square abutment generates a relatively larger maximum scour depth compared to the round abutment.

In order to compare the difference between square and round abutment, densimetric Froude number (F_o) can be calculated by using the following:

$$F_o = U_o / \sqrt{g(\Delta\rho / \rho)D_{50}} \tag{2}$$

where g is the gravitational acceleration, U_o is the approaching velocity, ϱ is the mass density of water, while the Δϱ is mass difference between sediment and water. D_{50} is the median grain size of sediments. An analysis using the densimetric Froude number is conducted to quantify the impact of abutment shape on maximum scour depth.

Furthermore, ice cover has a significant impact on the dimensions of the scour hole. In open channels, around the square abutment, the scour hole has a smaller slope compared to the scour holes under ice cover. It is also interesting to note that around the round abutment, the area of scour hole under the ice cover is larger than that of open channel. With the increase in ice cover roughness, there is a corresponding increase in scouring area. Around the square abutment, the scour hole retains a similar pattern with or without ice cover. While for round abutment, the scour hole under ice cover is larger than that from smooth cover and open channel.

To further examine the role of the ice cover, Figure 8 is plotted.

http://dx.doi.org/10.5772/61468

From Figure 8, at least two observations can be noted. Firstly, under all cover conditions, the overall trend of maximum scour depth increases with the increase in densimetric Froude number. Secondly, for a given F_o, the rough ice cover yields the largest maximum scour depth, while open channel has the smallest value. The data in Figure 8 also indicates the impact of ice cover on maximum scour depth. As mentioned previously, armor layer was detected in the scouring area around abutments.

Figure 5. Scour pattern with nonuniform sand from Case 1

Figure 9 shows armor layer sieve analysis compared with the original sediment sieve analysis. From the photos, it is interesting to note the proportion of coarse particles in the scouring area. Additionally, comparing the two analysis curves, it should become apparent that a smaller D_{50} yields small difference between armor layer and original sand, because smaller D_{50} for nonuniform sediment implies less coarse particles, hence the sediment size in the armor layer would decrease accordingly. Less coarse particles in the armor layer will provide less protection to foundation. Hence, a relatively larger maximum scour depth would be formed.

Dimensional analysis provides a convenient way for building a framework for parameters on which the maximum scour depth depends. Given the complexity of the interaction of various parameters, NCHRP [24] identified five major groups of dimensionless parameters affecting the maximum scour depth. However, there is still no clear indication on the impact of nonuniformity. In other words, the ice cover impact was not considered. Therefore, it is necessary to conduct a dimensionless analysis to investigate the ice cover impact on maximum scour depth. The following relationship can be noticed regarding maximum scour depth:

$$d_{\max} = f(U, \rho, \rho_s, g, d, n_b, n_i, D_{50}, l, B, H) \tag{3}$$

where

d_{max} is the maximum scour depth around the abutment,

U is the mean approach velocity,

ϱ is the mass density of the water,

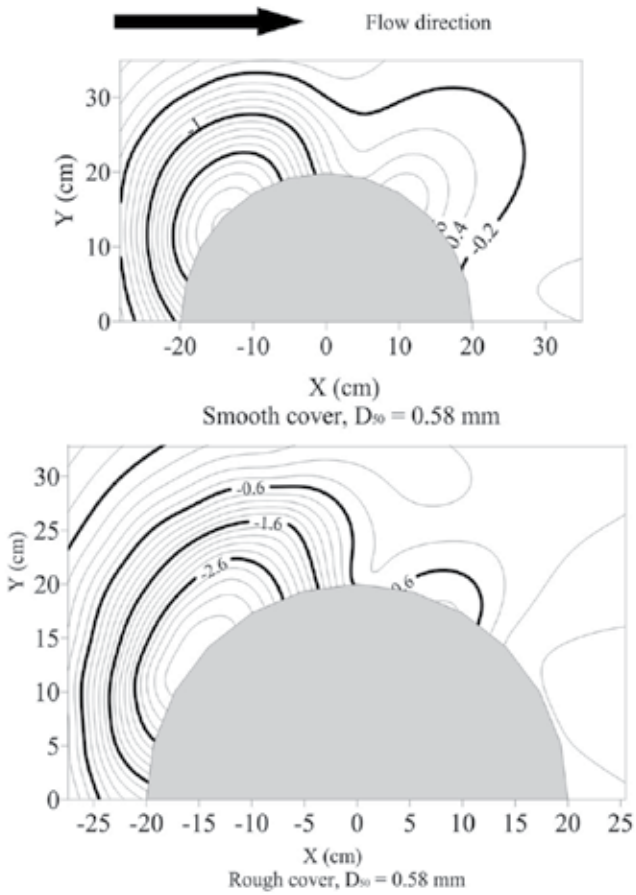

Figure 6. Scour profile around round abutment

ϱ_s is the mass density of nonuniform sediment,

d is the armor layer grain size,

n_b is the Manning's coefficient for the channel bed,

n_i is the Manning's coefficient of ice cover,

D_{50} is the median grain size,

l is the abutment width,

B is the flume width, and

H is the approaching water depth.

In the above relationship, the terms g, ϱ, and ϱ_s can be eliminated by introducing a combining parameter for a flow-sediment mixture. Additionally, abutment blockage ratio is also kept constant in the case study. To include the impacts of nonuniformity and armor layer, Meyer-

http://dx.doi.org/10.5772/61468

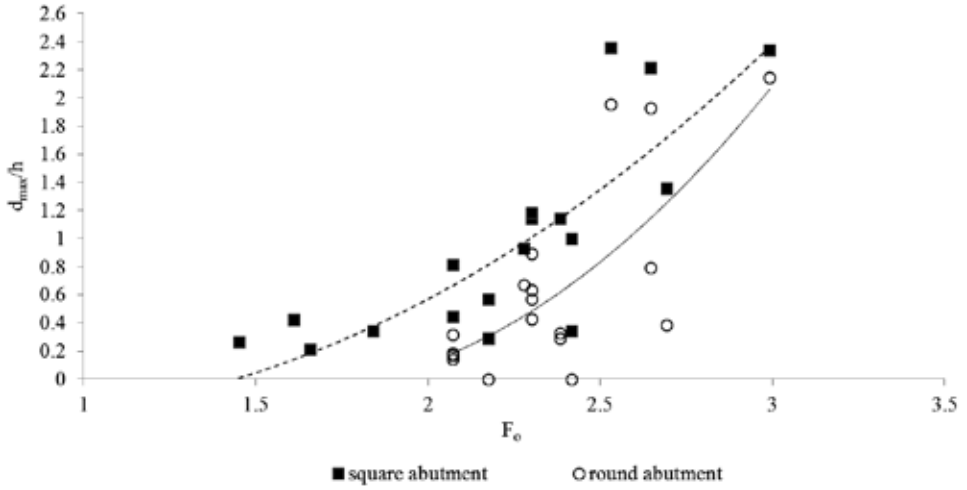

Figure 7. The dimensionless maximum scour depth variation with densimetric Froude number

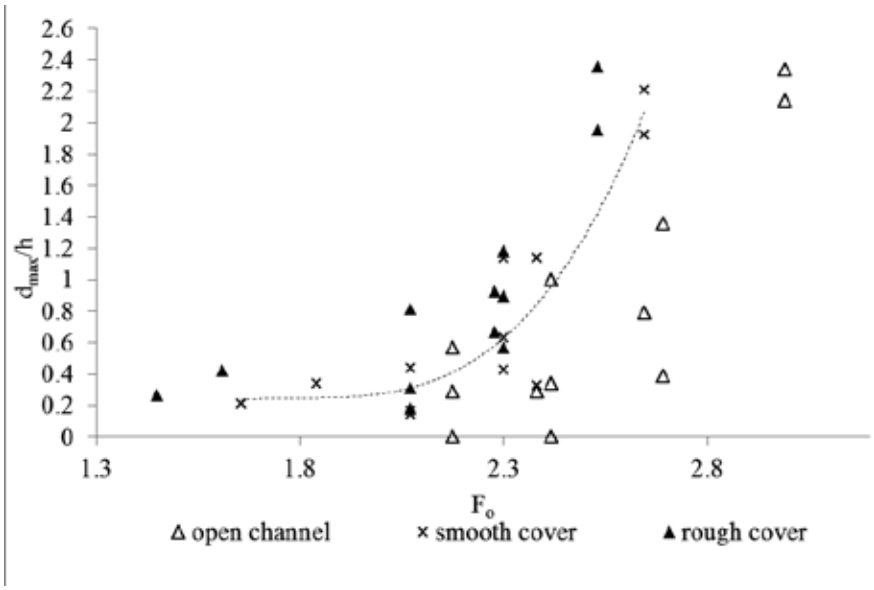

Figure 8. The comparison of dimensionless scour depth under different cover conditions (h is the flow depth)

Peter and Müller [20] developed the following equation by using one mean grain size of the bed to calculate the sediment size in the armor layer:

$$d = \frac{SD}{K_1\left(n / D_{90}^{1/6}\right)^{3/2}} \tag{4}$$

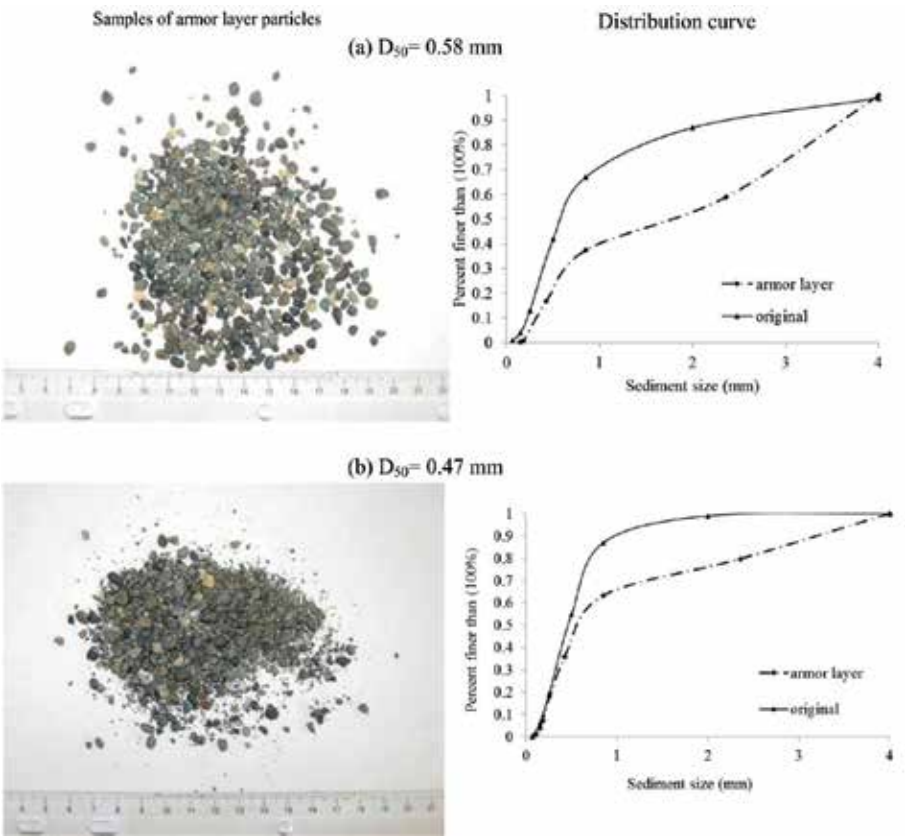

Figure 9. Samples of armor layer particle size and distribution curves

where

d is the armor layer sediment size,

S is the channel slope,

D is the mean water depth,

K_1 is the constant number, which equals to 0.058 when D is in meter,

n is the channel bottom Manning's roughness, and

D_{90} is the bed material size where 90% of the composition is finer.

Since the armor layer particle size is of the main interest here, d is introduced in the calculation of the densimetric Froude number:

$$F_o' = U / \sqrt{\left(\rho_s / \rho - 1\right) g d} \tag{5}$$

http://dx.doi.org/10.5772/61468

Figure 10 shows the variation of dimensionless maximum scour depth d_{max}/d with F_o' around both square and round abutments under all three flow conditions. It should be noted that under all flow conditions, with the increase in F_o', the value of d_{max}/d increases correspondingly. Around both square and round abutments, under the same F_o', the rough ice cover has the largest dimensionless maximum scour depth. Smooth ice cover has the second largest value. Meanwhile, the largest dimensionless maximum scour depth is located around square abutment in all flow conditions.

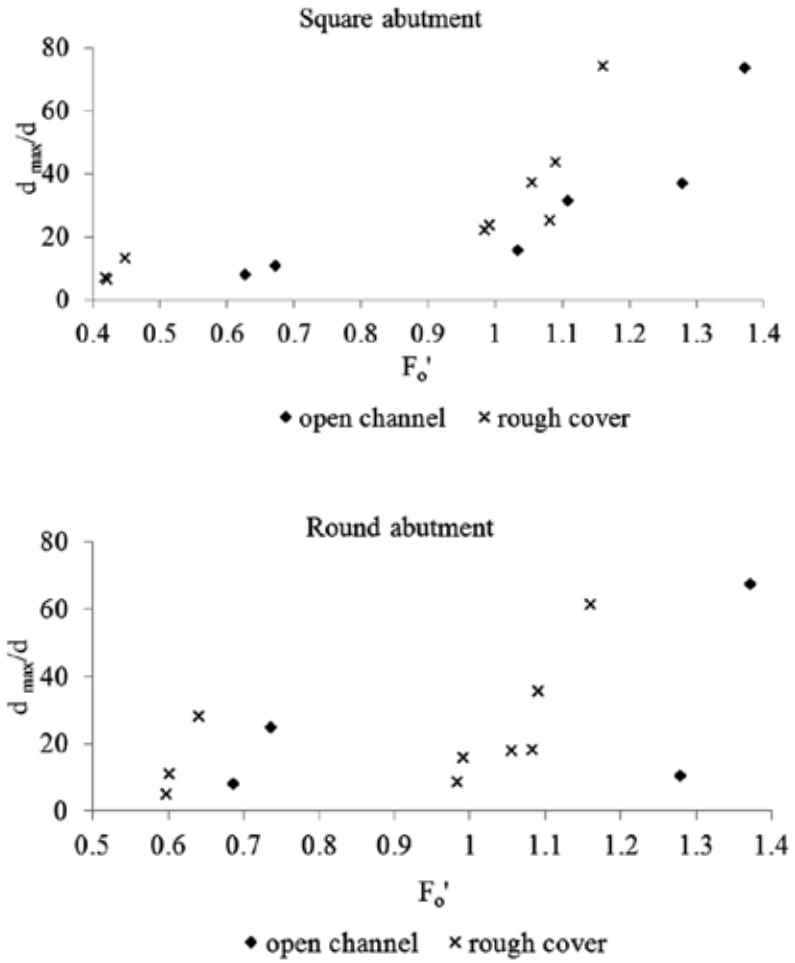

Figure 10. The dimensionless Froude number around both abutments under different cover conditions

From the above analysis, it is clear that ice cover has strong influence on local maximum scour depth around abutments. But rough ice cover has an even stronger impact.

Manning's roughness coefficient is between 0.01 and 0.0281 based on supporting field data as well as the observed ice cover characteristics [4]. In the case study, the Manning's coefficient

of 0.013 was adapted in accordance with Mays [18] for smooth ice cover. Rough ice cover was created by attaching small cubes with dimensions of 2.5 cm × 2.5 cm × 2.5 cm. The following equation was applied to calculate the Manning's coefficient [16]:

$$n_i = 0.039 k_s^{1/6} \tag{6}$$

where

k_s is the average roughness height of the ice underside.

In the first case study, rough ice cover has a Manning's coefficient of 0.021, which is located in the range as suggested by Carey [4]. The channel bed roughness is calculated by using the following equation from Hager [11]:

$$n_b = 0.039 D_{50}^{1/6} \tag{7}$$

As suggested by Wu et al. [30], the following relationships were developed to show the maximum scour depth under ice cover around square and round abutments:

$$\left(\frac{d_{\max}}{d}\right)_{square} \sim (F_o)^{3.73} \left(\frac{D_{50}}{d}\right)^{-1.78} \left(\frac{n_i}{n_b}\right)^{0.77} \left(\frac{H}{d}\right)^{3.01} \tag{8}$$

$$\left(\frac{d_{\max}}{d}\right)_{round} \sim (F_o)^{8.60} \left(\frac{D_{50}}{d}\right)^{-4.30} \left(\frac{n_i}{n_b}\right)^{1.00} \left(\frac{H}{d}\right)^{3.00} \tag{9}$$

The exponent of each parameter from the above relationships can be used to indicate the potential impact. The exponent of F_o, n_i/n_b, H/d is positive, while the exponent of D_{50} /d is negative. From the previous discussion, densimetric Froude number has a positive impact on maximum scour depth. Moreover, compared to the ice cover roughness, armor layer particle size also has a strong impact on the dimensionless maximum scour depth. With the increase in armor layer particle, the maximum scour depth decreases. This conclusion is in line with a previous study conducted by Sui et al. [26]. In natural river engineering, a mixture of coarse sediments in the vicinity of bridge foundations has the potential to reduce maximum scour depth.

2.2.2. Case 2

Figure 11 shows the impact of ice cover on bridge pier. Only one type of ice cover was used. Some of the results are presented by Wu and Balachandar [29]. At certain water depth, in this case, H = 108 mm, the scour contour and scour profile in the flow direction under ice cover is always larger than that in an open channel. The scour profiles in the flow direction also share some similarity. For example, the scour profiles almost overlap with each other in the upstream direction. While in the downstream of pier, the ice cover can clearly result in a movement of ridge toward downstream.

http://dx.doi.org/10.5772/61468

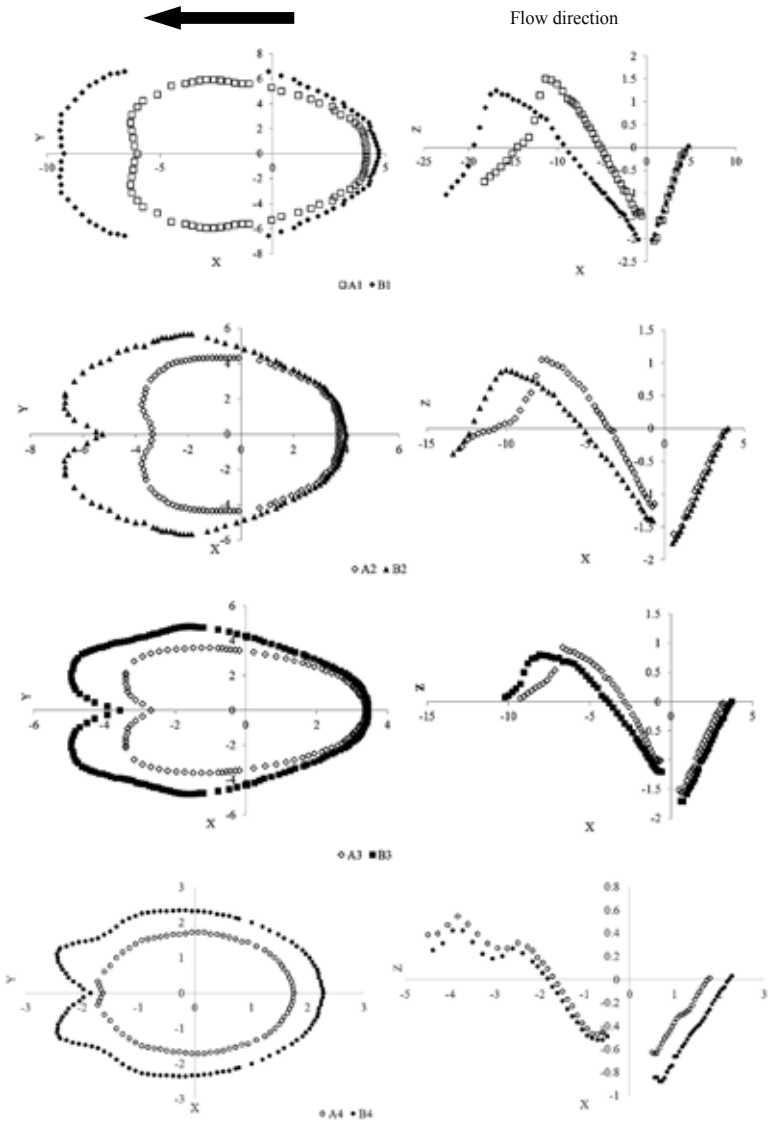

Figure 11. Scour comparison around piers under open channel (Group A) and ice cover (Group B) [29]

From the graphics presented above, the impact of ice cover on the local scour at bridge pier can be studied. It is evident from both case studies that, with the presence of ice cover, the maximum scour depth as well as the scour profile are increased.

2.2.3. Velocity profile under ice cover

By using the ADV data, the instantaneous velocity around the square abutment inside the scour hole was analyzed. The maximum scour depth is located at the upstream corner for the

square abutment. After each experiment, the velocity profile was measured at the upstream corner. Here, the parameter of interest is the maximum scour depth, so the velocity profile at the maximum scour depth location was plotted. The three-dimension velocity *u, v, w* in open channel, under both smooth ice cover, and rough ice cover are plotted in Figures 12 and 13.

For different sediments, the velocity profiles in the scour hole are slightly different. From these figures, one can notice the following:

- In open channel, the velocity in the X direction (flow direction) has the largest magnitude, while the velocity in Y direction (transverse direction) is second largest. One can also observe in open channel, the velocity in the X and Y directions changes direction from positive to negative or from negative to positive. Compared to the change of velocity direction in X and Y directions under ice cover, the open channel has the most turbulence in both the X and Y directions.
- Under ice-covered condition, the velocity magnitude in the Y direction has the largest magnitude followed by the velocity magnitude in X direction. This trend is clear in Figure 13 under both smooth and rough ice cover. At the same flow depth, the velocity in the Y direction inside the scour hole under rough ice cover has the largest value.
- Due to the impact of ice cover on the flow, the velocity in the Z direction is significantly different compared to that of open channels. Under ice-covered condition, the magnitudes in Z direction are larger than that from open channels. While under rough ice cover, the velocity gradient in Z direction is the largest. With decreasing D_{50}, the velocity in Z direction increases correspondingly. This is attributed to the presence of ice cover, which pushes the flow down toward the channel bed. A larger scour depth is formed. With the increase in ice cover roughness, the velocity in Z direction is increased correspondingly. With the decrease in D_{50} and increase in ice cover roughness, the variation of velocity in Z direction is obvious.
- Above the scour hole, the velocity gradients in both X and Y directions are decreased. The maximum velocity in X and Y direction is located at about the mid-depth from bottom of scour hole to the ice cover as shown in Figure 13.

2.2.4. Shear stress analysis

Bed shear stress and shear velocity are fundamental variables in river hydraulics to calculate the sediment transport, scour, and deposition. Dey and Barbhuiya [6] developed the Reynolds stresses method which is widely used by engineers. Biron et al. [3] compared several methods for bed shear stress calculation. For complex flow calculation, turbulent kinetic energy (TKE) method provided the best estimate of bed shear stress as it is not affected by local streamline variation and it takes into account the increased turbulent fluctuations. Using ADV data, Biron et al. [3], MacVirar and Roy [17], and Acharya [2] concluded that the TKE method is the most reliable to estimate the bed shear stress. Acharya [2] employed the TKE method for calculating bed shear stresses around spur dikes, yielding satisfactory results.

http://dx.doi.org/10.5772/61468

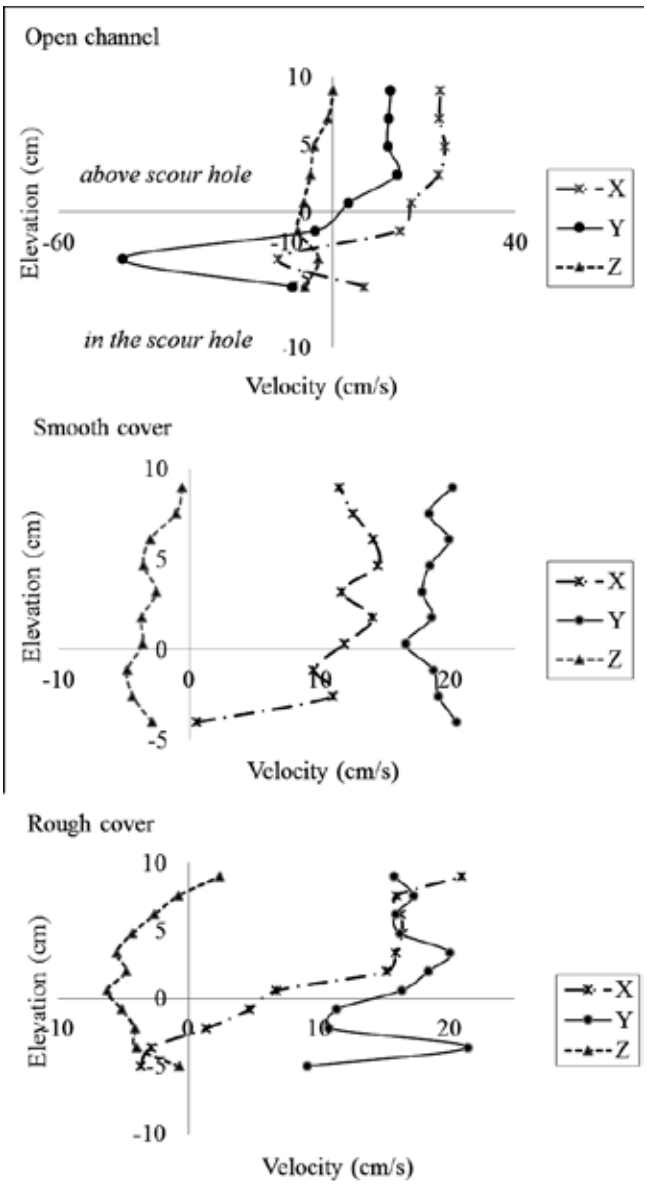

Figure 12. Three-dimensional velocity profile under different cover conditions (D_{50} = 0.58 mm)

Near-bed velocities were measured by placing the ADV probe in the scour hole. Three-dimensional velocity vectors were collected. For the instantaneous velocity component u, v, w in the X, Y, Z direction, the time-averaged velocity can be given as:

$$u = \overline{u} + u', v = \overline{v} + v', w = \overline{w} + w' \tag{10}$$

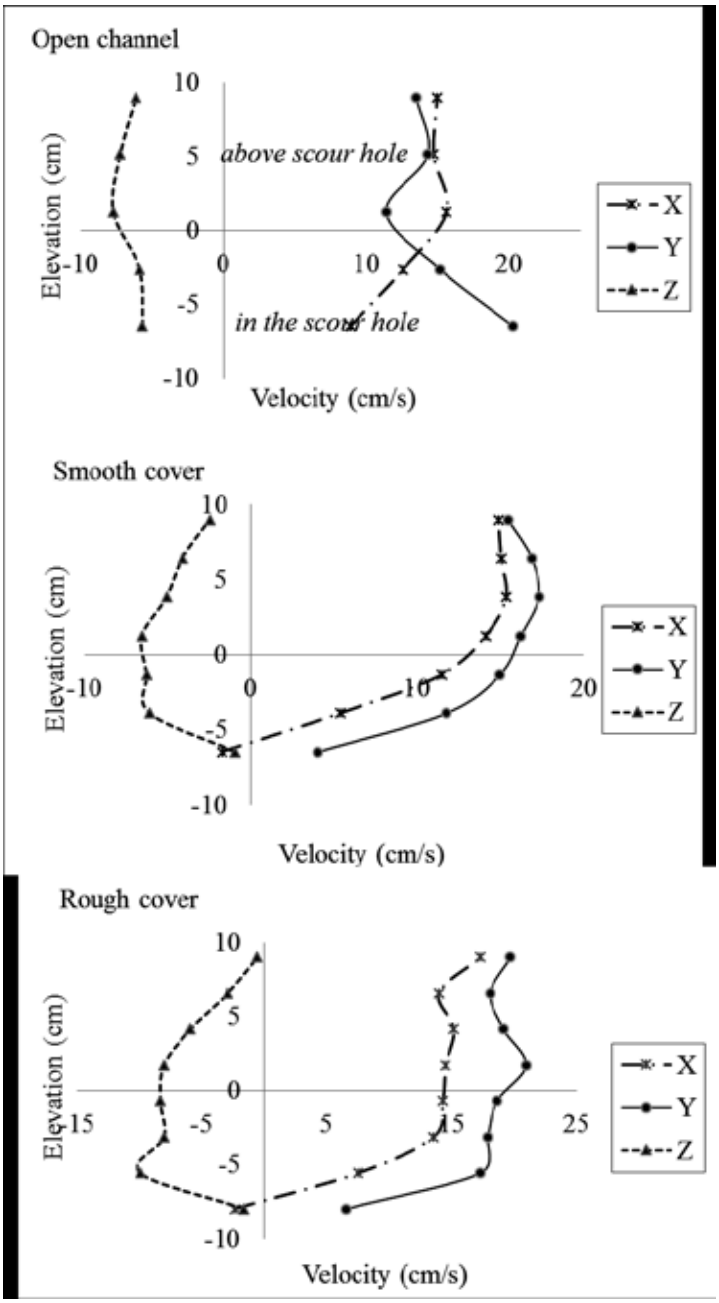

Figure 13. Three-dimensional velocity profile under different cover conditions (D_{50} = 0.47 mm)

where u′, v′, w′ denote the turbulent fluctuations in X, Y, and Z directions. The collected velocities at each point were processed to calculate the mean flow and turbulence characteristics at each point.

http://dx.doi.org/10.5772/61468

The bed shear stress was calculated by using TKE method as:

$$\tau_b = C_1\left[\frac{1}{2}\rho\left(u'^2 + v'^2 + w'^2\right)\right] \tag{11}$$

where C_1 is a proportionality constant which equals 0.19 [13]. Due to the fact that instrument noise errors associated with vertical velocity fluctuations were smaller than that of the horizontal velocity fluctuations, the above equation then can be simplified as:

$$\tau_b = C_2\rho\left(w'^2\right) \tag{12}$$

where $C_2 = 0.9$.

From discussions in Section 2.2.3, the velocity in Z direction plays a crucial role for the scouring process under ice cover. Hence, the above equation was used for calculation. The total bed shear stress in the scour hole can be expressed in dimensionless form as:

$$\hat{\tau} = \tau_b / \tau_0 \tag{13}$$

where τ_0 is the bed shear stress of the approaching flow calculated from $\tau_0=\varrho U_{*c}^2$, where U_{*c} is the critical shear velocity.

Figure 14 shows the variation of dimensionless shear stress at different elevations around the square abutment in open channel flow, smooth ice cover, and rough ice cover. The following conclusions can be drawn:

- Under rough ice cover condition, the rate of change of dimensionless shear stress is the largest compared with smooth ice cover and open channel. A larger bed shear stress is needed for the incipient motion in the scour region.
- Finer particles need relatively less dimensionless shear stress for the scouring under the same flow and cover conditions.
- Under rough ice cover condition, the dimensionless bed shear stress at the underside of ice has a relatively large magnitude. Additionally, the variation of dimensionless shear stress under ice cover has a shape of "S" as shown in Figure 14. However, more research should be conducted to validate this.

3. Conclusion

Ice cover and nonuniform sediment are two critical parameters for the development of scour around hydraulic structures, such as bridge piers and abutments. By using two case studies,

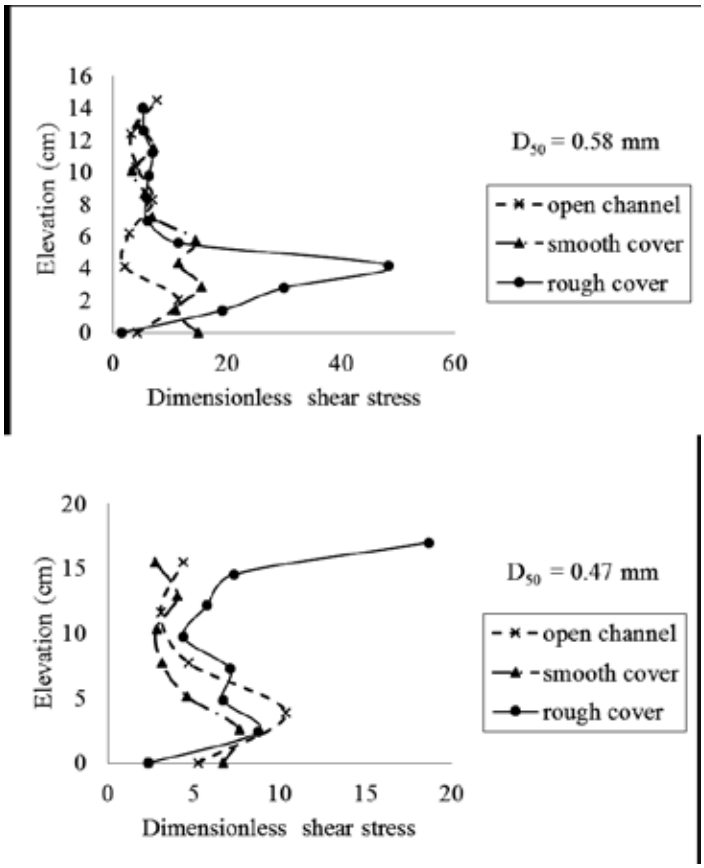

Figure 14. Comparison of measured dimensionless shear stress under different conditions

the impact of ice cover is presented in the chapter. With an increase in the densimetric Froude number, there is a corresponding increase in the dimensionless scour depth. For same nonuniform sediment, due to the formation of armor layer, less maximum scour depth was noted around bridge foundation structures. The increase in ice cover roughness can also result in a larger scour depth and profile. By analyzing the ADV data collected from Case 1, it was found that the velocity magnitude in Z direction is larger under ice covered flow in the scour hole than that under open channel flow. The velocity magnitude in Y direction has the largest magnitude under ice cover. More research is required to gain sufficient insight into the impact of ice cover on the local scour around hydraulic structures.

Acknowledgements

Experimental work was conducted at Quesnel River Research Center (QRRC), Likely, BC, and Sedimentation and Scour Study Laboratory at University of Windsor. Staff and colleagues provided great help.

http://dx.doi.org/10.5772/61468

Author details

Peng Wu[1], Jueyi Sui[2] and Ram Balachandar[3]

*Address all correspondence to: Peng.Wu@uregina.ca

1 Environmental Systems Engineering, University of Regina, Canada

2 Environmental Engineering Program, University of Northern British Columbia, Canada

3 Civil and Environmental Engineering, University of Windsor, Canada

References

[1] Ackermann N L, Shen H T, Olsson P, 2002. Local scour around circular piers under ice covers. *Proceeding of the 16th IAHR Internnational Symposium on Ice*, Internnational Association of Hydraulic Engineering Research, Dunedin, New Zealand.

[2] Acharya A, 2011. Experimental study and numerical simulation of flow and sediment transport around a series of spur dikes, PhD thesis, The University of Arizona, pp. 140-161.

[3] Biron P M, Robson C, Lapointe M F, Gaskin S J, 2004, Comparing different methods of bed shear stress estimates in simple and complex flow fields. *Earth Surf Process Landforms*, Vol. 29, pp. 1403-1415.

[4] Carey K L, 1966. Observed configuration and computed roughness of the underside of river ice, St Croix River, Wisconsin, Professional paper 550-B, US Geological Survey, pp. B192-B198.

[5] Chien N, Wan Z, 1999. *Mechanics of Sediment Transport*. ASCE Process. Reston, Virginia, USA.

[6] Dey S, Barbhuiya A K, 2005. Turbulent flow field in a scour hole at a semicircular abutment, Can J Civil Engin, Vol. 32, pp. 213-232.

[7] Duan J G, He L, Fu X, Wang Q, 2009, Mean flow and turbulence around experimental spur dike, *Adv Water Res*, Vol. 32, pp. 1717-1725.

[8] Ettema R, Braileanu F, Muste M, 2000. Method for estimating sediment transport in ice covered channels, *J Cold Region Engin*, *ASCE*, Vol. 14, No. 3, pp. 130-144.

[9] Ettema R, Daly S, 2004. Sediment transport under ice. ERDC/CRREL TR-04-20. Cold Regions Research and Engineering Laboratory U.S. Army Engineer Research and Development Center 72 Lyme Road Hanover, New Hampshire 03755.

[10] Goring D G, Nikora V I, 2002, Despiking acoustic Doppler velocimeter data. *J Hydraul Engin, ASCE*, Vol. 128, No. 1, pp. 117-126.

[11] Hager W H, 1999. *Wastewater Hydraulics: Theory and Practice*, Springer, Berlin, New York, pp. 17 – 54.

[12] Hains D B, 2004. An experimental study of ice effects on scour at bridge piers, PhD Dissertation, Lehigh University, Bethlehem, PA.

[13] Kim S C, Friedrichs C T, Maa J P Y, Wright L D, 2000. Estimating bottom stress in tidal boundary layer from acoustic Doppler velocimeter data, *J Hydraul Engin*, Vol. 126, No. 6, pp. 399-406.

[14] Kuhnle R A, Jia Y, Alonso C V, 2008. Measured and simulated flow near a submerged spur dike, *J Hydraul Engin, ASCE*, Vol. 134, No. 7, pp. 916-924.

[15] Lau Y L, Krishnappan B G, 1985. Sediment transport under ice cover, *J Hydraul Engin, ASCE*, 111(6), pp. 934-950.

[16] Li S S, 2012. Estimates of the Manning's coefficient for ice covered rivers, *Water Management, Proc Institut Civil Engin*, Vol. 165, Issue WM9, pp. 495-505.

[17] MacVirar B J, Roy A G, 2007. Hydrodynamics of a forced riffle pool in a gravel bed river: Mean velocity and turbulence intensity, *Water Res Res*, Vol. 43, Issue 12, DOI: 10.1029/2006WR005272.

[18] Mays L W, 1999. *Hydraulic Design Handbook*, McGraw-Hill, pp. 3.12.

[19] Melville B W, 1997. Pier and Abutment scour: integrated approach, *J Hydraul Engin, ASCE*, Vol. 123(2), pp. 125-136.

[20] Meyer-Peter E, Müller R, 1948. Formula for bed-load transport, Proceedings of International Association for Hydraulic Research, 2nd Meeting, Delft, Netherlands, pp. 39-64.

[21] Morse B, Hicks F, 2005. Advances in river ice hydrology 1999-2003, *Hydrol Process*, Vol. 19, Issue 1, pp. 247-263.

[22] Munteanu A, 2004. Scouring around a cylindrical bridge pier under partially ice-covered flow condition, Master thesis, University of Ottawa, Ottawa, Ontario, Canada.

[23] Munteanu A, Frenette R, 2010. Scouring around a cylindrical bridge pier under ice covered flow condition-experimental analysis, R V Anderson Associates Limited and Oxand report.

[24] NCHRP Web-only Document 181, 2011. Evaluation of Bridge-Scour Research: Abutment and Contraction Scour Processes and Prediction. NCHRP Project 24-27(02).

[25] Rehmel M, 2007. Application of Acoustic Doppler Velocimeter for streamflow measurements, *J Hydraul Engin, ASCE*, Vol. 133, Special Issue: Acoustic Velocimetry for Riverine Environments, pp. 1433–1438.

http://dx.doi.org/10.5772/61468

[26] Sui J, Wang J, He Y, Krol F, 2010. Velocity profile and incipient motion of frazil particles under ice cover, *Int J Sedim Res*, Vol. 25(1), pp. 39-51.

[27] Smith B T, Ettema R, 1997. Flow resistance in ice covered alluvial channels, *J Hydraul Engin ASCE*, Vol. 123(7), pp. 592-599.

[28] Wahl T L, 2000, Analyzing data using WinADV, 2000 Joint Conference on water resources engineering and water resources planning and management, Minneapolis, Minnesota, pp. 1-10.

[29] Wu P, Balachandar R, 2015. Measurement of scour profiles around bridge piers in channel flow with and without ice-cover, 22nd Canadian Hydrotechnical Conference, April 29-May 3, Montreal, Quebec, Canada, pp. 1-11.

[30] Wu P, Hirshfield F, Sui J, 2014a, Armor layer analysis of local scour around bridge abutments under ice cover. *River Research and Applications*, published online in Wiley Online Library, DOI: 10.1002/rra.2771.

[31] Wu P, Hirshfield F, Sui J. 2014b, Further studies of incipient motion and shear stress on local scour around bridge abutment under ice cover, *Can J Civil Engin*. Vol. 41(10), pp. 892-899.

[32] Wu P, Hirshfield F, Sui J, 2015. Local scour around bridge abutments under ice covered conditions – an experimental study, *Int J Sedim Res*, Vol. 30 (1), pp. 39-47.

[33] Yang C T, 2003. *Sediment Transport, Theory and Practice*. Krieger Publishing Company, Krieger Drive, Malabar, Florida 32950.

Edited by Vlassios Hrissanthou

Sediment transport is a significant part of the scientific area of river hydraulics. Therefore, the first section of the present book presents effects of sediment transport on hydraulic structures, that concern alluvial channel hydraulics. The second section refers to a serious consequence of river sediment transport, namely reservoir sedimentation. Sediment transported in a river originates from the corresponding basin, that is eroded by rainfall water. Hence, the quantification of soil erosion is also addressed in the second section. While soil erosion is the original physical process that causes reservoir sedimentation, the latter process may increase coastal erosion in case that the river feeding the reservoir, discharges its water into the sea. So, the effect of reservoir sedimentation on coastal erosion is further treated in the second section. Finally, the third section of the book is dedicated to the phenomenon of local scour around bridge piers, in particular the conditions of ice cover.

ISBN 978-953-51-5060-2

IntechOpen